iScience

CellPress
OPEN ACCESS

Article

Assembling Shape-Persistent High-Order Sierpiński Triangular Fractals

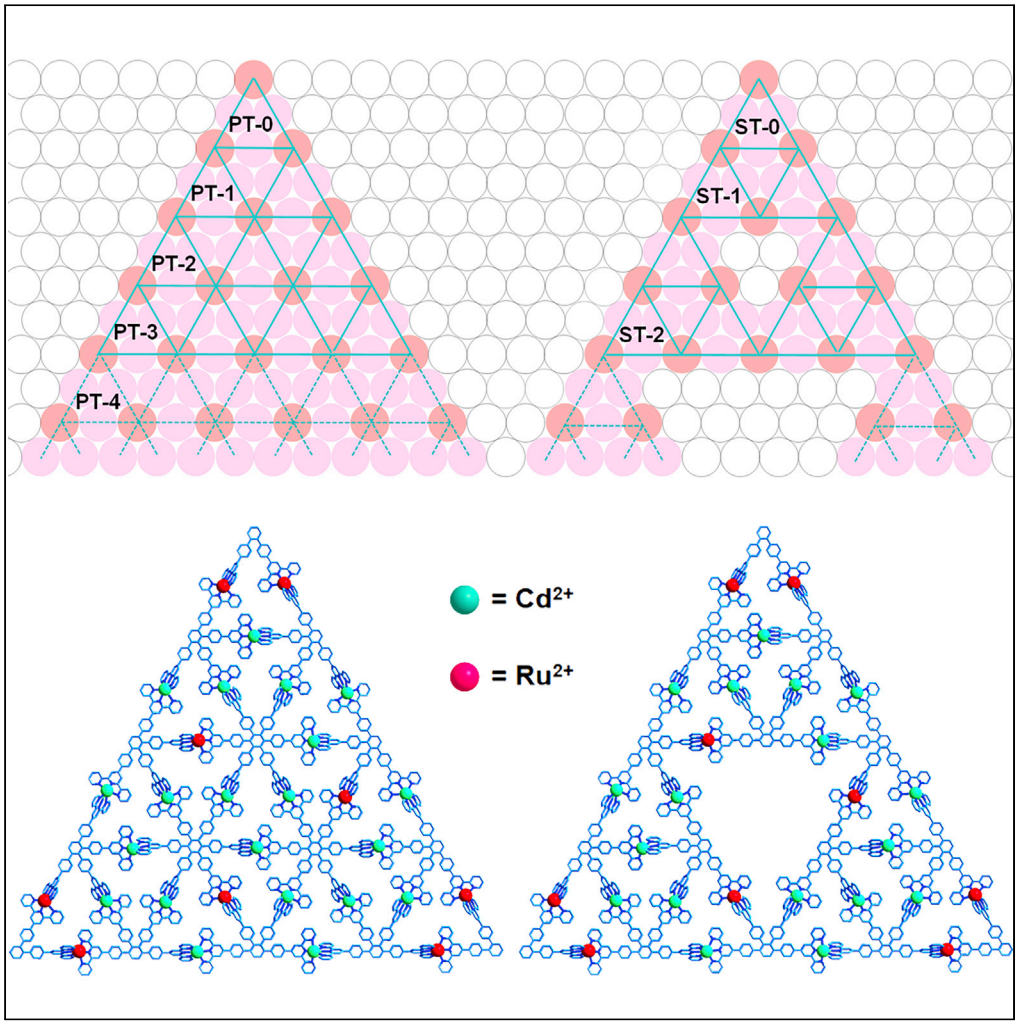

Zhilong Jiang, Die Liu, Mingzhao Chen, ..., Xiaopeng Li, George R. Newkome, Pingshan Wang

jinyulinzhao@foxmail.com (M.C.)
newkome@uakron.edu (G.R.N.)
chemwps@csu.edu.cn (P.W.)

HIGHLIGHTS

Giant supramacromolecular Sierpiński and Pascal's triangles

The design and use of small synthons to assemble high-order molecular fractals

A retro-assembly modular construction strategy for complicated molecular fractals

The dense-packed counterions of architectures could form supramolecular hydrogels

Jiang et al., iScience 23, 101064
May 22, 2020
https://doi.org/10.1016/j.isci.2020.101064

iScience

CellPress
OPEN ACCESS

Article

Assembling Shape-Persistent High-Order Sierpiński Triangular Fractals

Zhilong Jiang,[1,5] Die Liu,[1,5] Mingzhao Chen,[1,*] Jun Wang,[2] He Zhao,[2] Yiming Li,[3] Zhe Zhang,[1] Tingzheng Xie,[1] Feng Wang,[2] Xiaopeng Li,[3] George R. Newkome,[4,*] and Pingshan Wang[1,2,6,*]

SUMMARY

Fractals are a series of intricate patterns with aesthetic, mathematic, and philosophic significance. The Sierpiński triangles have been known for more than one hundred years, but only recently discrete shape-persistent low-generation (mainly ST-1) fractal supramolecules have been realized. Herein, we report a retro-assembly pathway to the nanometer-scale, supra-macromolecular second-generation Sierpiński triangle and its third-generation saturated counterpart (Pascal's triangle). These gigantic triangular assemblies are unambiguously confirmed by NMR, DOSY, ESI-MS, TWIM-MS, TEM, and AFM analyses. Notably, the dense-packed counterions of these discrete triangular architectures could further form supramolecular hydro-gels in water. This work not only provides a fundamental chemical pathway to explore various giant supramolecular constructs and further overcome the synthetic limitation of complicated molecular fractals, but also presents a new type of supramolecular hydro-gels with potential in controlled release applications.

INTRODUCTION

Self-similar fractals were described as "exactly the same at every scale or nearly the same at different scales" by Mandelbrot in 1975 (Mandelbrot, 1982; Peitgen et al., 1992). Examples of such fractal patterns are apparent in Nature, such as clouds, trees, and coast lines, but chemists need to find new one-step routes traditional and yet unknown fractal structures by simple one-step chemical methods (Lehn, 1985; Wang et al, 2015, 2018; Newkome et al., 2006; Newkome and Moorefield, 2015; Grayson and Fréchet, 2001; Sugiura et al., 1999; Rousseaux et al., 2015; Kempkes et al., 2018). As a basic example of self-similar fractal set, the Sierpiński triangle (**ST**; Figure 1) is a mathematically generated pattern that possesses the overall shape of an equilateral triangle and subdivided infinitely into smaller equilateral triangles. It was mathematically defined by the Polish mathematician Waclaw Sierpiński in 1916 via a series of interrelated equilateral triangles (Sierpinski, 1916). For Pascal's triangle (**PT**; Figure 1), it is a triangular array of the binomial coefficients, which is named after the French mathematician Blaise Pascal (Wolfram, 1984). If coloring the Pascal's triangle with 2n rows the even numbers blue and the odd numbers yellow, the result is an approximation to the Sierpiński triangle (Figure 1).

The earliest molecular-scale STs in experimental systems were achieved by self-assembly of DNA tiles (Brune et al., 1994). In recent years, efforts have been made to construct molecular **STs**, especially via different self-assembly strategy on surfaces (Shang et al., 2015; Li et al., 2017; Qiang et al., 2015; Rastgoo-Lahrood et al., 2016; Zhang et al., 2015; Nieckarz and Szabelski, 2016). For example, Wu's group and Wang's group have demonstrated a series of defect-free **STs** on noble metal surface at strictly low temperatures and under high-vacuum conditions from the 120° backbone of building blocks (Shang et al., 2015; Li et al., 2017). Wang and co-workers recently reported that covalent **STs** based on dynamic covalent chemistry could be prepared in solution on highly oriented pyrolytic graphite (HOPG) surface (Mo et al., 2019). In addition, driving forces including hydrogen bond and metal-ligand interaction were also used to prepare ordered STs on different surfaces (Qiang et al., 2015; Rastgoo-Lahrood et al., 2016; Cai et al., 2017).

It is worth noting that the on-surface construction of **STs** tends to form a mixture of different generations of **STs** rather than a discrete shape-persistent architecture. Alternatively, the self-assembly of supramolecular architectures through coordination of metal ions and predesigned ligands is an important part of

[1]Institute of Environmental Research at Greater Bay Area; Key Laboratory for Water Quality and Conservation of the Pearl River Delta, Ministry of Education; Guangzhou Key Laboratory for Clean Energy and Materials, Guangzhou University, Guangzhou-510006, China

[2]Hunan Key Laboratory of Micro & Nano Materials Interface Science; College of Chemistry and Chemical Engineering, Central South University, Changsha, Hunan-410083, China

[3]Department of Chemistry, University of South Florida, Tampa, FL 33620, USA

[4]Center for Molecular Biology and Biotechnology, Florida Atlantic University, Jupiter, FL 33428, USA

[5]These authors contributed equally

[6]Lead Contact

*Correspondence: jinyulinzhao@foxmail.com (M.C.), newkome@uakron.edu (G.R.N.), chemwps@csu.edu.cn (P.W.)

https://doi.org/10.1016/j.isci.2020.101064

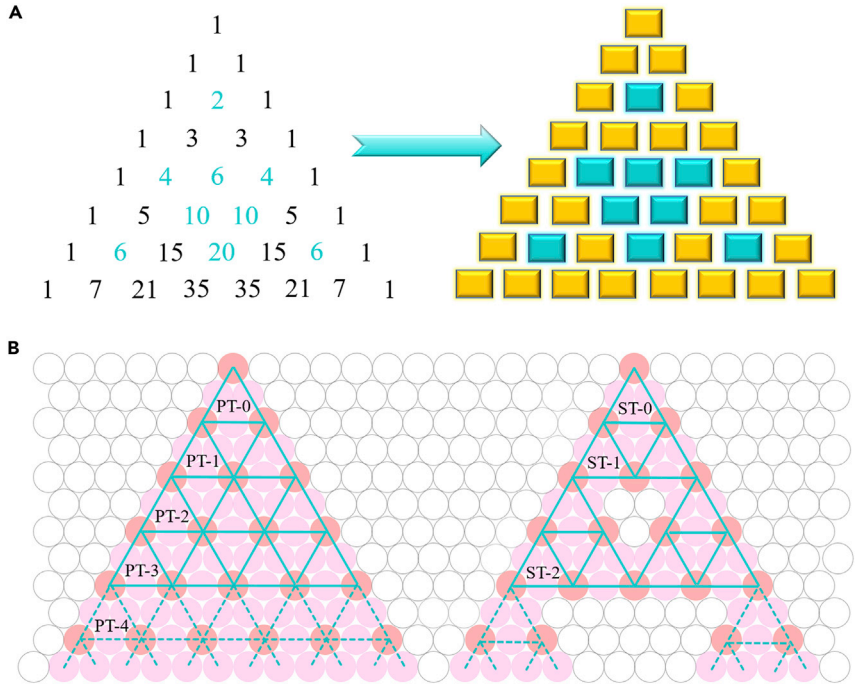

Figure 1. Mathematical Triangular Array of the Binomial Coefficients

(A) The first few lines of binomial coefficients (yellow rectangles indicate the odd numbers and blue rectangles indicate the even numbers, the result is an approximation to the Sierpiński triangle).

(B) The Pascal triangle (**PT**) and Sierpiński triangle (**ST**) pattern.

supramolecular chemistry (Safont-Sempere et al., 2011; Swiegers and Malefetse, 2000; Yam et al., 2015; Holliday and Mirkin, 2001; De et al., 2010). Since Pt(II), Pd(II), and Fe(II) have been used as vertices to link different ligands leading to the construction of complicated 2D and 3D architectures, the use of precise organic-based vertices expands on this concept in which the ligand-metal-ligand component is used to appear as the sides of the construct (Byrne et al., 2017; Chakrabarty et al., 2011; Chichak et al., 2004; Cullen et al., 2016; Danon et al., 2017; Fujita et al., 2016a, 2016b; K. Li et al., 2014; Z. Y. Li et al., 2014; Lu et al., 2017; Ronson et al., 2017). Among these coordination-driven constructs, fractal macromolecules are regarded as the most aesthetical design. However, it has been synthetically challenging especially those with multi asymmetric heterogeneous ligands, and thus limited examples have thus far been reported (Sarkar et al., 2014; Jiang et al., 2017a, 2017b; Wang et al., 2014; Wu et al., 2017).

Recently, the low generation of **ST** and **PT** were synthesized in solution by Newkome group and our group (Sarkar et al., 2014; Jiang et al., 2017a, 2017b; Schultz et al., 2012), but the construction of their next-generation architectures by employing similar methods carries significant challenges (Figures S1–S3). To the best of our knowledge, the single defect-free G2 **ST** and G3 **PT** have not been reported yet. Herein, we present the extremely challenging classical structures by molecular self-assembly based on three predesigned < tpy-Ru^{2+}-tpy > monomers in solution for the first time (tpy = 2,2′:6′,2″-terpyridine), which consist of sixteen and twelve small triangles, respectively. The resultant giant architectures with a fractal feature can be assumed as a recursive mathematical form that possesses a self-similar structure, i.e., triangles of different sizes or levels.

Motivated by the retrosynthetic path devised by Corey Corey, 1991, an assembly strategy has been applied to analyze the geometrical patterns of target G2 **ST** and G3 **PT** (Figure 2A). Thus, the disconnections of metallo-terpyridinyl G2 **ST** and G3 **PT** fractals are the coordinated metal ions, instead of disconnecting the covalent bonds in a conventional retrosynthesis. Based on the triangular connections, the precursor for G2 **ST** and G3 **PT** could be distinguished as separate key metallo-organic ligands **L1**, **L2**, and **L3**, which utilize stable < tpy-Ru^{2+}-tpy > as a linker. Thus, using three key expanded synthons, "V"-shaped, "K"-shaped, and "Star"-shaped ligands (Figure 2A), the desired multi-direct precursors could be specifically constructed

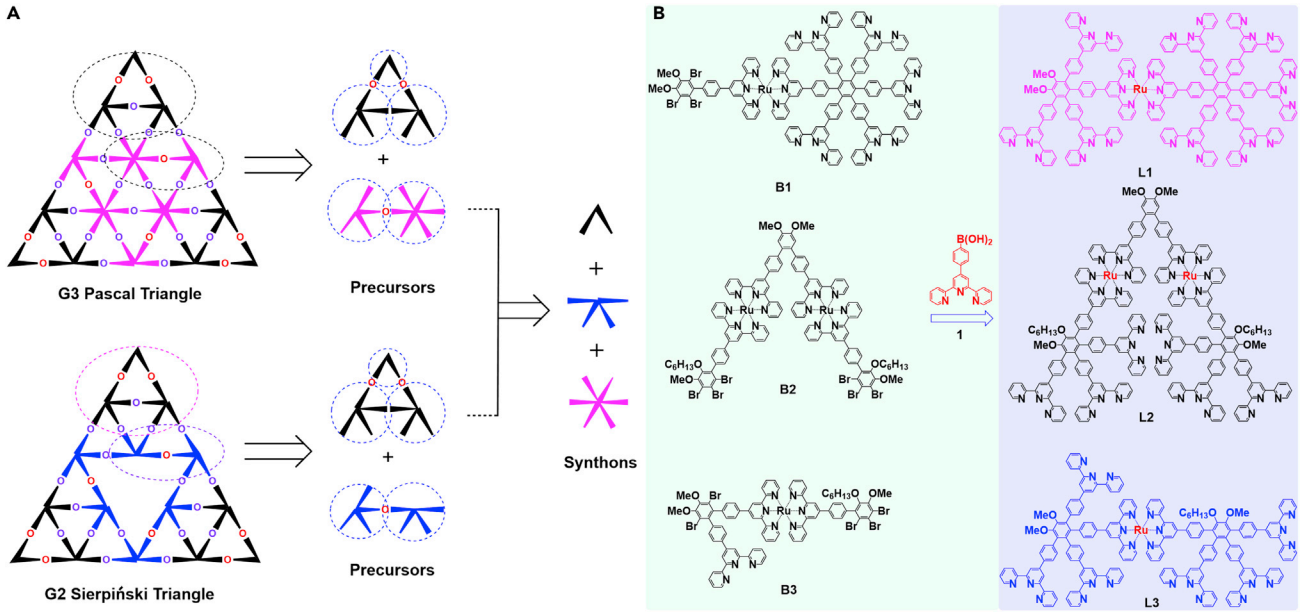

Figure 2. Retrosynthetic Analysis and Ligands Synthesis

(A) Illustrating the disconnection of G3 **PT** and G2 **ST** to three precursors and three simplified synthons by the retrosynthetic analysis.

(B) Synthesis of modular Metallo-organic Ligands through a multi-fold Pd^0-catalyzed Suzuki coupling reaction on Ru-complexes. Reagents and conditions: CH_3CN, $Pd(PPh_3)_4$, K_2CO_3, reflux.

by the Suzuki coupling reactions on complexes using the stable designer < tpy-Ru^{2+}-tpy > derivatives. These pre-organized modular units may help the precursors and metal ions accurately assemble to generate the ultimate desirable architectures overcoming the entropy effect, as a result of thermodynamic control.

RESULTS AND DISCUSSION

Ligands Synthesis

In terpyridyl chemistry, Ru(II) has been regarded as one of the most important metal ions to coordinate with terpyridine moieties to generate the inert <tpy-Ru^{2+}-tpy> bonds. In our previous work, the synthetic route to <tpy-Ru^{2+}-tpy> complexes containing uncoordinated terpyridine moieties utilized Suzuki coupling reactions (Jiang et al., 2017a, 2017b; Chakraborty and Newkome, 2018). Based on this premise, the key metallo-organic ligands **L1**, **L2**, and **L3** were designed and successfully synthesized by multiple Suzuki-coupling of corresponding Br-substituent Ru^{2+}-terpyridine complexes **B1**, **B2**, **B3** and 4′-(4-boronophenyl)-terpyridine **1** in a mixed solvent system with Pd(0) as catalyst, respectively (Figure 2B). The initial organic ligands were synthesized via known procedures (Jiang et al., 2017a, 2017b; Chen et al., 2018a, 2018b). Those multi-bromo-substituted complexes were prepared by the coordination of the tpy-$RuCl_3$ adducts with the "Star"-shaped hexa-tepyridine, "V"-shaped bisterpyridines under reducing conditions and simple column chromatography, respectively (Scheme S1). The detailed synthetic routes and procedures and characterizations are available in the Supporting Information (Figures S4–S40 and S51–S58). All the metallo-organic ligands and their precursors were fully characterized by nuclear magnetic resonance (NMR), including ^1H, ^{13}C, Homonuclear Chemical Shift Correlation Spectroscopy (COSY), and Nuclear Overhauser Effect Spectroscopy (NOESY).

The ^1H NMR spectrum of **L2** features two peaks at 9.41 and 9.02 ppm with identified integral could be assigned to $tpyH^{3',5'}$ of <tpy-Ru^{2+}-tpy> moieties, singlets and doublets appeared at 8.77–8.54 ppm were assigned to the $tpyH^{3',5'}$, $tpyH^{3,3''}$, and $tpyH^{6,6''}$ for the free terpyridine ligands (Figure S30). In addition, two sharp OCH_3 singlets at 4.05 and 3.75 ppm and one triplet at 3.99 ppm for the OCH_2 with a 3:3:2 integral ratio also confirmed the expected structure. The ^1H NMR spectrum of **L1** and **L3** was complicated owing to several chemical environments of the terpyridine protons within the asymmetrical structure; there were ten and eight different terpyridine moieties in **L1** and **L3**, respectively. As for the ^1H NMR spectrum

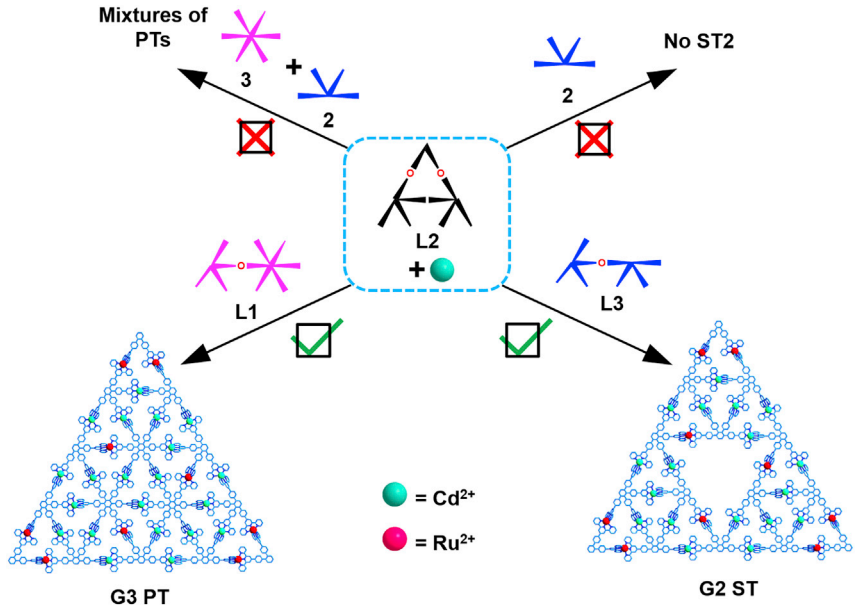

Figure 3. Schematic Illustrations of Preparing the Sierpiński-type Triangular Fractals from the Multicomponent Assembly

Direct assembly of L2 with organic ligands failed to gain the expected architectures.

of **L1** (Figure S21), it is clear that there were two groups of representative $tpyH^{3',5'}$ singlets at above 9.0 ppm, which were assigned to $tpyH^{3',5'}$ of the <tpy-Ru^{2+}-tpy> moieties and four singlets below 9.0 ppm corresponding to free $tpyH^{3',5'}$. Double singlets with an integration ratio 1:1 were found at 4.07, 4.05 ppm, which were assigned to the different methoxy groups. The ^1H NMR spectrum of **L3** displayed two singlets at 8.87 and 9.07 ppm with identified integral could be assigned to $tpyH^{3',5'}$ of <tpy-Ru^{2+}-tpy> moieties, and the resonance absorption peaks ranging from 8.45 to 8.75 ppm correspond to protons of free terpyridine groups (Figure S38). Three sharp singlets around 3.75 ppm and one triplet at 3.97 ppm were in accordance with methoxyl and methylene groups of desired compound **L3**. All peaks assignments were confirmed based on 2D COSY and NOESY NMR spectra. To further establish the structure of these modules, electrospray ionization mass spectrometry (ESI-MS) was employed to show that all experimental values of ligands **L1–L3** are consistent with the theoretical values (Figures S54, S56, and S58).

Self-Assembly of the Third-Generation Pascal's Triangle

According to the geometric prediction, it was proposed that **L2**, K-shaped organic ligand **2**, and star shaped **3** could assemble with Cd^{2+} to form the desired G3 **PT** directly (Figure 3). The product was characterized by ESI-MS spectroscopy; unfortunately, only the G2 **PT** metallo-triangle architecture and a trace amount of G3 **PT** could be obtained (Figure S50). This was attributed to the fact that the self-assembly is an entropy-driven process, which needs to conquer the entropy reduction effect during the assembly. Similarly, the attempt to obtain G2 **ST** was, however, unsuccessful by directly mixing ligand **L2** and **2** with metal ions in a precise stoichiometric ratio of 1:2:7 via the one-pot procedure; the resultant product was unidentified by ESI-MS (Figures S49). We speculated that random assortment of free K-shaped ligands led to form the defective structures. Therefore, the Ru^{2+}-tpy-based metallo-organic ligands **L1** and **L3** were redesigned through a retro-assembly analysis of targeted G2 **ST** and G3 **PT** (Video S1).

Fortunately, after mixing modules **L1** and **L2** with $Cd(NO_3)_2$ in the precise ratio of 1:1:7 in MeOH/$CHCl_3$ (1:1, v/v) at 75°C for 12 h, the multiple predesigned components were accurately assembled into the third-generation supramolecular Pascal's triangle G3 **PT**. Compared with the sharp ^1H NMR signals of the ligands, the spectra of the supramolecular G3 **PT** displayed remarkable broaden peaks at aromatic area, owing to their much slower tumbling motion on the NMR timescale (Sun et al., 2010). But at aliphatic area, singlets of the methoxy groups and the triplet signal corresponding to the methylene group of G3 **PT** were observed at around 4.00 ppm; it showed complicated but sharp signals indicating the formation of a single assembly. All assignments were further confirmed by 2D COSY and NOESY spectra (Figures S41–S43). In

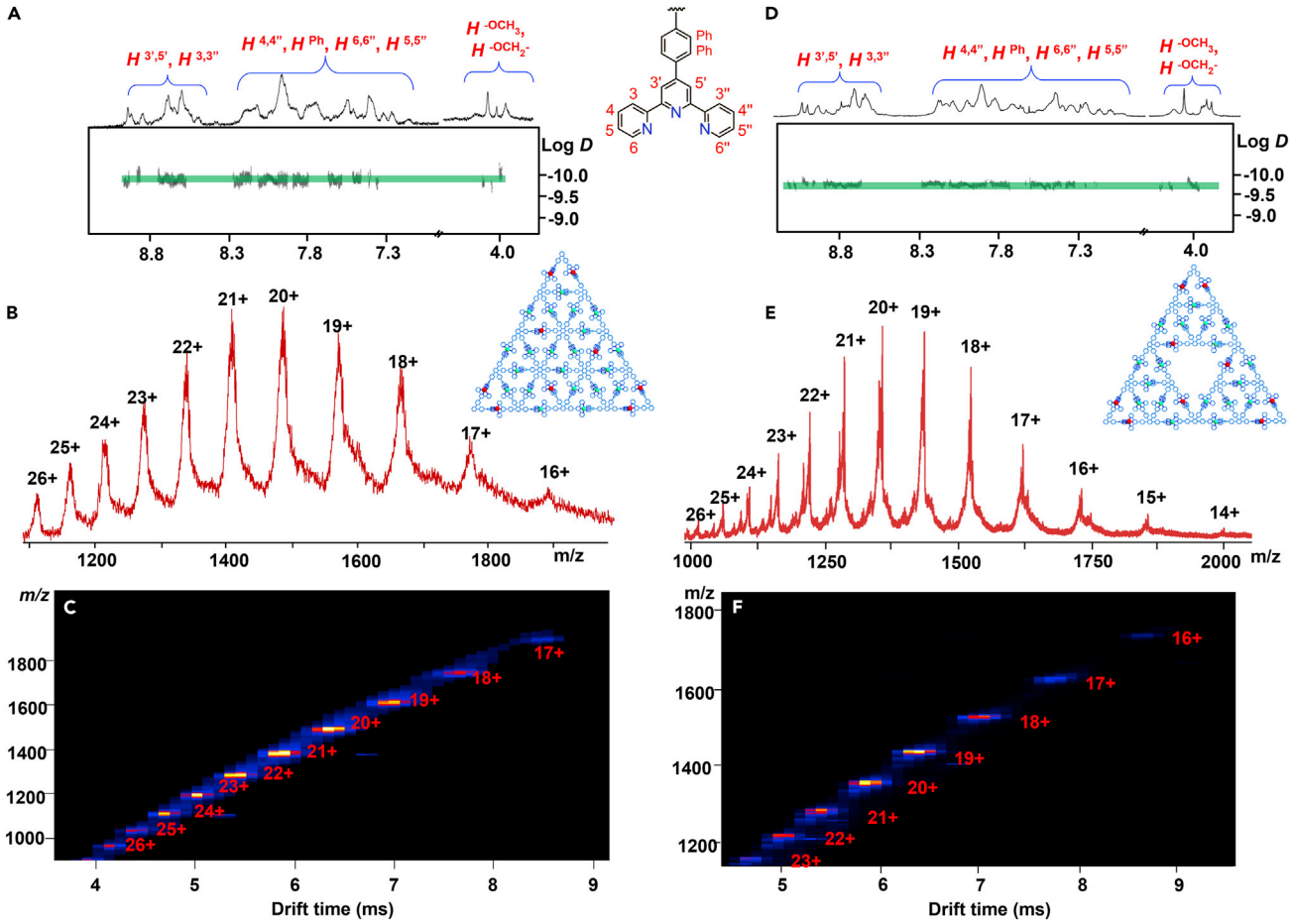

Figure 4. NMR Spectrum and Mass Spectrometry for Pascal's Triangle G3 PT and the Sierpiński Triangle G2 ST

(A) 2D DOSY spectrum (500 MHz, CD_3CN, 298 K) of G3 **PT**.

(B) Electrospray ionization-mass spectrometry (ESI-MS) of G3 **PT**.

(C) Traveling wave ion mobility mass spectrometry (TWIM-MS) of G3 **PT**.

(D) 2D DOSY spectrum (500 MHz, CD_3CN, 298 K) of G2 **ST**.

(E) ESI-MS of G2 **ST**.

(F) TWIM-MS of G2 **ST**.

particular, the diffusion-ordered spectroscopy (DOSY) spectrum of supramolecular G3 **PT** exhibited the only narrow band, confirming a single product was formed (Figure 4A). The observation of diffusion coefficient at 1.22×10^{-10} m^2 s^{-1}, according to the Stokes-Einstein equation (Einstein, 1956), the radius is determined to be 5.1 $\pm$ 0.5 nm, suggested the diameter of the supramolecular G3 **PT** is d = 10.2 $\pm$ 1.0 nm, which is consistent with the data of computer modeling (11.2 nm).

The ESI-MS spectrum of G3 **PT** (Figure 4B) exhibited a series of peaks at m/z 1,898.20, 1,780.04, 1,673.49, 1,577.27, 1,491.28, 1,413.47, 1,342.58, 1,277.56, 1,218.59, 1,164.32, and 1,113.54, with charge states from 16 + to 26 + via the loss of corresponding PF_6 anions. Based on these signals, the molecular weight was calculated to be 32,725.88 Da, and this value was consistent with the theoretical ones (32,722.10 Da) that derived from the assembled composition of G3 **PT**. Unfortunately, the experimental isotopic pattern of each charge state was not obtained, possibly owing to the giant molecular weight beyond resolution of our ESI mass spectrometer, and such giant metallo-architecture may easily encapsulate numbers of solvent molecules owing to the large cavities. Moreover, traveling wave ion mobility mass spectrometry (TWIM-MS) was employed to verify the structural information; only one set of peaks on TWIM-MS excluded the formation of other isomers or conformers (Figure 4C). The valence change of Cd and Ru species was further confirmed by X-ray photoelectron spectroscopy (XPS) data. XPS peaks that appear at 281.1 and 285.3 eV

are characteristic peaks of the Ru^{2+} and those that appear at 405.3 and 412.0 eV are characteristic peaks of the Cd^{2+} centers of G3 **PT** (Figure S59).

Self-Assembly of the Second-Generation Sierpiński Triangle

The self-assembly of G2 **ST** was performed with modules **L2**, **L3**, and Cd^{2+} in a precise stoichiometric 1:1:7 ratio (Figure 3). The structure of G2 **ST** was confirmed by ESI-MS and NMR. The ^{1}H NMR spectrum of G2 **ST** was also inevitably complicated owing to the presence of eighteen different terpyridine units and the slow tumbling motion of large complexes on the NMR timescale. Nevertheless, considerable structural information could be obtained by means of 2D COSY and NOESY NMR spectroscopy (Figures S44–S46). All $tpyH^{6,6''}$ protons from the previously uncomplexed tpy units significantly shifted upfield owing to the electron shielding effects. The DOSY NMR of G2 **ST** that showed a distinct band with the diffusion coefficients at 1.13×10^{-10} m^2 s^{-1} at 298 K indicated the formation of single product (Figure 4D). The diameter of the supramolecular G3 **ST** is also consistent with the result of computer modeling.

Mass spectrometry ESI-MS was primarily applied to characterize the G2 **ST** assembly. ESI-MS spectrum exhibited a series of peaks with charge states from 14 + to 26+, owing to the successive loss of PF_6. These peaks were consistent very well with theoretical values of each charge state (Figure 4E). In addition, the exchange of the anions with PF_6 also played a vital role in ESI-MS determination; the enlarged drawing exhibits two additional +19 ion peaks near $[M\text{-}19PF_6]^{19+}$, which was consistent with $[M\text{-}20PF_6\text{+}NO_3]^{19+}$ and $[M\text{-}21PF_6\text{+}2NO_3]^{19+}$. Such results were caused by an incomplete exchange of PF_6 owing to the large number of exchangeable counter anions (Figure S47). The molecular weight for G2 **ST** was determined to be 30,061.54 Da, which was in accordance with the formula of $[Cd_{18}(C_{244}H_{180}N_{30}O_6Ru_2)_3(C_{189}H_{134}N_{24}O_4Ru)_3]^{54+}$ $(PF_6)^{54}$. When a moderate ESI capillary voltage was applied, peaks with charge states from 12 + to 26+ were observed as a result of incorporating a different number of small solvent molecules (Figures S48 and S49). The TWIM-MS plot of G2 **ST** was obtained that can further serve as a good evidence for the absence of isomers as well as the high structural rigidity of the G2 **ST** (Figure 4F). Similarly, the presence of Cd^{2+} and Ru^{2+} ions was detected after deconvolution of the XPS data (Figure S60).

Transmission Electron Microscopy and Atomic Force Microscopy Analysis

Any attempt to grow X-ray single crystals was unsuccessful. Alternatively, transmission electron microscopy (TEM) and atomic force microscopy (AFM) experiments were done to confirm the size and shape of the G3 **PT** and G2 **ST** (Figure 5). The deposition of G3 **PT** and G2 **ST** was conducted in a dilute ($\sim10^{-6}$ M) MeCN solution on carbon-coated grids (Cu, 400 mesh). From TEM pictures, both architectures were observed to be triangle-shadow patterns and the length of sides were about 11.6 $\pm$ 0.5 nm; the results were in agreement with the optimized molecular models (Figures S62 and S64). Specifically, a few patterns resembling the Star of David were also found in the TEM formed by the stacking of two G2 **ST** triangles (Figure S61), which was also shown for the G1 **ST**. (Sarkar et al., 2014) AFM images of G3 **PT** and G2 **ST** revealed a triangle-shadow morphology by dropping a dilute MeCN solution ($\sim10^{-7}$ M) on the mica surface, which were much larger than those of TEM and the theoretical simulation (Figures S63 and S65). Such results were derived from a tip broadening effect (Radmacher et al., 1994). However, the height of 0.8 $\pm$ 0.2 nm determined by AFM images matched well with energy-minimized (0.8 nm) structure obtained by molecular modeling (Bauer et al., 2011).

The Reversible Gelation Behavior

Notably, the self-assembled triangular architectures G3 **PT** and G2 **ST** were found to form supramolecular hydro-gels in water. By heating the solution of G3 **PT** and G2 **ST** in the mixture solvent of H_2O/CH_3CN (v/v, 10:1) and then cooling to room temperature gave red hydro-gels, respectively. It is interesting that the reversible gel-sol transitions could be realized through temperature stimuli; when the temperature increased, the formed supramolecular hydro-gels gradually turned into solutions, and the gels were able to reform when the temperature cooled down (Figures 6Aa and 6Ab). TEM and SEM (scanning electron microscopy) were employed to investigate the morphologies of the hydro-gel. As shown in Figures 6B–6E, the TEM images of G3 **PT**-based hydro-gel were observed to be nanofiber networks. The similar three-dimensional bulk networks were observed in the SEM images, which displayed the microstructures of the obtained hydro-gels. We expected that the supramolecular hydro-gels were generated owing to the dense-packed counterions of the coordinative and ionic interactions, hydrophobic interactions, solvent effect, $\pi-\pi$ stacking, et al. (Cordier et al., 2008; Li et al., 2014a, 2014b).

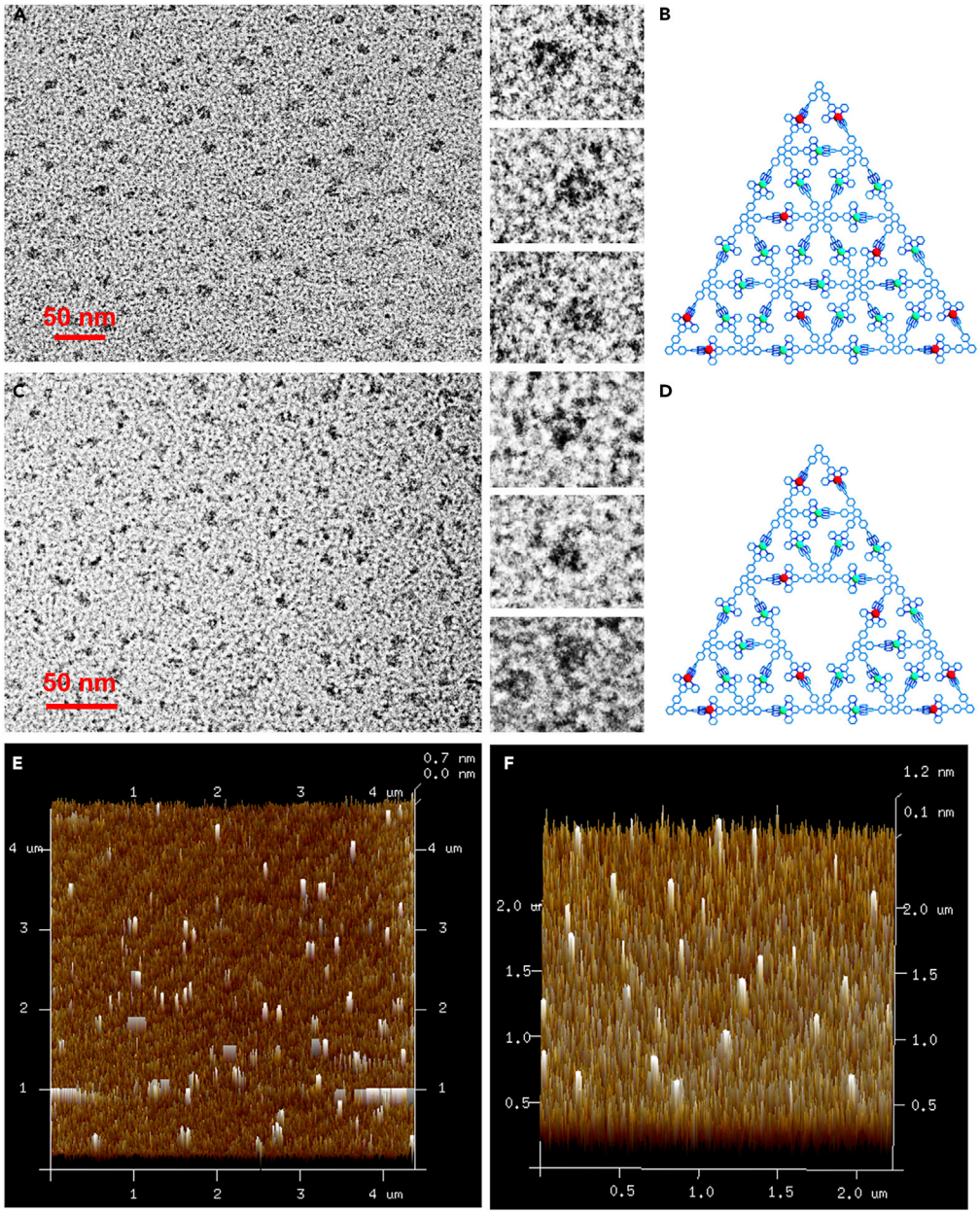

Figure 5. TEM and AFM Images

TEM images of (A) Pascal's triangle G3 **PT** and (C) Sierpiński triangle G2 **ST**.

Representative energy-minimized structures from molecular modeling of (B) G3 **PT** and (D) G2 **ST**.

AFM images of (E) G3 **PT** and (F) G2 **ST**.

The supramolecular hydro-gel properties of the dense-packed counterions in these gigantic triangular assemblies could further promote the application of hydro-gel to adsorb and release water-soluble functional molecules. Take 5-fluorouracil as a representative; upon adding the aqueous solutions of the small molecule into acetonitrile solution of G3 **PT**, similar observation was obtained as described above, red transparent hydro-gel (Figures 6A–6C). The UV-vis spectra of molecule 5-fluorouracil, supramolecular hydro-gel G3 **PT**, and their mixture are shown in Figure 6F. The absorption of 5-fluorouracil in hydro-gel G3 **PT** shows a little difference from 5-fluorouracil with absorbance positions 267 and 263 nm, respectively, suggesting that the 5-fluorouracil was loaded in the hydro-gel. In fact, the latter formed supramolecular hydro-gel also possesses the reversible temperature-responsive gel-sol phase transitions; thus the small

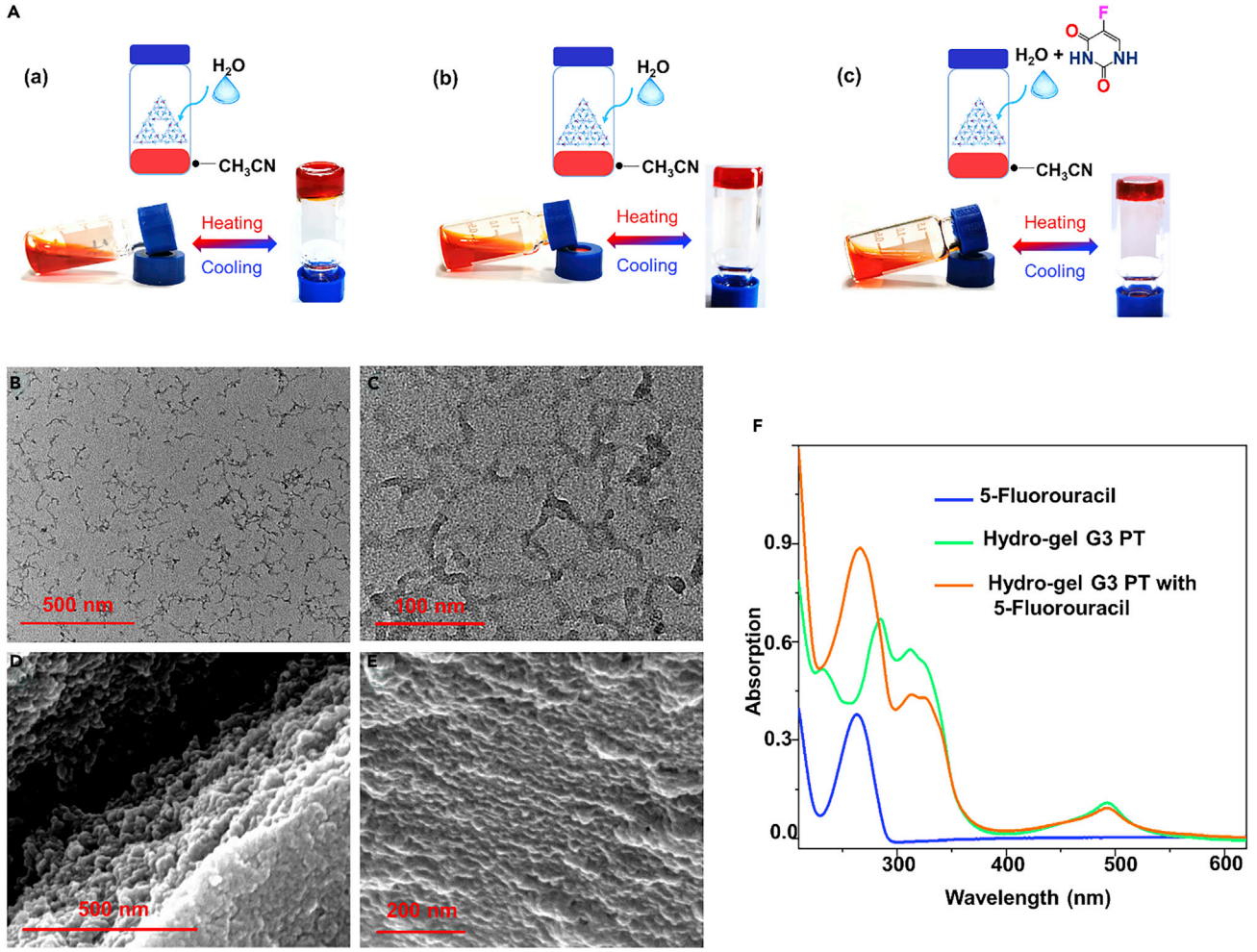

Figure 6. Reversible Gel-Sol Transitions of Supramolecular Hydro-Gels

(A) Photographs of supramolecular hydro-gels formation in H_2O and their thermal reversible gel-sol transitions (a: G2 **ST**, b: G3 **PT**, c: G3 **PT** with 5-fluorouracil).

(B: scale bar 500 nm and C: scale bar 100 nm) TEM images of the solution of supramolecular hydro-gels G3 **PT** in H_2O.

(D: scale bar 500 nm and E: scale bar 200 nm) SEM images of the aggregates of the supramolecular hydro-gels G3 **PT** in H_2O.

(F) UV-vis absorption spectra of 5-fluorouracil, supramolecular hydro-gels G3 **PT,** and supramolecular hydro-gels G3 **PT** with 5-fluorouracil (10^{-5} M) in ethanol.

molecule was able to release in case of heating. The adsorption and release properties of such novel hydro-gels were expected (Chen et al., 2018a, 2018b).

Conclusions

In conclusion, the supramolecular shape-persistent second-generation Sierpiński triangle and third-generation Pascal's triangle fractals were assembled from three metallo-precursors, which were redesigned through a retro-assembly analysis and synthesized via multi-fold Suzuki coupling reactions. The self-assembly of G2 **ST** and G3 **PT** with fractal features was employed by a modular strategy using <tpy-Ru^{2+}-tpy> and <tpy-Cd^{2+}-tpy> connectivity. Compared with one-pot self-assembly, modular strategy showed a highly spontaneous matching and avoided self-sorting as well as formation of oligomers; such predesigned ligands were more likely to form giant 2D architectures by self-assembly. Moreover, these gigantic triangular assemblies with dense-packed counterions and ionic interactions possess reversible gelation properties with potential applications in drug release. This work supports new pathways to design and construct giant discrete shape-persistent supramolecules based on terpyridine ligands or other ligands through retro-

assembly analysis and modular strategy. These simple procedures also open the door to new precise functional nanomaterials by modification of simple directed monomers.

METHODS

All methods can be found in the accompanying Transparent Methods supplemental file.

SUPPLEMENTAL INFORMATION

Supplemental Information can be found online at https://doi.org/10.1016/j.isci.2020.101064.

ACKNOWLEDGMENTS

This research was supported by the National Natural Science Foundation of China (21971257), the Distinguished Professor Research Fund from Guangzhou University, China (to P.W.), project of Guizhou Province Science and Technology, China (QianKeHe Foundation[2018]1146) to Z.J., the Natural Science Foundation of Guangdong Province, China (grant number 2019A1515011358) to Z.Z. Authors acknowledge the NMR, AFM, and TEM measurements from The Modern Analysis and Testing Center of Central South University, China.

AUTHOR CONTRIBUTIONS

Z.J., D.L., M.C., G.R.N., and P.W. designed the research and wrote the paper. Z.J., D.L., and M.C. completed the syntheses. Z.J., D.L., M.C., J.W., H.Z., Y.L., Z.Z., T.X., and F.W. carried out the characterization studies. Z.J., D.L., M.C., G.R.N., and P.W. analyzed the data and wrote the manuscript. All the authors discussed the results and commented and proofread the manuscript.

DECLARATION OF INTERESTS

The authors declare no competing interests.

Received: December 1, 2019
Revised: March 8, 2020
Accepted: April 9, 2020
Published: May 22, 2020

REFERENCES

Bauer, T., Zheng, Z., Renn, A., Enning, R., Stemmer, A., Sakamoto, J., and Schluter, A.D. (2011). Synthesis of free-standing, monolayered organometallic sheets at the air/water interface. Angew. Chem. Int. Ed. *50*, 7879–7884.

Brune, H., Romainczyk, C., Röder, H., and Kern, K. (1994). Mechanism of the transition from fractal to dendritic growth of surface aggregates. Nature *369*, 469–471.

Byrne, K., Zubair, M., Zhu, N., Zhou, X.P., Fox, D.S., Zhang, H., Twamley, B., Lennox, M.J., Duren, T., and Schmitt, W. (2017). Ultra-large supramolecular coordination cages composed of endohedral Archimedean and Platonic bodies. Nat. Commun. *8*, 15268–15277.

Cai, L., Sun, Q., Bao, M., Ma, H., Yuan, C., and Xu, W. (2017). Competition between hydrogen bonds and coordination bonds steered by the surface molecular coverage. ACS Nano *11*, 3727–3732.

Chakrabarty, R., Mukherjee, P.S., and Stang, P.J. (2011). Supramolecular coordination: self-assembly of finite two- and three-dimensional ensembles. Chem. Rev. *111*, 6810–6918.

Chakraborty, S., and Newkome, G.R. (2018). Terpyridine-based metallosupramolecular constructs: tailored monomers to precise 2D-motifs and 3D-metallocages. Chem. Soc. Rev. *47*, 3991–4016.

Chen, M., Wang, J., Wang, S.C., Jiang, Z., Liu, D., Liu, Q., Zhao, H., Yan, J., Chan, Y.T., and Wang, P. (2018a). Truncated sierpinski triangular assembly from a molecular mortise-tenon joint. J. Am. Chem. Soc. *140*, 12168–12174.

Chen, W.-H., Liao, W.-C., Sohn, Y.S., Fadeev, M., Cecconello, A., Nechushtai, R., and Willner, I. (2018b). Stimuli-responsive nucleic acid-based polyacrylamide hydrogel-coated metal–organic framework nanoparticles for controlled drug release. Adv. Funct. Mater. *28*, 1705137.

Chichak, K.S., Cantrill, S.J., Pease, A.R., Chiu, S.H., Cave, G.W., Atwood, J.L., and Stoddart, J.F. (2004). Molecular borromean rings. Science *304*, 1308–1312.

Cordier, P., Tournilhac, F., Soulié-Ziakovic, C., and Leibler, L. (2008). Self-healing and thermoreversible rubber from supramolecular assembly. Nature *451*, 977–980.

Corey, E.J. (1991). The logic of chemical synthesis: multistep synthesis of complex carbogenic molecules (Nobel Lecture). Angew. Chem. Int. Ed. *30*, 455–465.

Cullen, W., Misuraca, M.C., Hunter, C.A., Williams, N.H., and Ward, M.D. (2016). Highly efficient catalysis of the Kemp elimination in the cavity of a cubic coordination cage. Nat. Chem. *8*, 231–236.

Danon, J.J., Krüger, A., Leigh, D.A., Lemonnier, J.F., Stephens, A.J., Vitoricayrezabal, I.J., and Woltering, S.L. (2017). Braiding a molecular knot with eight crossings. Science *355*, 159–162.

De, S., Mahata, K., and Schmittel, M. (2010). Metal-coordination-driven dynamic heteroleptic architectures. Chem. Soc. Rev. *39*, 1555–1575.

Einstein, A. (1956). Investigations on the Theory of Brownian Movement (Dover).

Fujita, D., Ueda, Y., Sato, S., Mizuno, N., Kumasaka, T., and Fujita, M. (2016a). Self-assembly of tetravalent Goldberg polyhedra from 144 small components. Nature *540*, 563–567.

Fujita, D., Ueda, Y., Sato, S., Yokoyama, H., Mizuno, N., Kumasaka, T., and Fujita, M. (2016b). Self-assembly of $M_{30}L_{60}$ icosidodecahedron. Chem *1*, 91–101.

Grayson, S.M., and Fréchet, J.M.J. (2001). Convergent dendrons and Dendrimers: from

synthesis to applications. Chem. Rev. *101*, 3819–3868.

Holliday, B.J., and Mirkin, C.A. (2001). Strategies for the construction of supramolecular compounds through coordination chemistry. Angew. Chem. Int. Ed. *32*, 2022–2043.

Jiang, Z., Li, Y., Wang, M., Liu, D., Yuan, J., Chen, M., Wang, J., Newkome, G.R., Sun, W., Li, X., et al. (2017a). Constructing high-generation Sierpiński triangles by molecular puzzling. Angew. Chem. Int. Ed. *56*, 11450–11455.

Jiang, Z., Li, Y., Wang, M., Song, B., Wang, K., Sun, M., Liu, D., Li, X., Yuan, J., Chen, M., et al. (2017b). Self-assembly of a supramolecular hexagram and a supramolecular pentagram. Nat. Commun. *8*, 15476–15484.

Kempkes, S.N., Slot, M.R., Freeney, S.E., Zevenhuizen, S.J.M., Vanmaekelbergh, D., Swart, I., and Smith, C.M. (2018). Design and characterization of electrons in a fractal geometry. Nat. Phys. *15*, 127–131.

Lehn, J.M. (1985). Supramolecular Chemistry: Concepts and Perspectives (VCH).

Li, K., Zhang, L.Y., Yan, C., Wei, S.C., Pan, M., Zhang, L., and Su, C.Y. (2014a). Stepwise assembly of Pd(6)(RuL(3))(8) nanoscale rhombododecahedral metal-organic cages via metalloligand strategy for guest trapping and protection. J. Am. Chem. Soc. *136*, 4456–4459.

Li, Z.Y., Zhang, Y., Zhang, C.W., Chen, L.J., Wang, C., Tan, H., Yu, Y., Li, X., and Yang, H.B. (2014b). Cross-linked supramolecular polymer gels constructed from discrete multi-pillar[5]arene metallacycles and their multiple stimuli-responsive behavior. J. Am. Chem. Soc. *136*, 8577–8589.

Li, C., Zhang, X., Li, N., Wang, Y., Yang, J., Gu, G., Zhang, Y., Hou, S., Peng, L., Wu, K., et al. (2017). Construction of Sierpiński triangles up to the fifth order. J. Am. Chem. Soc. *139*, 13749–13753.

Lu, Y., Deng, Y.-X., Lin, Y.-J., Han, Y.-F., Weng, L.-H., Li, Z.-H., and Jin, G.-X. (2017). Molecular borromean rings based on dihalogenated ligands. Chem *3*, 110–121.

Mandelbrot, B.B. (1982). The Fractal Geometry of Nature (W. H. Freeman and Company).

Mo, Y., Chen, T., Dai, J., Wu, K., and Wang, D. (2019). On-surface synthesis of highly ordered covalent Sierpiński triangle fractals. J. Am. Chem. Soc. *141*, 11378–11382.

Newkome, G.R., and Moorefield, C.N. (2015). From 1–> 3 dendritic designs to fractal supramacromolecular constructs: understanding the pathway to the Sierpinski gasket. Chem. Soc. Rev. *44*, 3954–3967.

Newkome, G.R., Wang, P., Moorefield, C.N., Cho, T.J., Mohapatra, P.P., Li, S., Hwang, S.H., Lukoyanova, O., Echegoyen, L., Palagallo, J.A., et al. (2006). Nanoassembly of a fractal polymer: a molecular "Sierpinski hexagonal gasket. Science *312*, 1782–1785.

Nieckarz, D., and Szabelski, P. (2016). Chiral and fractal: from simple design rules to complex supramolecular constructs. Chem. Commun. (Camb.) *52*, 11642–11645.

Peitgen, H.O., Jürgens, H., and Saupe, D. (1992). Chaos and Fractals: New Frontiers of Science (Springer-Verlag).

Qiang, S., Liangliang, C., Honghong, M., Chunxue, Y., and Wei, X. (2015). On-surface construction of a metal-organic Sierpiński triangle. Chem. Commun. (Camb.) *51*, 14164–14166.

Radmacher, M., Fritz, M., Hansma, H.G., and Hansm, P.K. (1994). Direct observation of enzyme activity with the atomic force microscope. Science *265*, 1577–1579.

Rastgoo-Lahrood, A., Martsinovich, N., Lischka, M., Eichhorn, J., Szabelski, P., Nieckarz, D., Strunskus, T., Das, K., Schmittel, M., Heckl, W.M., et al. (2016). From Au–thiolate chains to thioether Sierpiński triangles: the versatile surface chemistry of 1,3,5-Tris(4-mercaptophenyl) benzene on Au(111). ACS Nano *10*, 10901–10911.

Ronson, T.K., Meng, W., and Nitschke, J.R. (2017). Design principles for the optimization of guest binding in aromatic-paneled $Fe(II)_4L_6$ cages. J. Am. Chem. Soc. *139*, 9698–9707.

Rousseaux, S.A., Gong, J.Q., Haver, R., Odell, B., Claridge, T.D., Herz, L.M., and Anderson, H.L. (2015). Self-assembly of Russian doll concentric porphyrin nanorings. J. Am. Chem. Soc. *137*, 12713–12718.

Safont-Sempere, M.M., Fernandez, G., and Wurthner, F. (2011). Self-sorting phenomena in complex supramolecular systems. Chem. Rev. *111*, 5784–5814.

Sarkar, R., Guo, K., Moorefield, C.N., Saunders, M.J., Wesdemiotis, C., and Newkome, G.R. (2014). One-step multicomponent self-assembly of a first-generation Sierpinski triangle: from fractal design to chemical reality. Angew. Chem. Int. Ed. *53*, 12182–12185.

Schultz, A., Cao, Y., Huang, M., Cheng, S.Z., Li, X., Moorefield, C.N., Wesdemiotis, C., and Newkome, G.R. (2012). Stable, trinuclear Zn(II)- and Cd(II)-metallocycles: TWIM-MS, photophysical properties, and nanofiber formation. Dalton Trans. *41*, 11573–11575.

Shang, J., Wang, Y., Chen, M., Dai, J., Zhou, X., Kuttner, J., Hilt, G., Shao, X., Gottfried, J.M., and Wu, K. (2015). Assembling molecular Sierpiński triangle fractals. Nat. Chem. *7*, 389–393.

Sierpinski, W. (1916). Sur une courbe cantorienne qui contient une image biunivoquet et continue detoute courbe donnée. C R. Acad. Paris *162*, 629–632.

Sugiura, K.-i., Tanaka, H., Matsumoto, T., Kawai, T., and Sakata, Y. (1999). A mandala-patterned bandanna-shaped porphyrin oligomer, $C_{1244}H_{135}0N_{84}Ni_{20}O_{88}$, having a unique size and geometry. Chem. Lett. *28*, 1193–1194.

Sun, Q.F., Iwasa, J., Ogawa, D., Ishido, Y., Sato, S., Ozeki, T., Sei, Y., Yamaguchi, K., and Fujita, M. (2010). Self-assembled M24L48 polyhedra and their sharp structural switch upon subtle ligand variation. Science *328*, 1144–1147.

Swiegers, G.F., and Malefetse, T.J. (2000). New self-assembled structural motifs in coordination chemistry. Chem. Rev. *100*, 3483–3538.

Wang, M., Wang, C., Hao, X.Q., Liu, J., Li, X., Xu, C., Lopez, A., Sun, L., Song, M.P., Yang, H.B., et al. (2014). Hexagon wreaths: self-assembly of discrete supramolecular fractal architectures using multitopic terpyridine ligands. J. Am. Chem. Soc. *136*, 6664–6671.

Wang, W., Chen, L.J., Wang, X.Q., Sun, B., Li, X., Zhang, Y., Shi, J., Yu, Y., Zhang, L., Liu, M., et al. (2015). Organometallic rotaxane dendrimers with fourth-generation mechanically interlocked branches. Proc. Natl. Acad. Sci. U S A *112*, 5597–5601.

Wang, L., Liu, R., Gu, J., Song, B., Wang, H., Jiang, X., Zhang, K., Han, X., Hao, X.Q., Bai, S., et al. (2018). Self-assembly of supramolecular fractals from generation 1 to 5. J. Am. Chem. Soc. *140*, 14087–14096.

Wolfram, S. (1984). Geometry of binomial coefficients. Am. Math. Mon *91*, 566–571.

Wu, T., Yuan, J., Song, B., Chen, Y.S., Chen, M., Xue, X., Liu, Q., Wang, J., Chan, Y.T., and Wang, P. (2017). Stepwise self-assembly of a discrete molecular honeycomb using a multitopic metallo-organic ligand. Chem. Commun. (Camb.) *53*, 6732–6735.

Yam, V.W., Au, V.K., and Leung, S.Y. (2015). Light-emitting self-assembled materials based on d(8) and d(10) transition metal complexes. Chem. Rev. *115*, 7589–7728.

Zhang, X., Li, N., Gu, G.C., Wang, H., Nieckarz, D., Szabelski, P., He, Y., Wang, Y., Xie, C., and Shen, Z. (2015). Controlling molecular growth between fractals and crystals on surfaces. ACS Nano *9*, 11909–11915.

iScience, Volume *23*

Supplemental Information

Assembling Shape-Persistent High-Order Sierpiński Triangular Fractals

Zhilong Jiang, Die Liu, Mingzhao Chen, Jun Wang, He Zhao, Yiming Li, Zhe Zhang, Tingzheng Xie, Feng Wang, Xiaopeng Li, George R. Newkome, and Pingshan Wang

Supporting Information

Assembling shape-persistent high-order Sierpiński triangle fractals

Zhilong Jiang, Die Liu, Mingzhao Chen, Jun Wang, He Zhao, Yiming Li, Zhe Zhang, Tingzheng Xie, Feng Wang, Xiaopeng Li, George R. Newkome and Pingshan Wang

The Pascal triangle and Sierpiński Triangle pattern

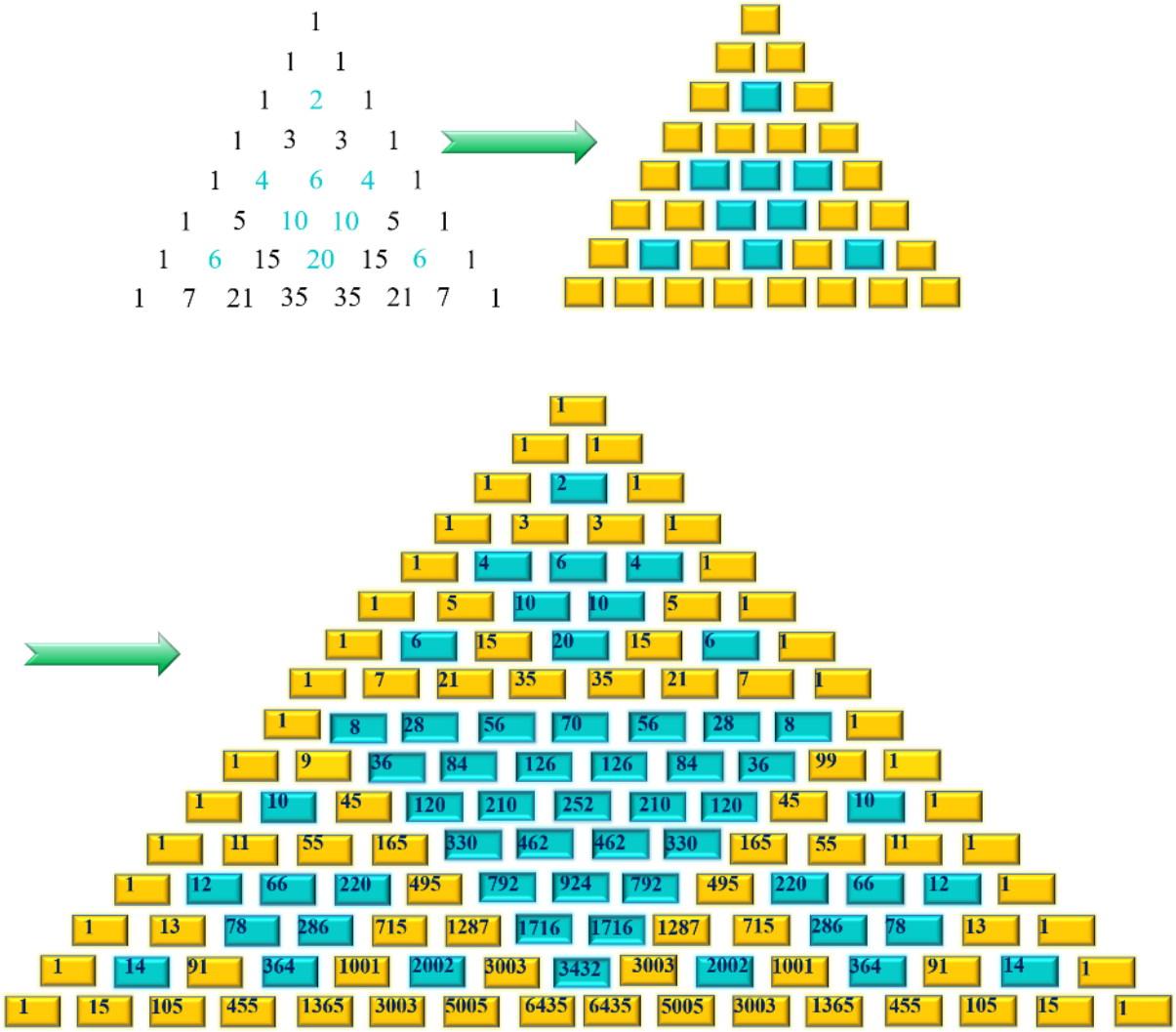

Figure S1. Mathematical triangular array of the binomial coefficients (yellow rectangles indicate the odd numbers and blue rectangles indicate the even numbers). Related to Figure 1.

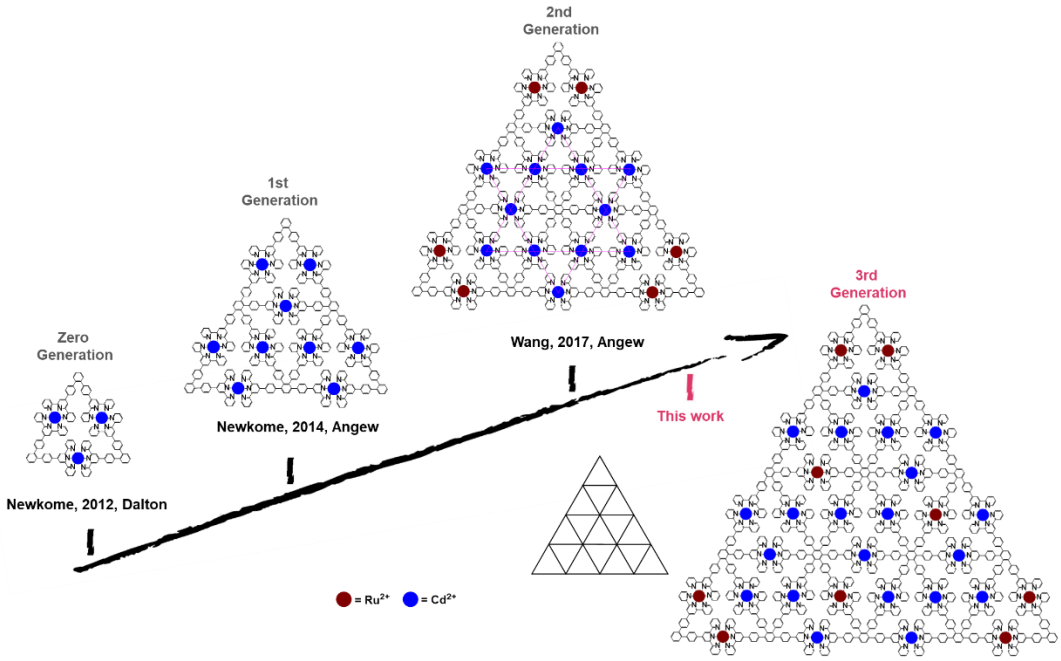

Figure S2. The whole family of the synthesized molecular PTs. Related to Figure 2.

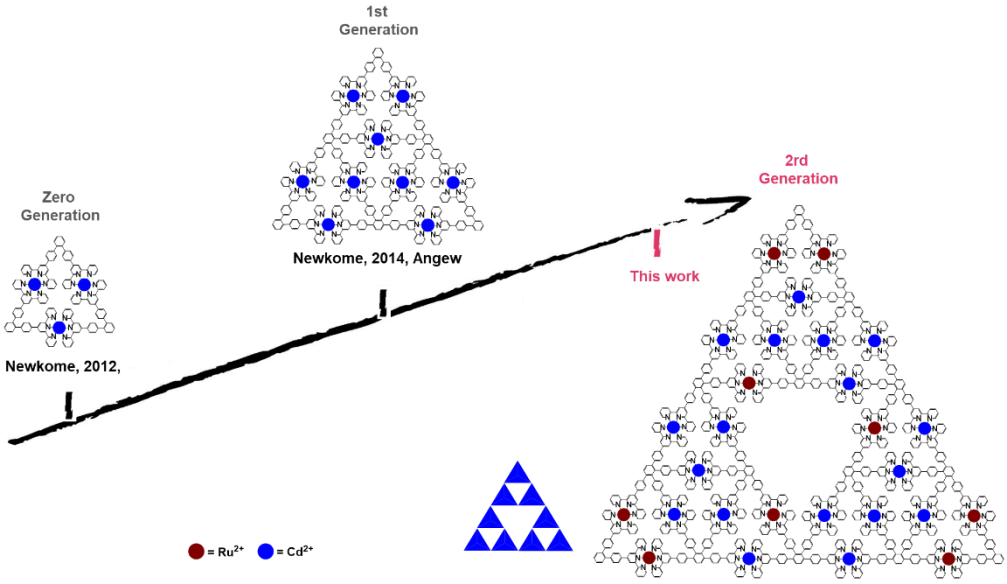

Figure S3. The whole family of the synthesized molecular STs. Related to Figure 2.

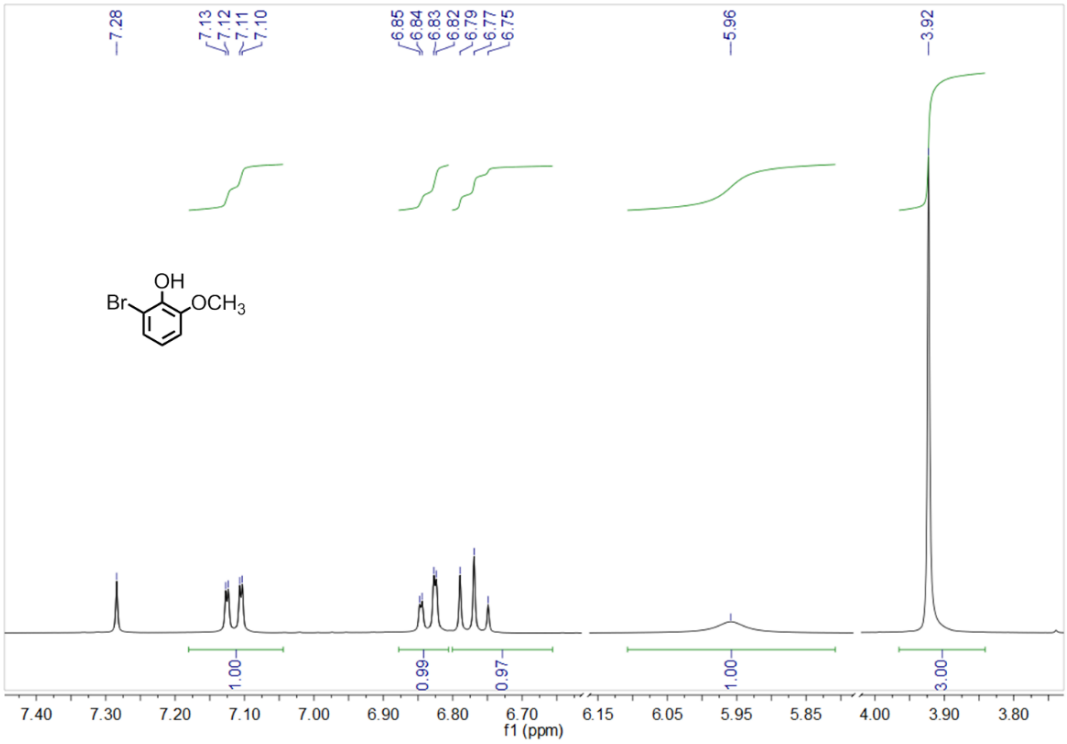

Figure S4. The ^{1}H NMR spectrum of **S2** (400 MHz) in $CDCl_3$. Related to Figure 2.

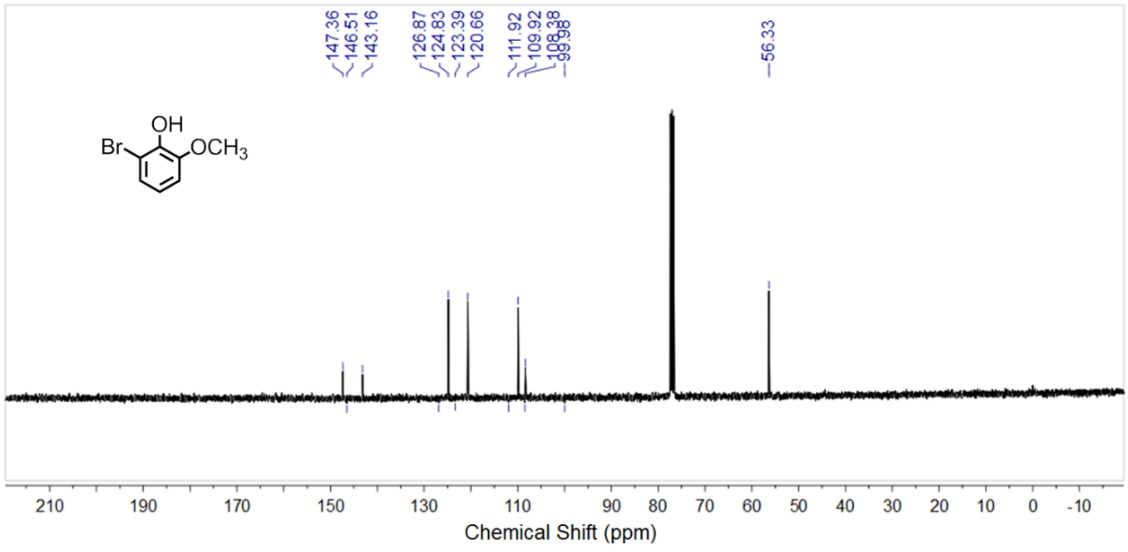

Figure S5. The ^{13}C NMR spectrum of **S2** (101 MHz) in $CDCl_3$. Related to Figure 2.

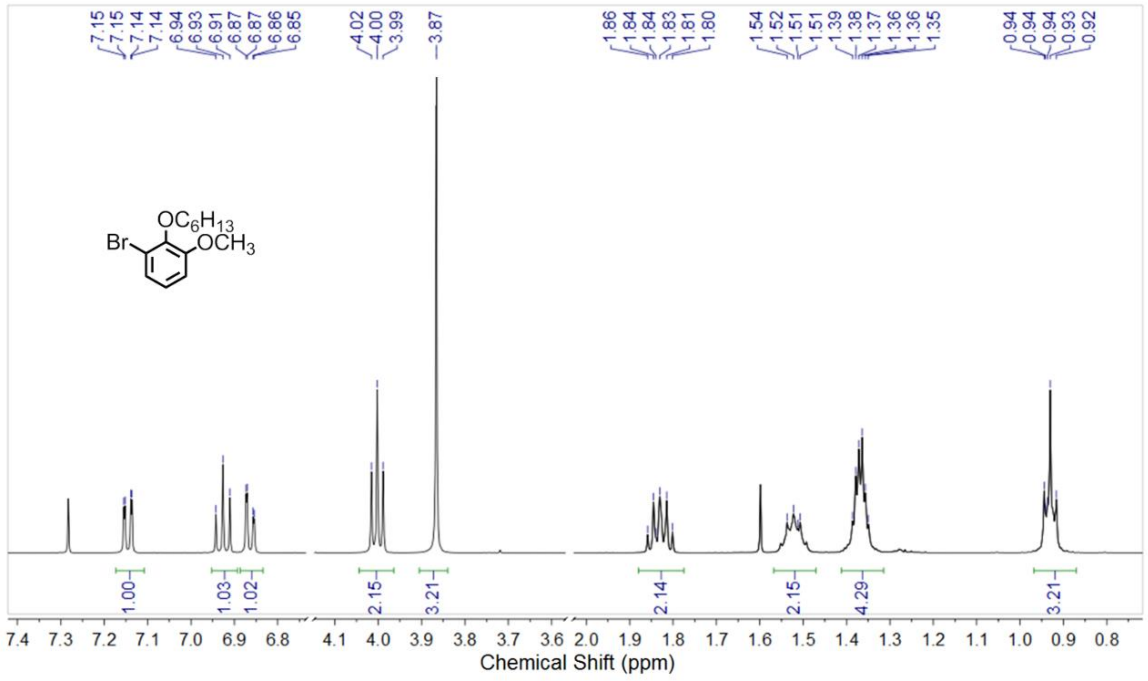

Figure S6. The ^{1}H NMR spectrum of **S3** (500 MHz) in $CDCl_3$. Related to Figure 2.

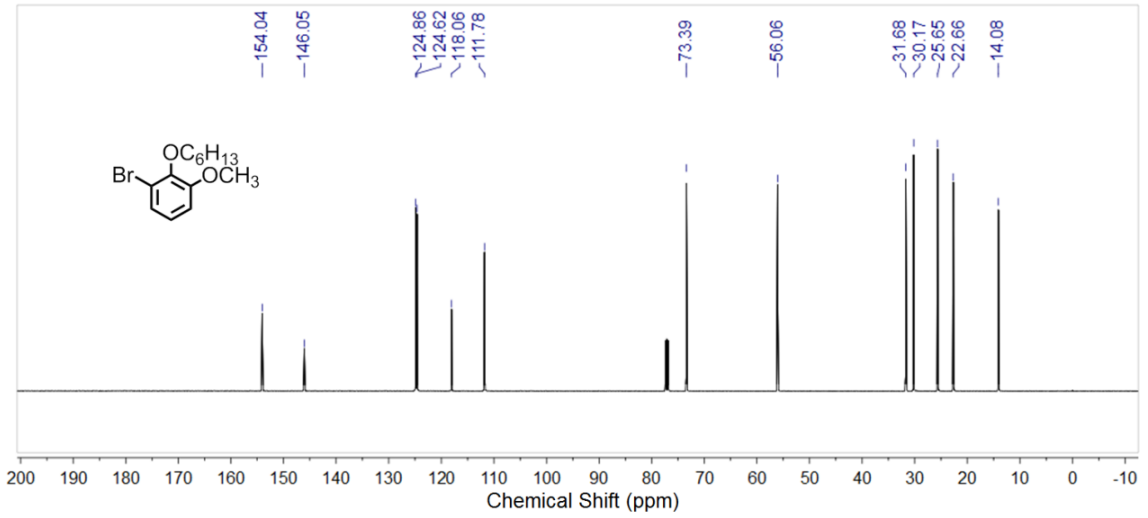

Figure S7. The ^{13}C NMR spectrum of **S3** (126 MHz) in $CDCl_3$. Related to Figure 2.

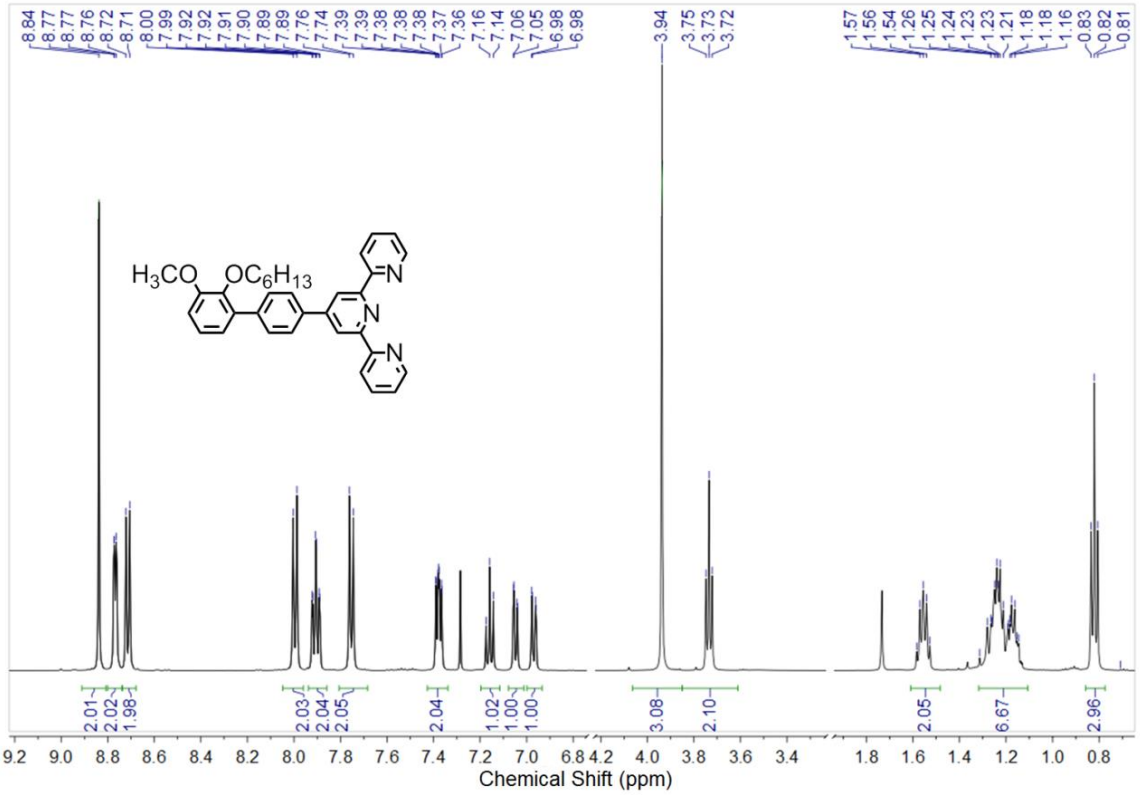

Figure S8. The ^{1}H NMR spectrum of **S4** (500 MHz) in $CDCl_3$. Related to Figure 2.

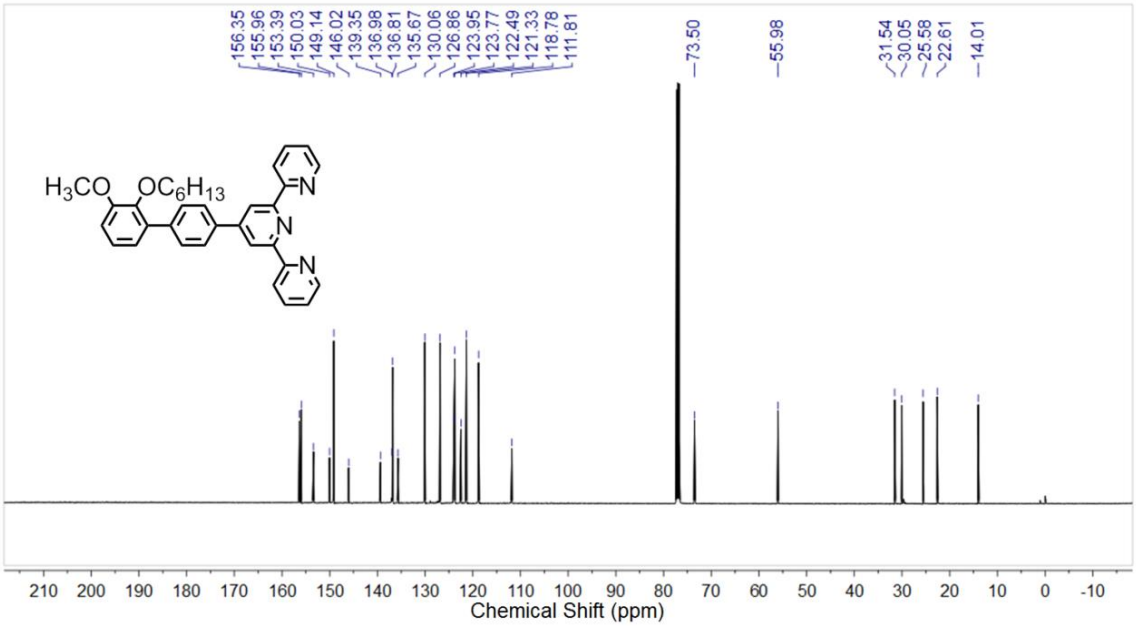

Figure S9. The ^{13}C NMR spectrum of **S4** (126 MHz) in $CDCl_3$. Related to Figure 2.

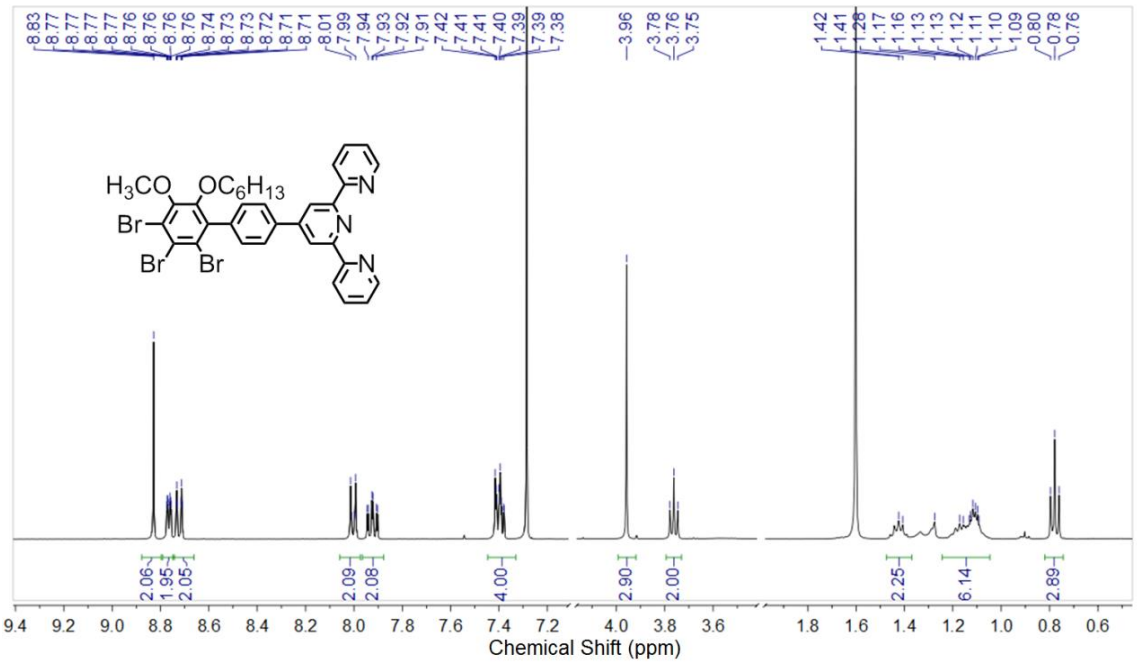

Figure S10. The ^{1}H NMR spectrum of **S5** (400 MHz) in $CDCl_3$. Related to Figure 2.

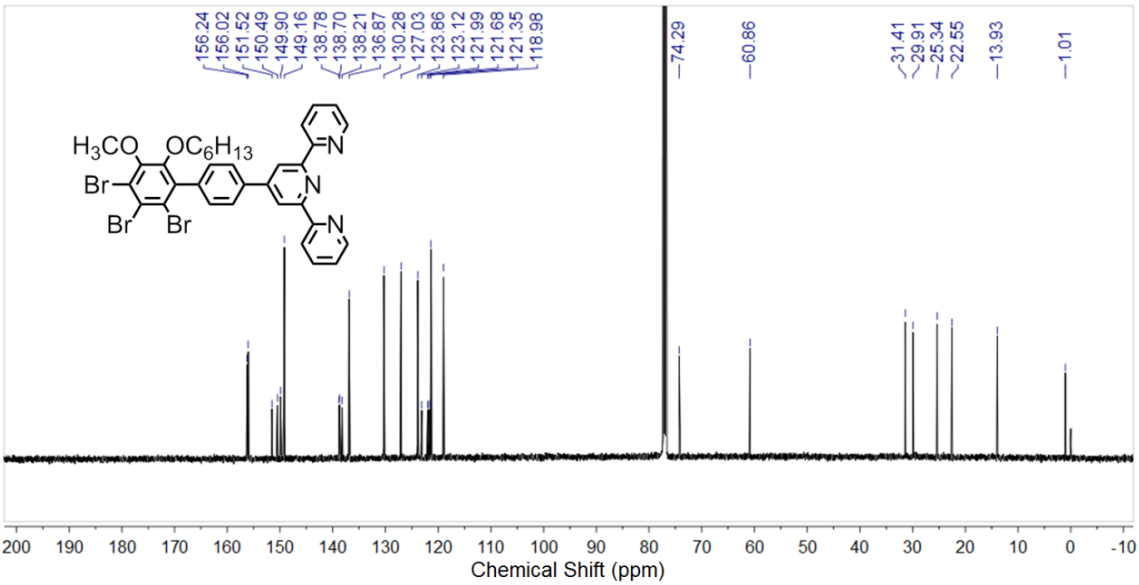

Figure S11. The ^{13}C NMR spectrum of **S5** (126 MHz) in $CDCl_3$. Related to Figure 2.

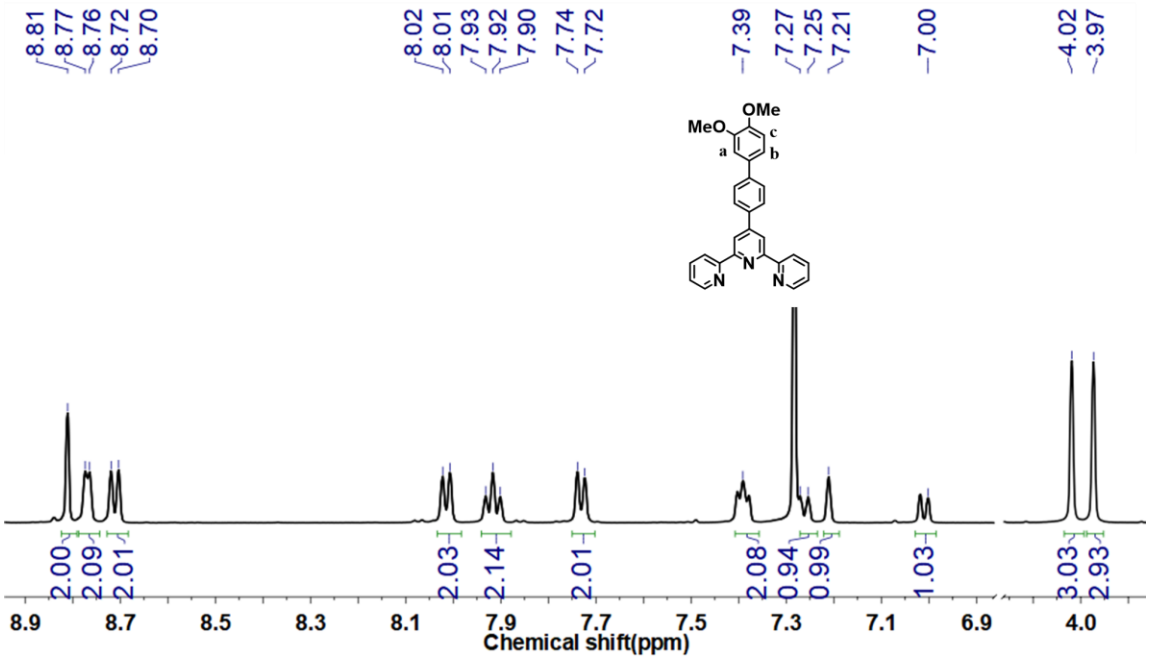

Figure S12. The ^{1}H NMR spectrum of **S7** (500 MHz) in $CDCl_3$. Related to Figure 2.

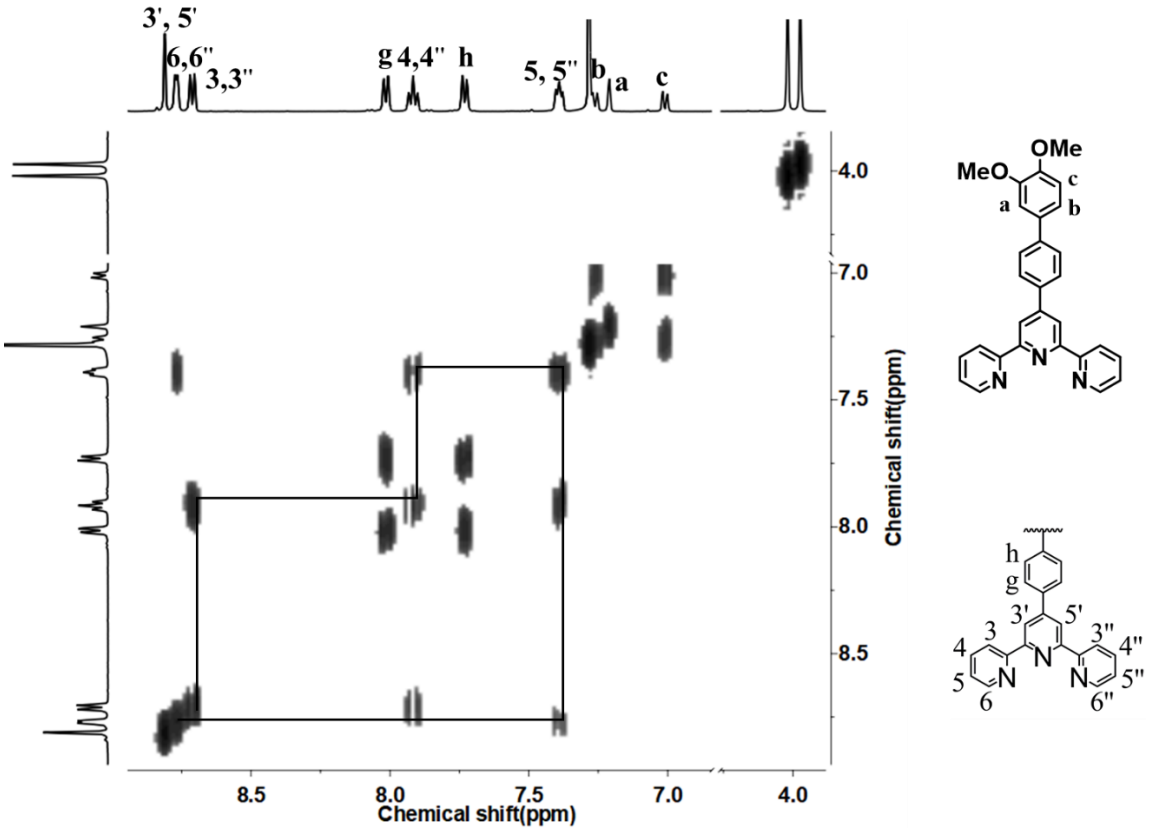

Figure S13. The 2D-COSY spectrum of **S7**(500 MHz) in $CDCl_3$. Related to Figure 2.

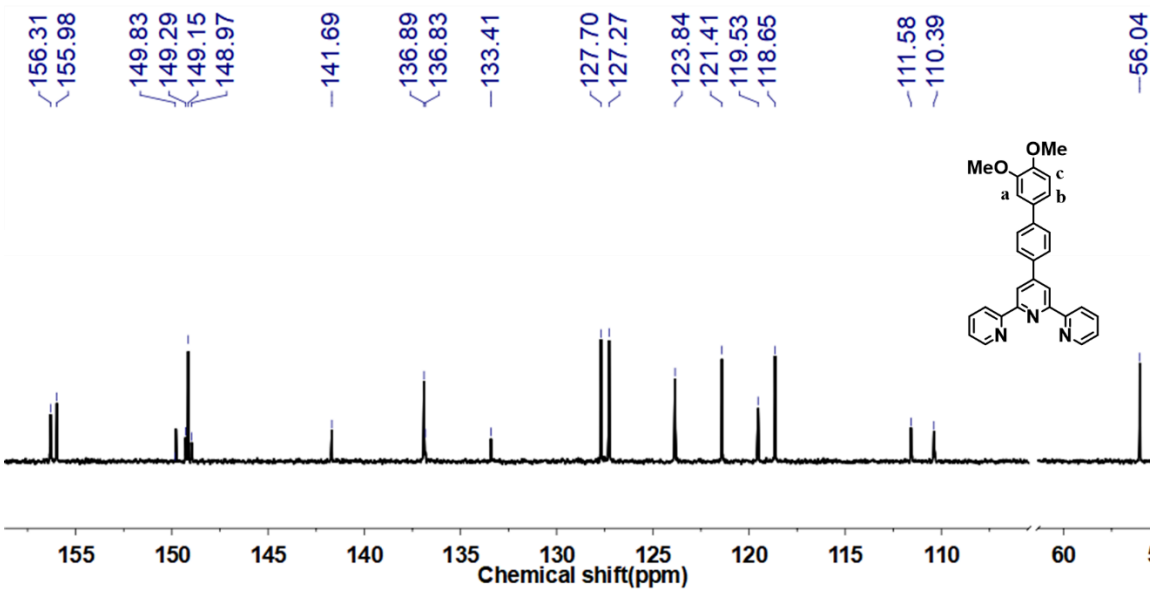

Figure S14. The ^{13}C NMR spectrum of **S7** (126 MHz) in $CDCl_3$. Related to Figure 2.

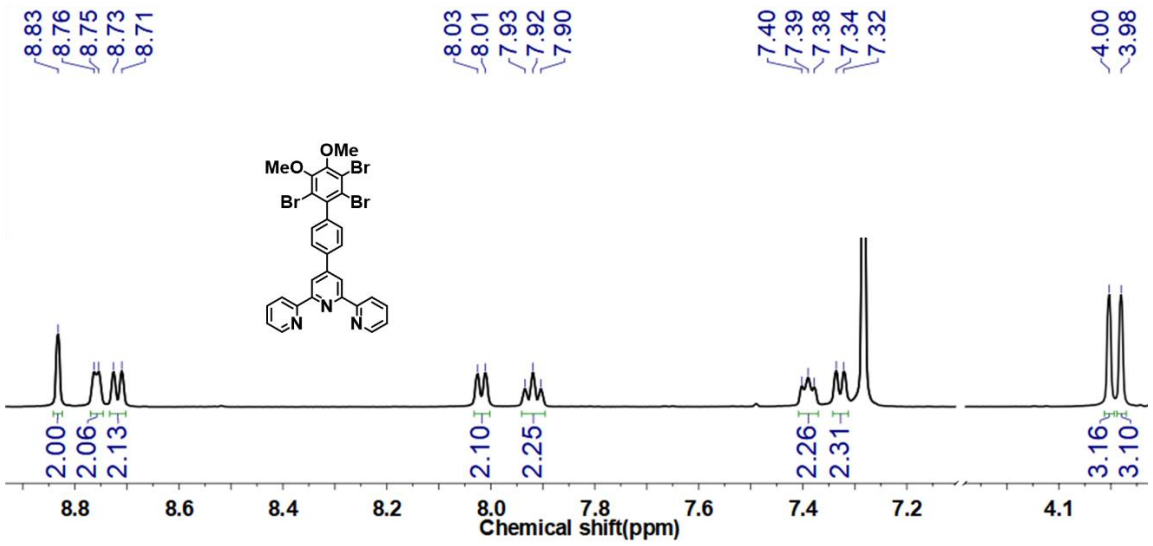

Figure S15. The ^{1}H NMR spectrum of **S8** (500 MHz) in $CDCl_3$. Related to Figure 2.

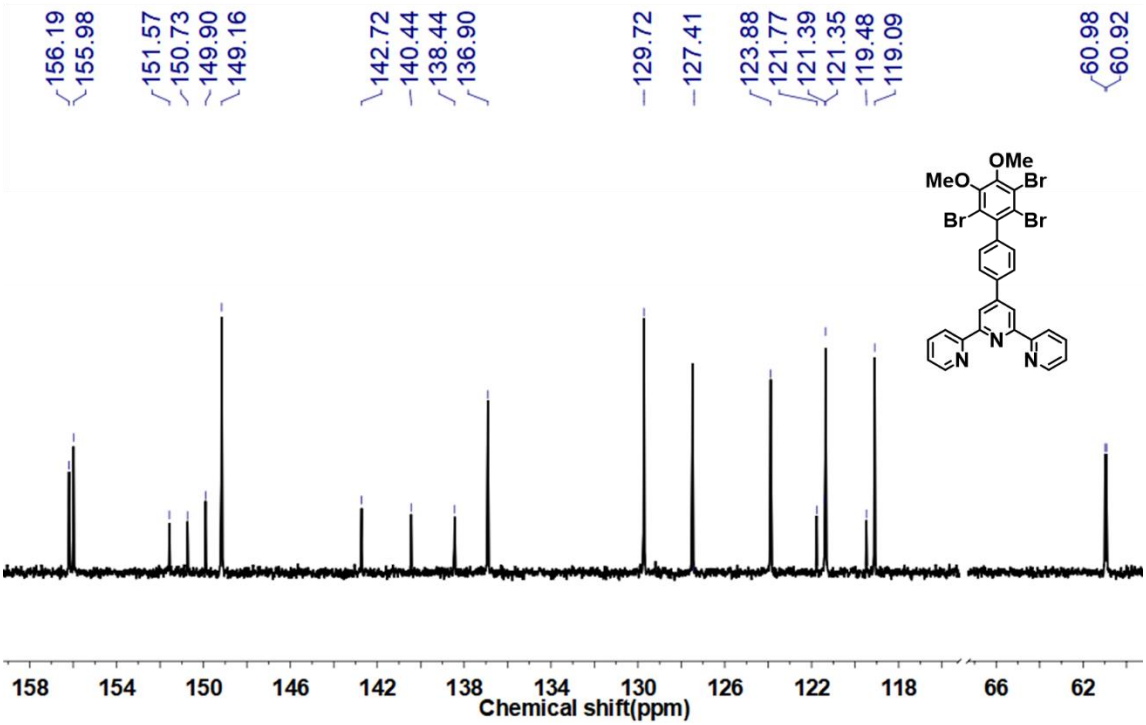

Figure S16. The ^{13}C NMR spectrum of **S8** (126 MHz) in $CDCl_3$. Related to Figure 2.

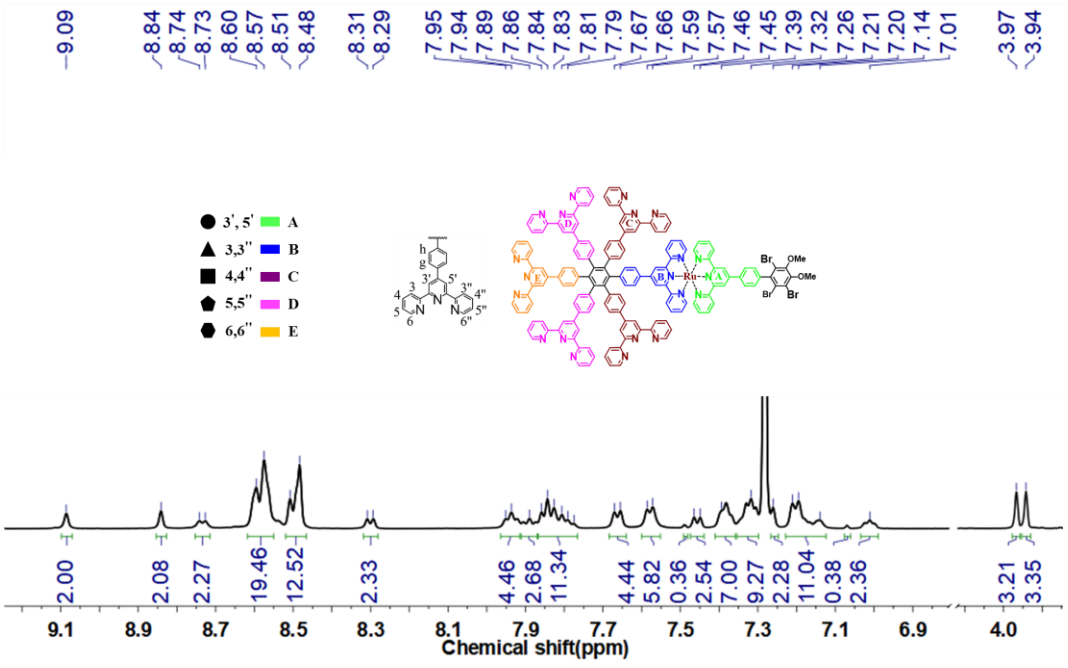

Figure S17. The ^{1}H NMR spectrum of **B1** (500 MHz) in $CDCl_3$. Related to Figure 2.

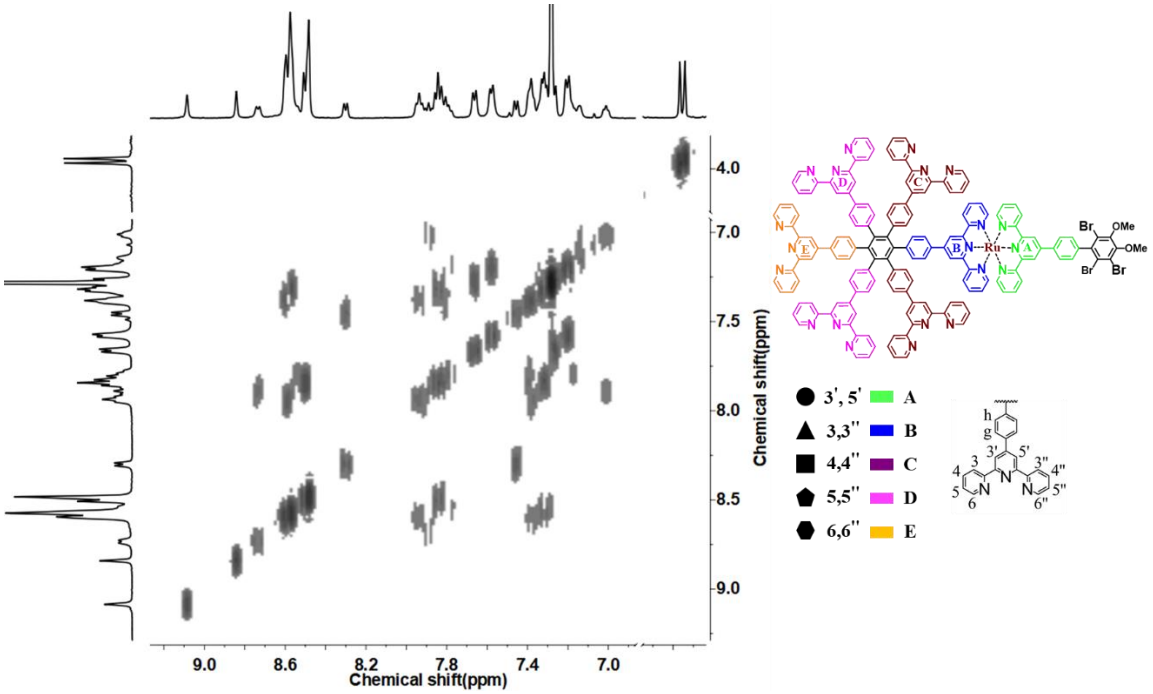

Figure S18. The 2D-COSY spectrum of **B1** (500 MHz) in $CDCl_3$. Related to Figure 2.

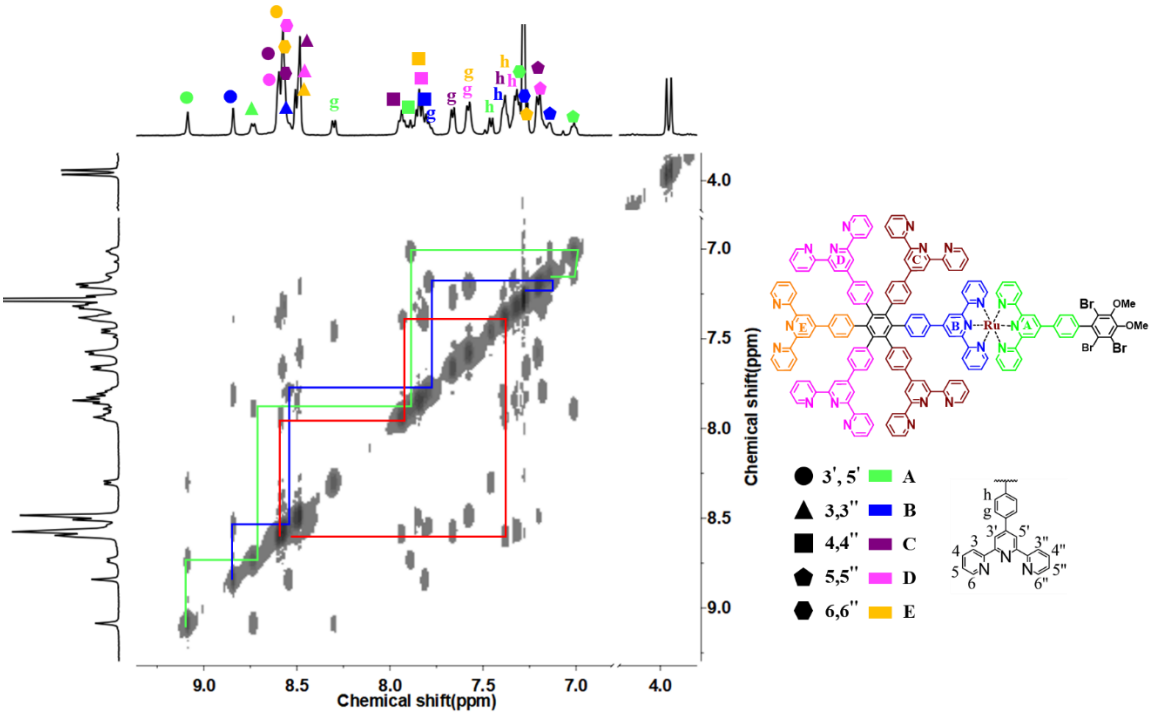

Figure S19. The 2D-NOESY spectrum of **B1** (500 MHz) in $CDCl_3$. Related to Figure 2.

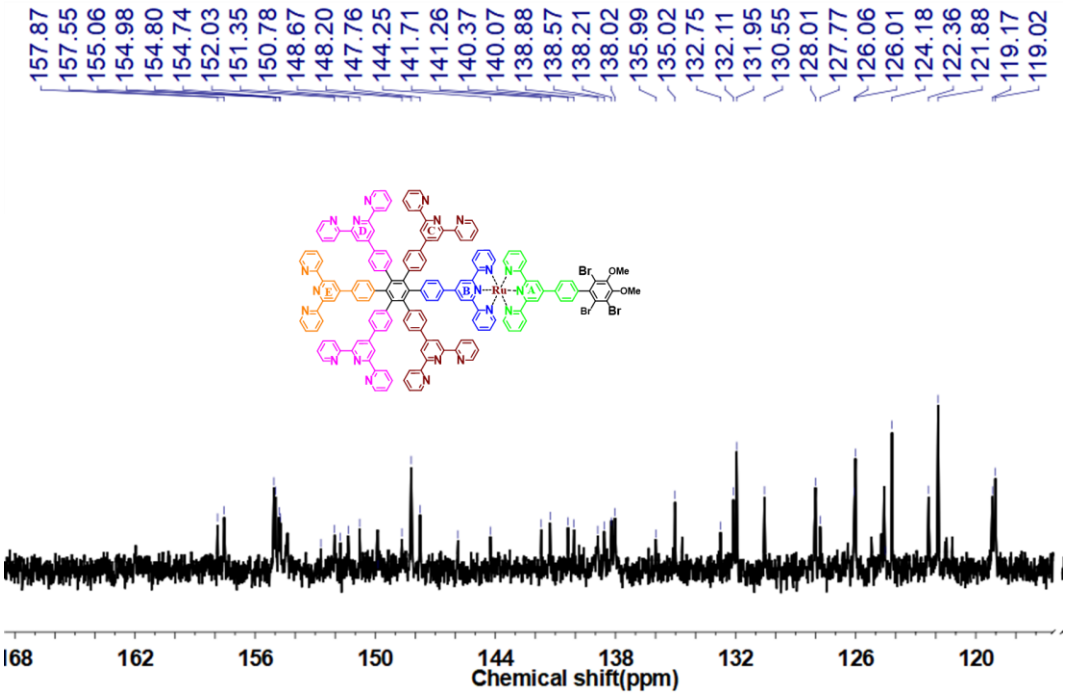

Figure S20. The ^{13}C NMR spectrum of **B1** (126 MHz) in $CDCl_3$. Related to Figure 2.

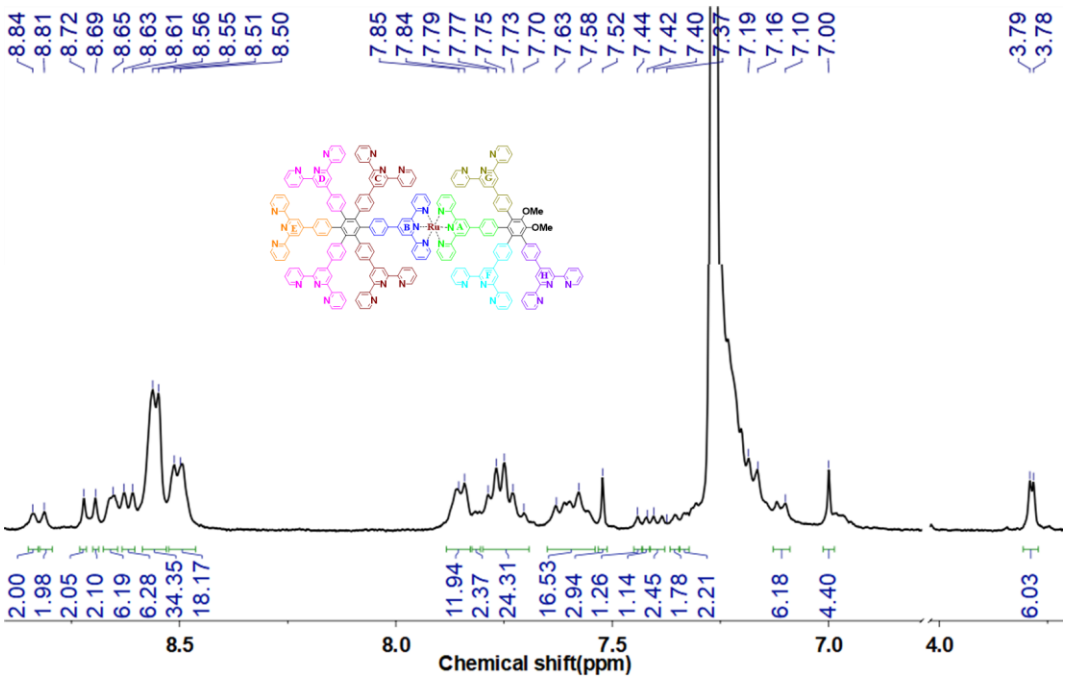

Figure S21. The ^{1}H NMR spectrum of **L1** (400 MHz) in $CDCl_3$. Related to Figure 2.

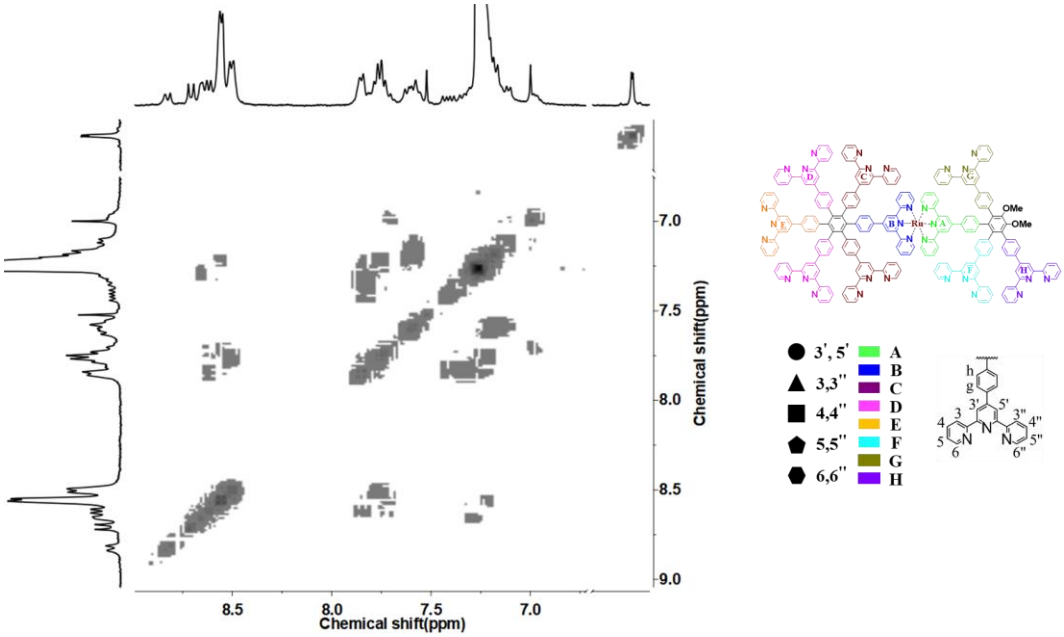

Figure S22. The 2D-COSY spectrum of **L1** (400 MHz) in $CDCl_3$. Related to Figure 2.

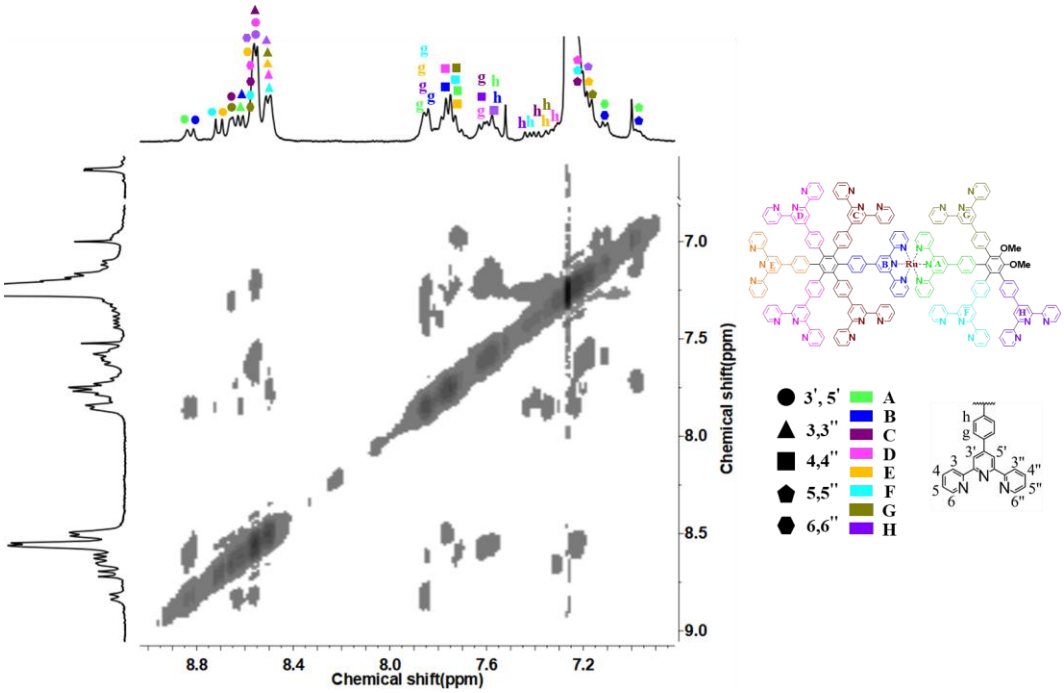

Figure S23. The 2D-NOESY spectrum of **L1** (400 MHz) in $CDCl_3$. Related to Figure 2.

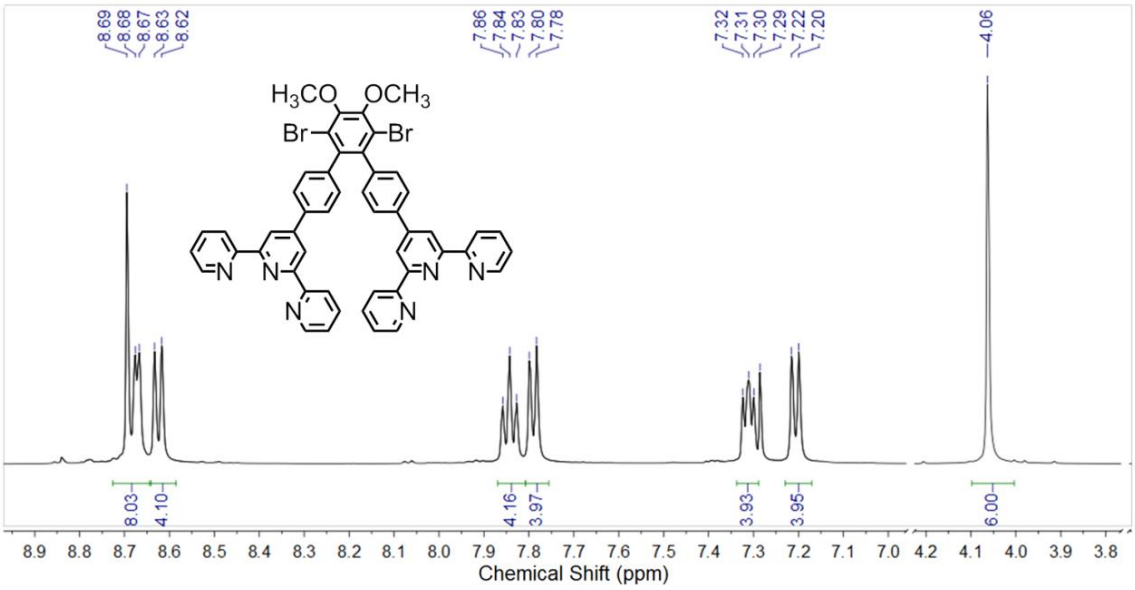

Figure S24. ^{1}H NMR spectrum of **S11** (500 MHz) in $CDCl_3$. Related to Figure 2.

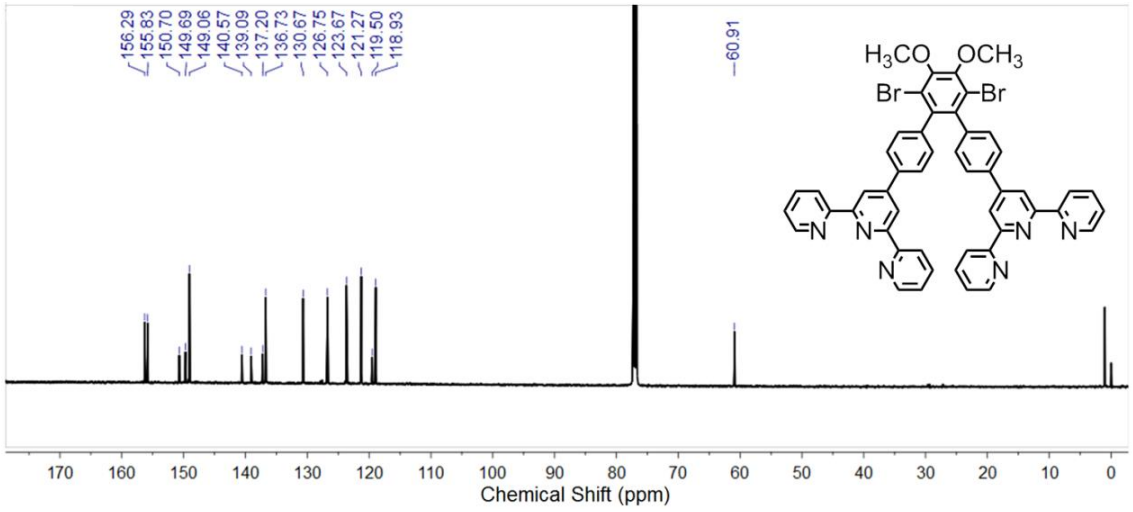

Figure S25. ^{13}C NMR spectrum of **S11** (126 MHz) in $CDCl_3$. Related to Figure 2.

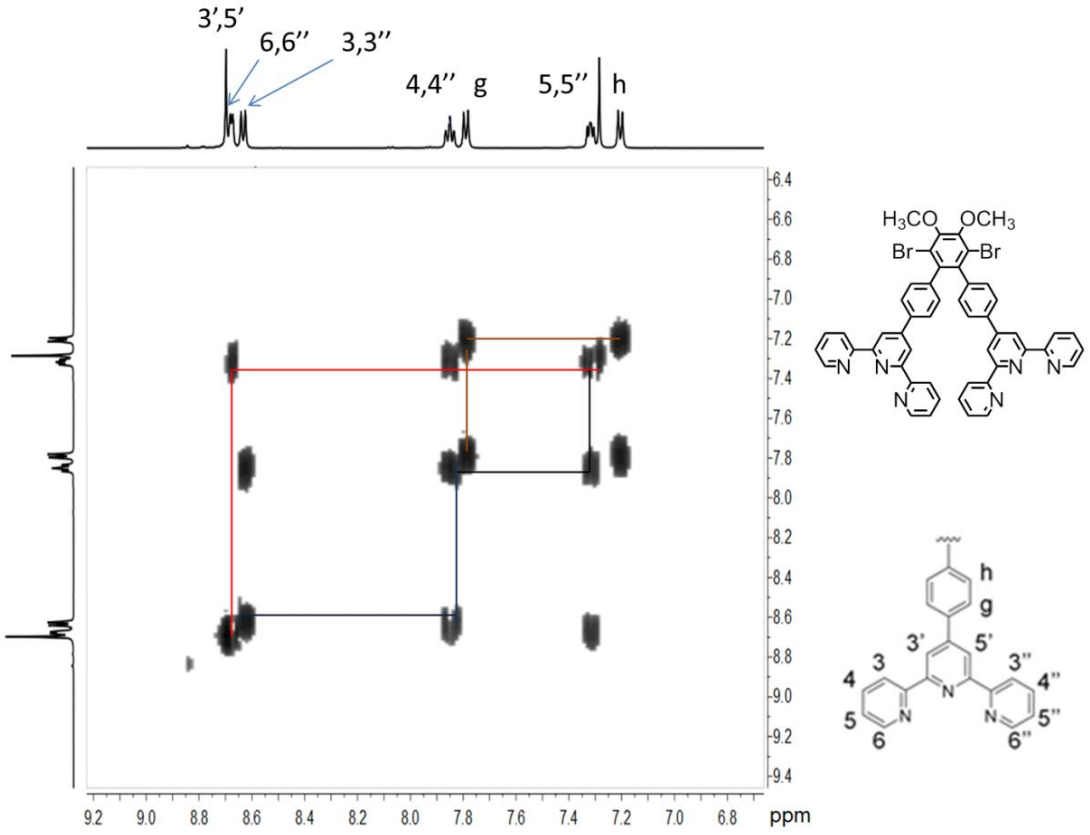

Figure S26. The 2D-COSY spectrum of **S11** (500 MHz) in $CDCl_3$. Related to Figure 2.

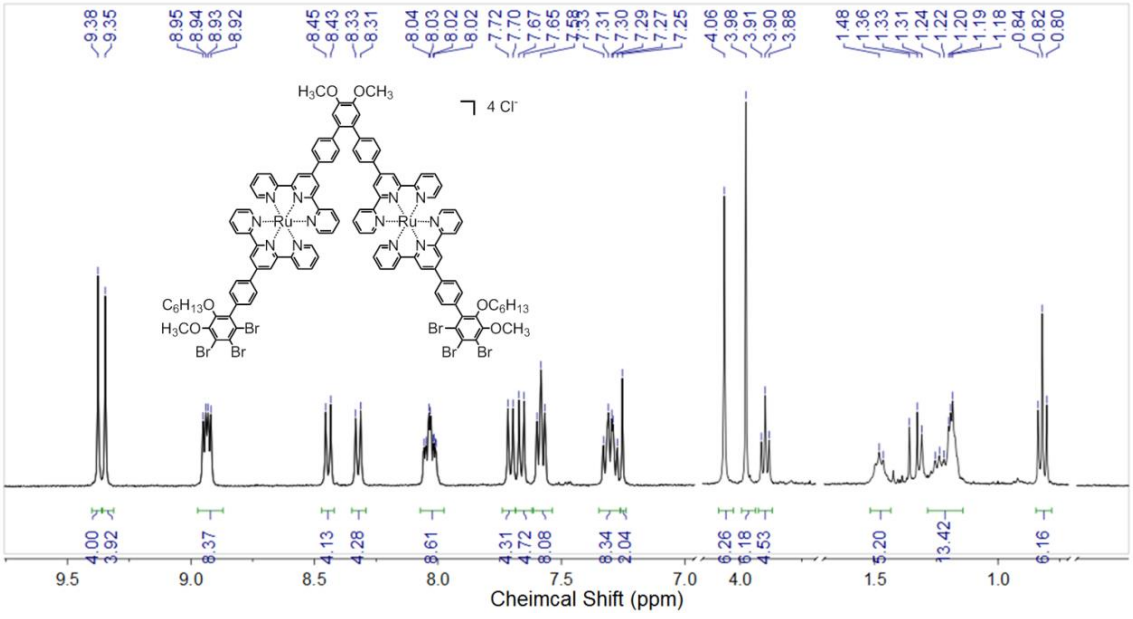

Figure S27. ^1H NMR spectrum of **B2** (400 MHz) in CD_3CN. Related to Figure 2.

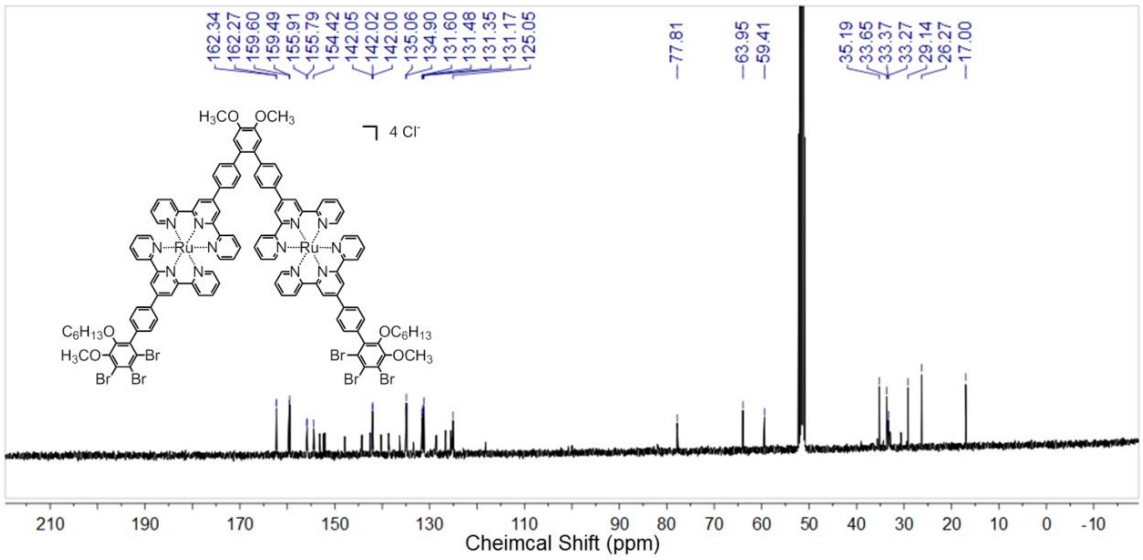

Figure S28. The ^{13}C NMR spectrum of **B2** (101 MHz) in CD_3CN. Related to Figure 2.

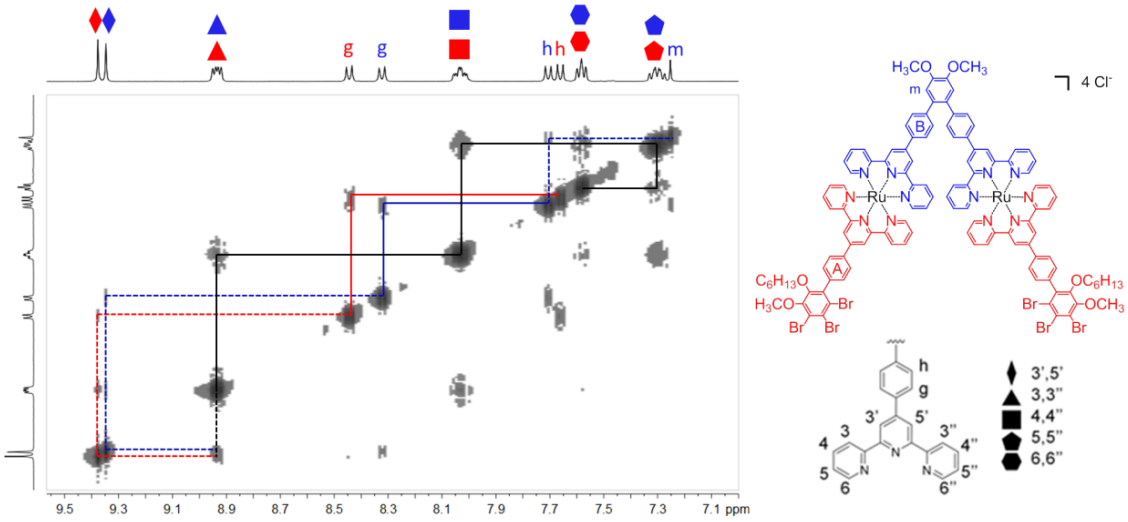

Figure S29. The NOESY spectrum of **B2** (500 MHz) in CD_3CN. Related to Figure 2.

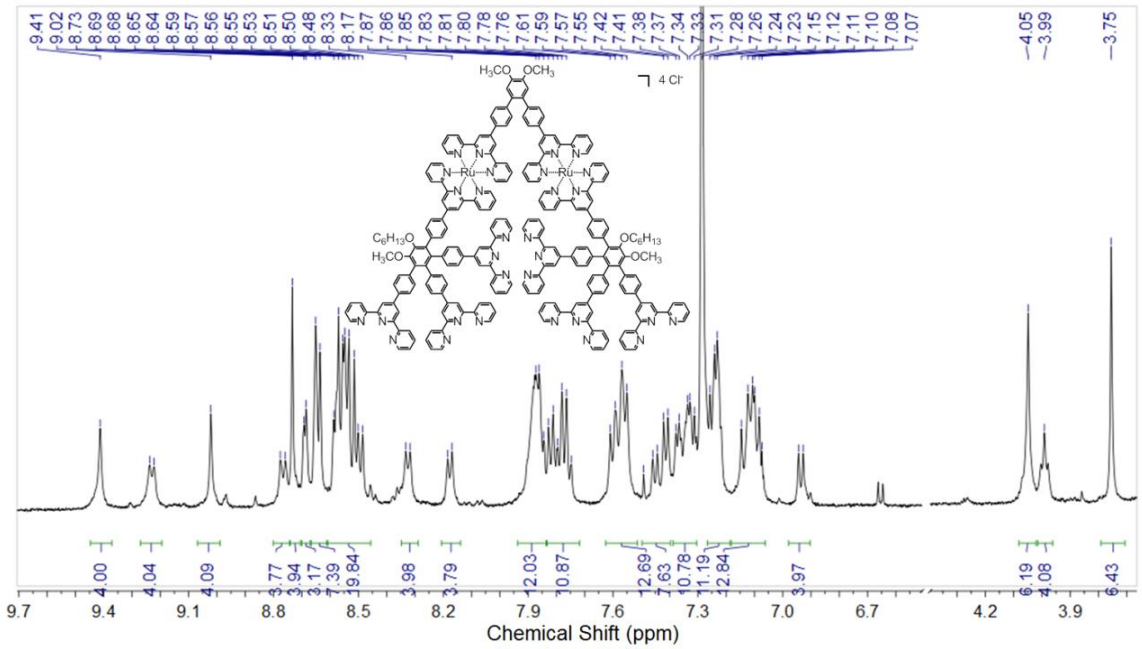

Figure S30. The ^{1}H NMR spectrum of **L2** (500 MHz) in CD_3CN. Related to Figure 2.

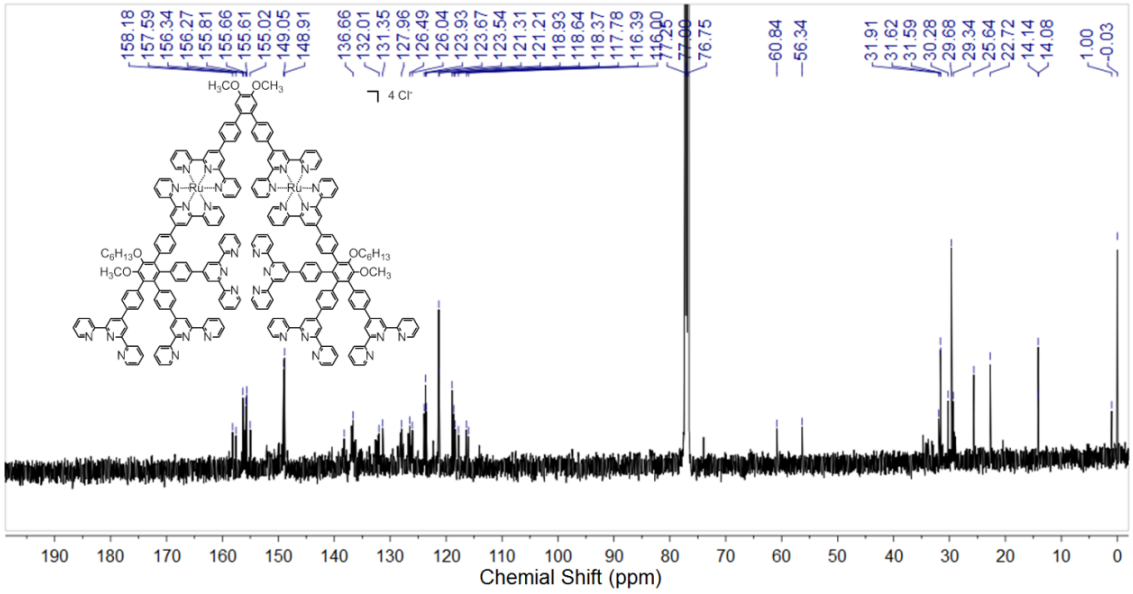

Figure S31. The ^{13}C NMR spectrum of **L2** (126 MHz) in CD_3CN. Related to Figure 2.

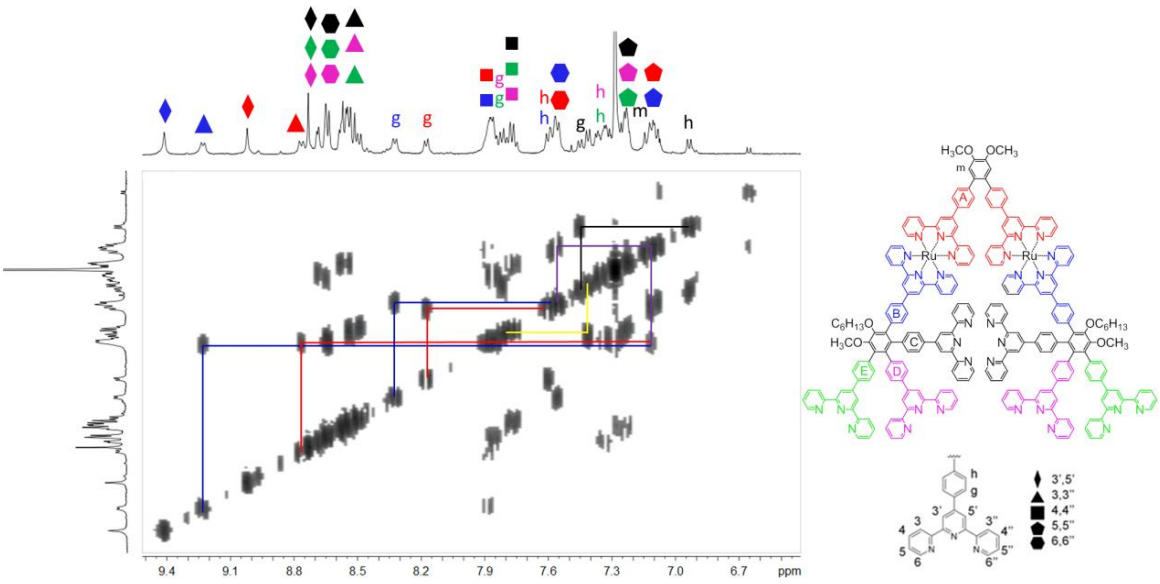

Figure S32. The 2D-COSY spectrum of **L2** (500 MHz) in CD_3CN. Related to Figure 2.

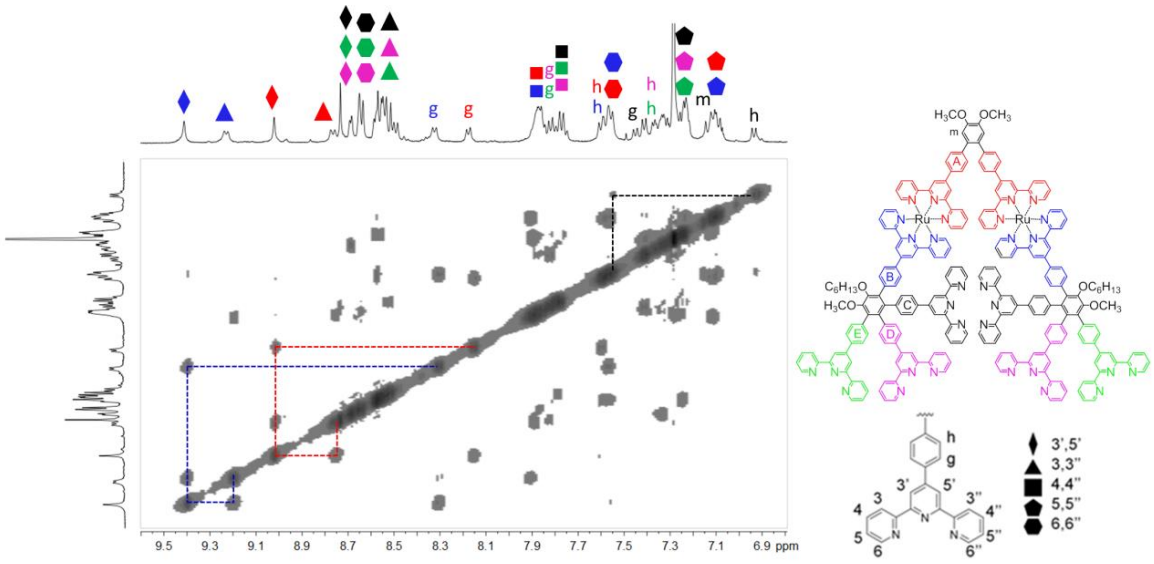

Figure S33. The NOESY spectrum of **L2** (500 MHz) in CD_3CN. Related to Figure 2.

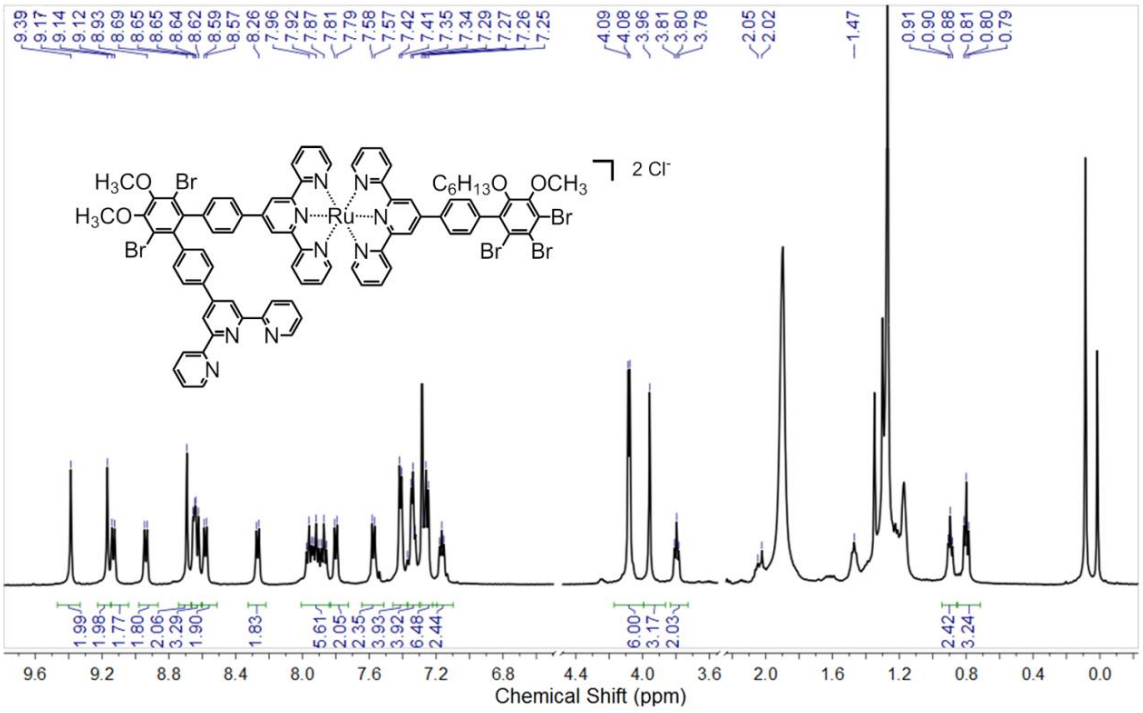

Figure S34. The ^{13}C NMR spectrum of **B3** (500 MHz) in $CDCl_3$. Related to Figure 2.

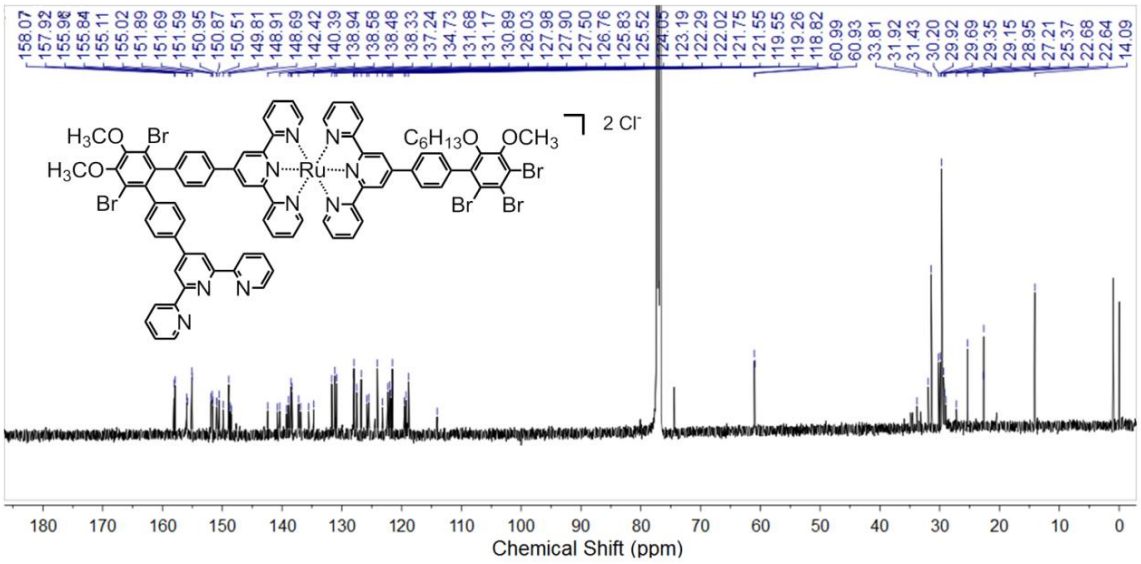

Figure S35. The ^{1}H NMR spectrum of **B3** (126 MHz) in $CDCl_3$. Related to Figure 2.

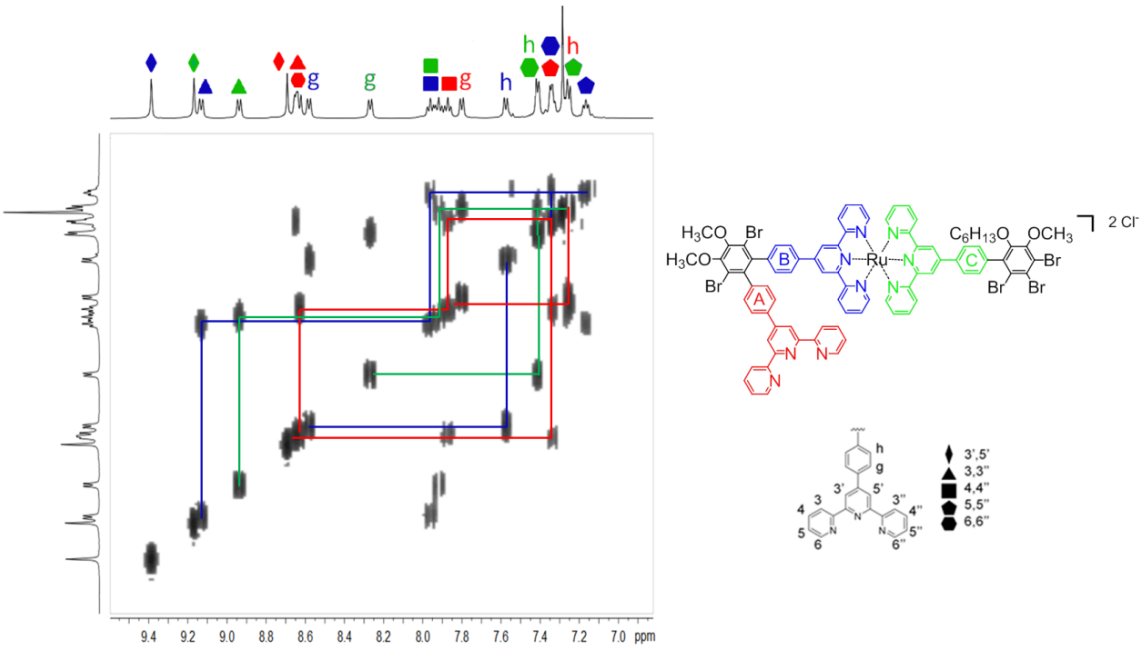

Figure S36. The COSY spectrum of **B3** (500 MHz) in $CDCl_3$. Related to Figure 2.

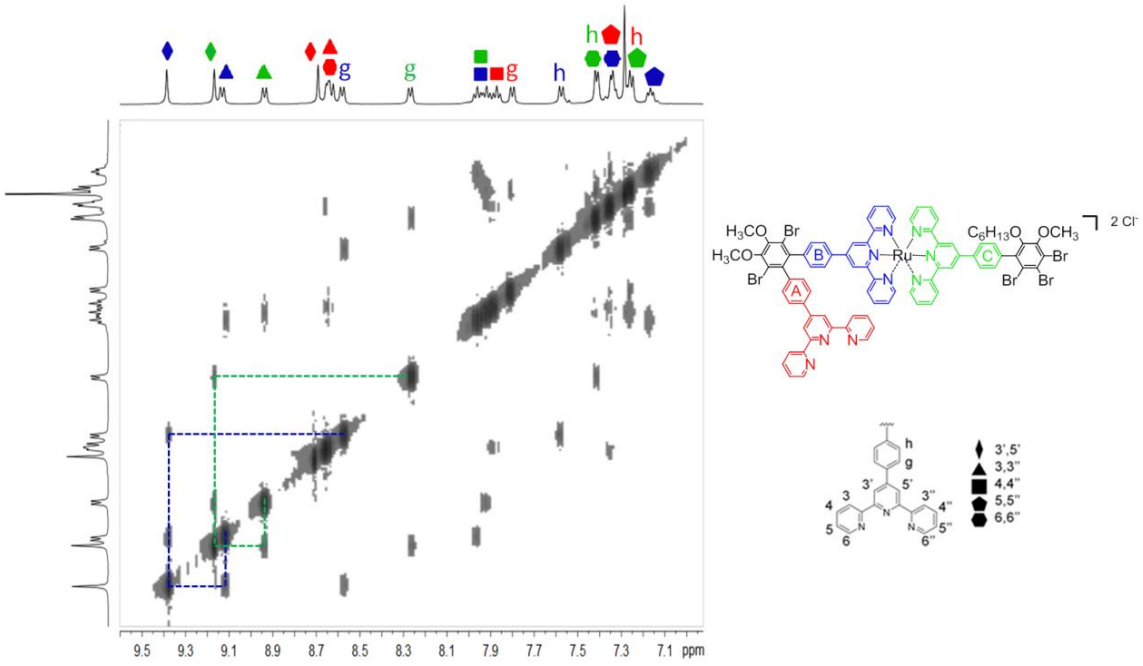

Figure S37. The NOESY spectrum of **B3**(500 MHz) in $CDCl_3$. Related to Figure 2.

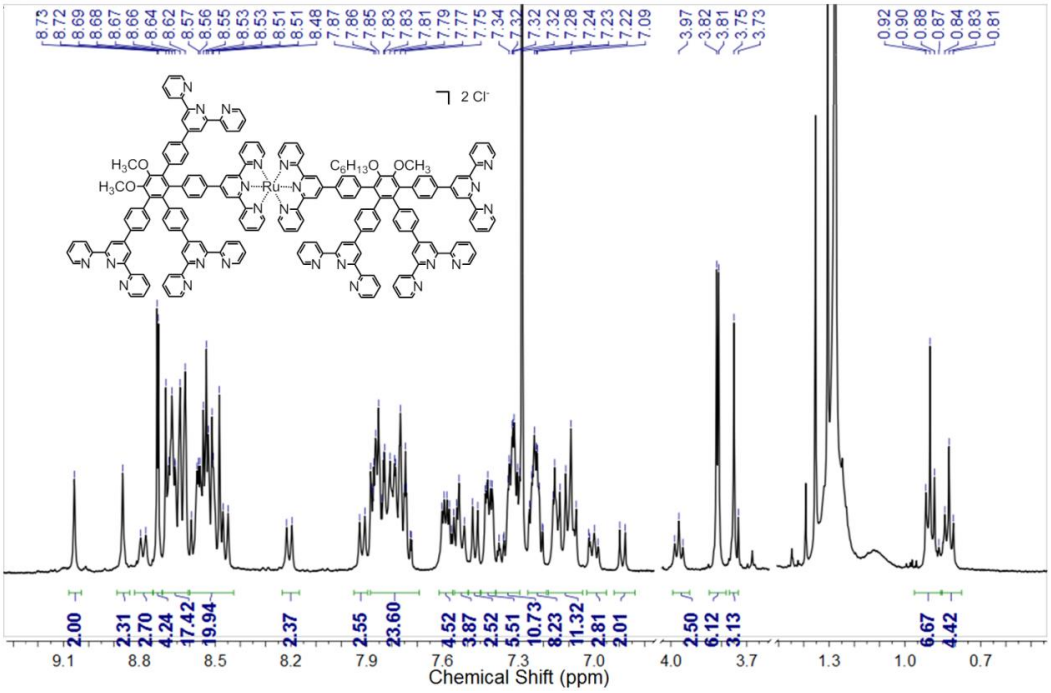

Figure S38. The ^{1}H NMR spectrum of **L3** (400 MHz) in $CDCl_3$. Related to Figure 2.

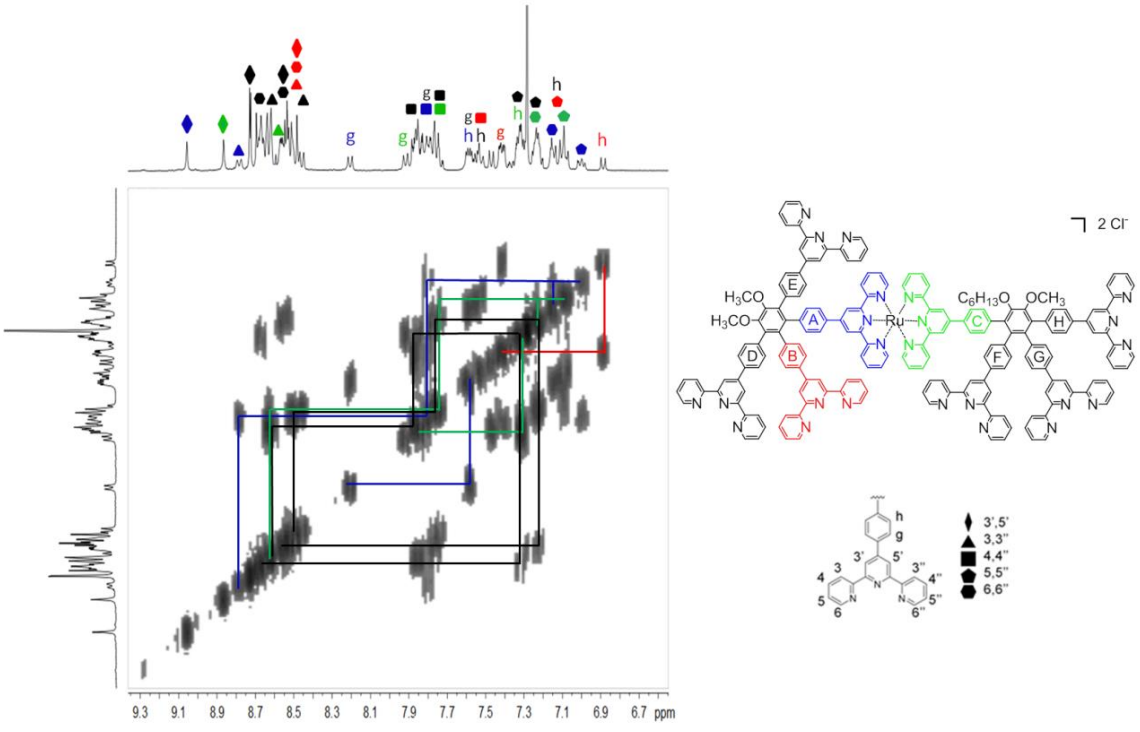

Figure S39. The 2D-COSY spectrum of **L3** (500 MHz) in $CDCl_3$. Related to Figure 2.

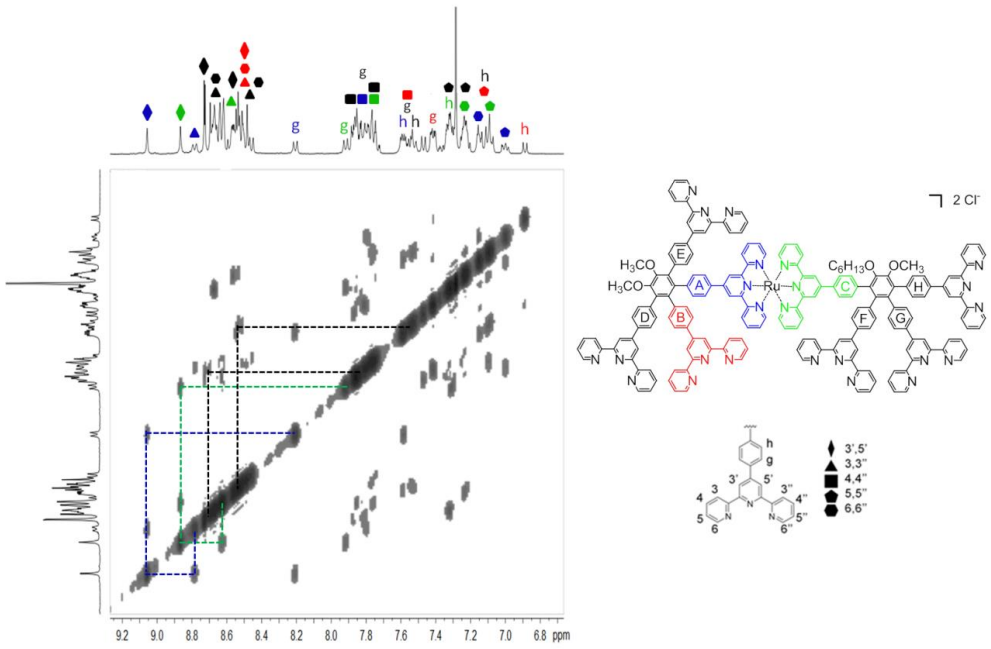

Figure S40. The 2D-NOESY spectrum of **L3** (500 MHz) in $CDCl_3$. Related to Figure 2.

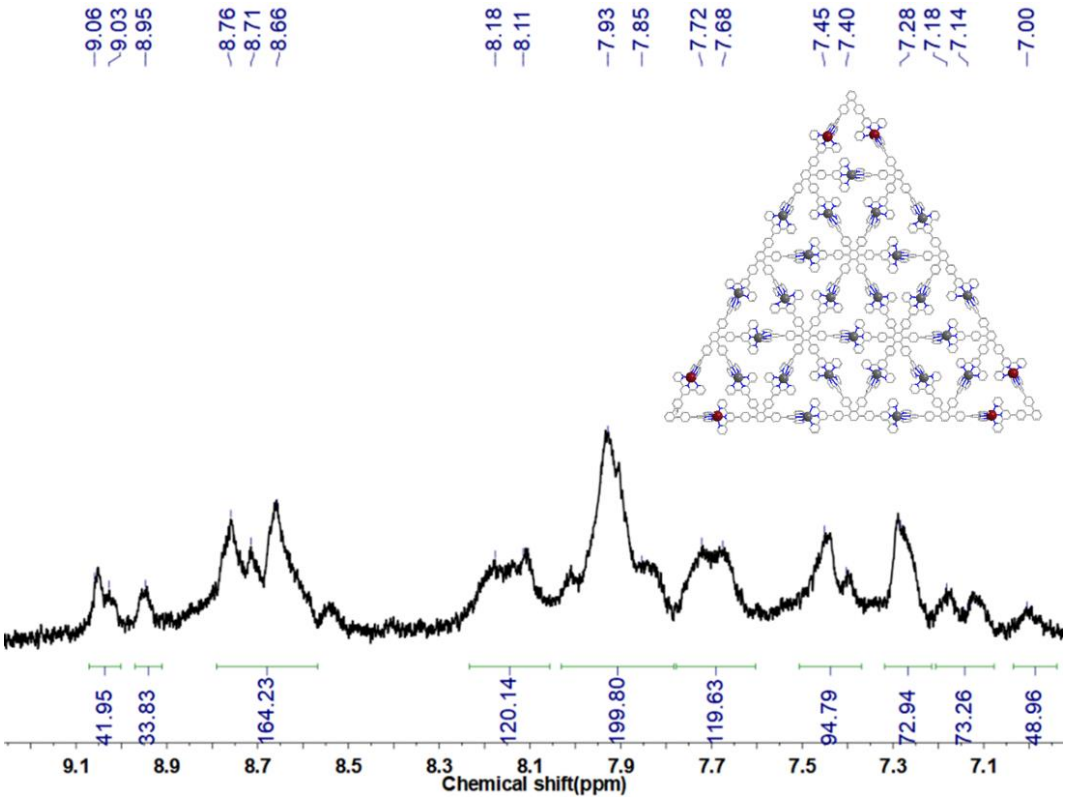

Figure S41. The ^{1}H NMR spectrum of G3 **PT-3** (500 MHz) in CD_3CN. Related to Figure 4.

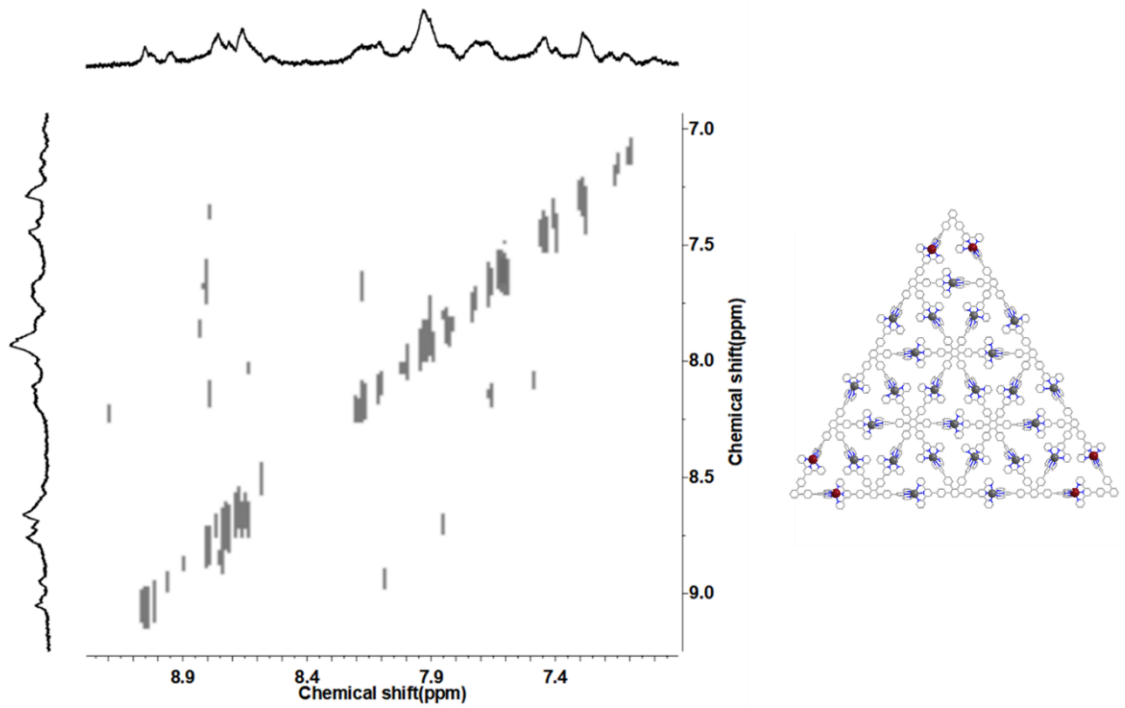

Figure S42. The 2D-COSY spectrum of G3 **PT-3** (500 MHz) in CD_3CN. Related to Figure 4.

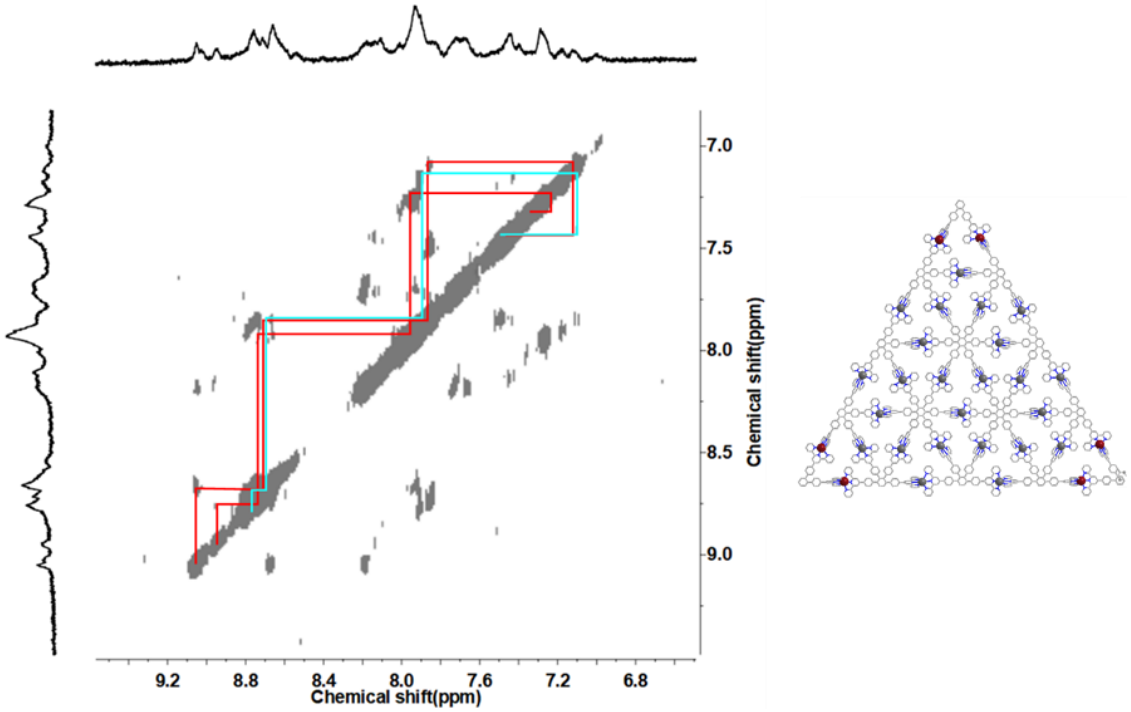

Figure S43. The 2D-NOESY spectrum of G3 **PT-3** (500 MHz) in CD_3CN. Related to Figure 4.

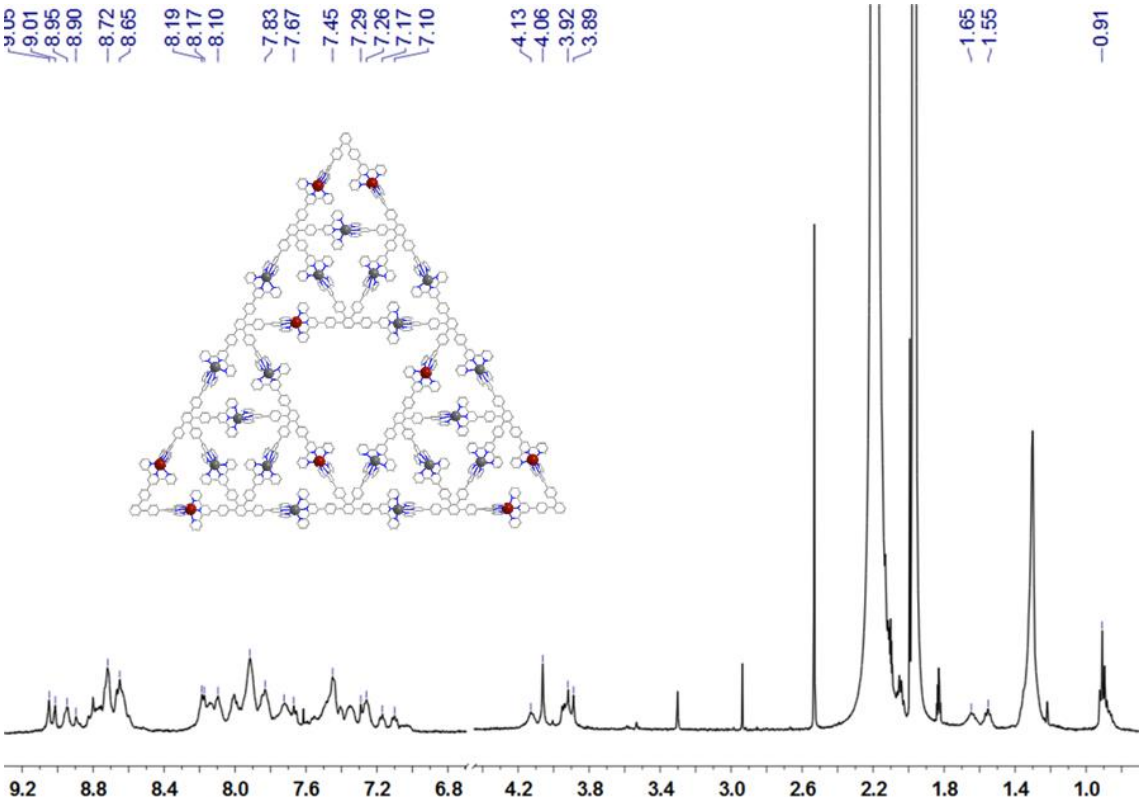

Figure S44. The ^{1}H NMR spectrum of G2 **ST** (500 MHz) in CD_3CN. Related to Figure 4.

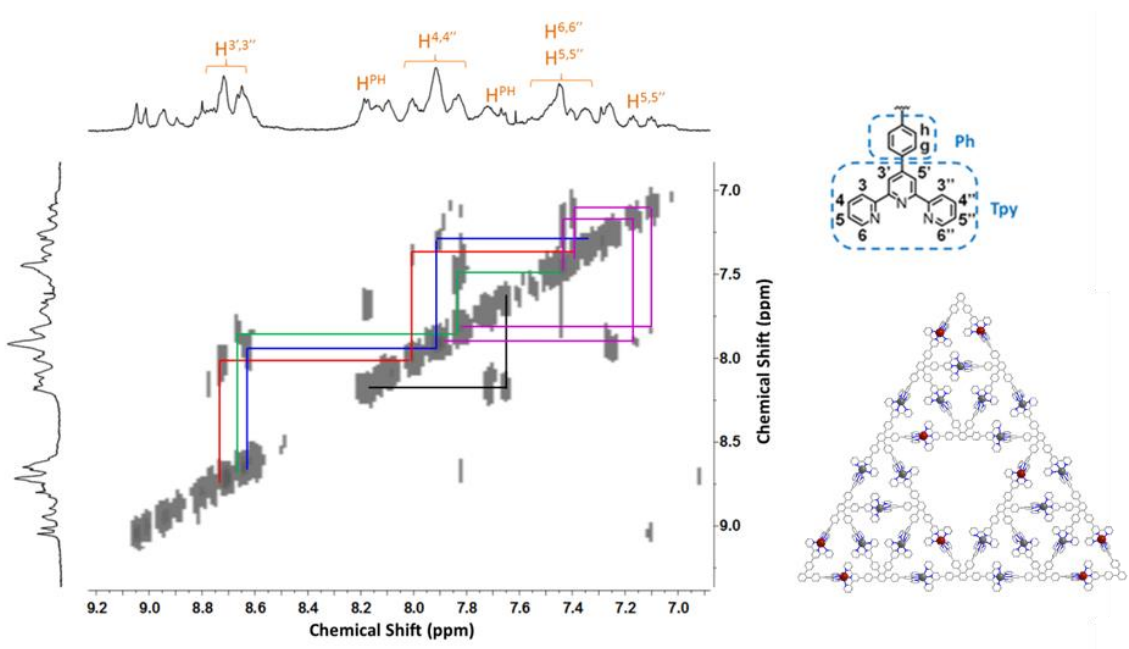

Figure S45. The 2D-COSY spectrum of G2 **ST** (500 MHz) in CD_3CN. Related to Figure 4.

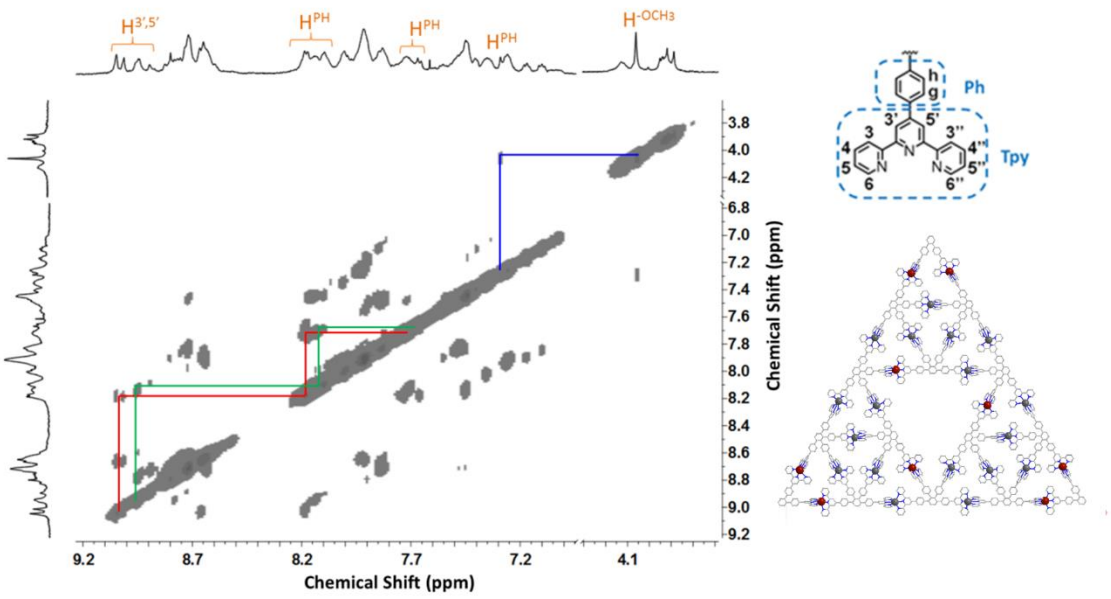

Figure S46. The 2D-NOESY spectrum of G2 **ST** (500 MHz) in CD_3CN. Related to Figure 4.

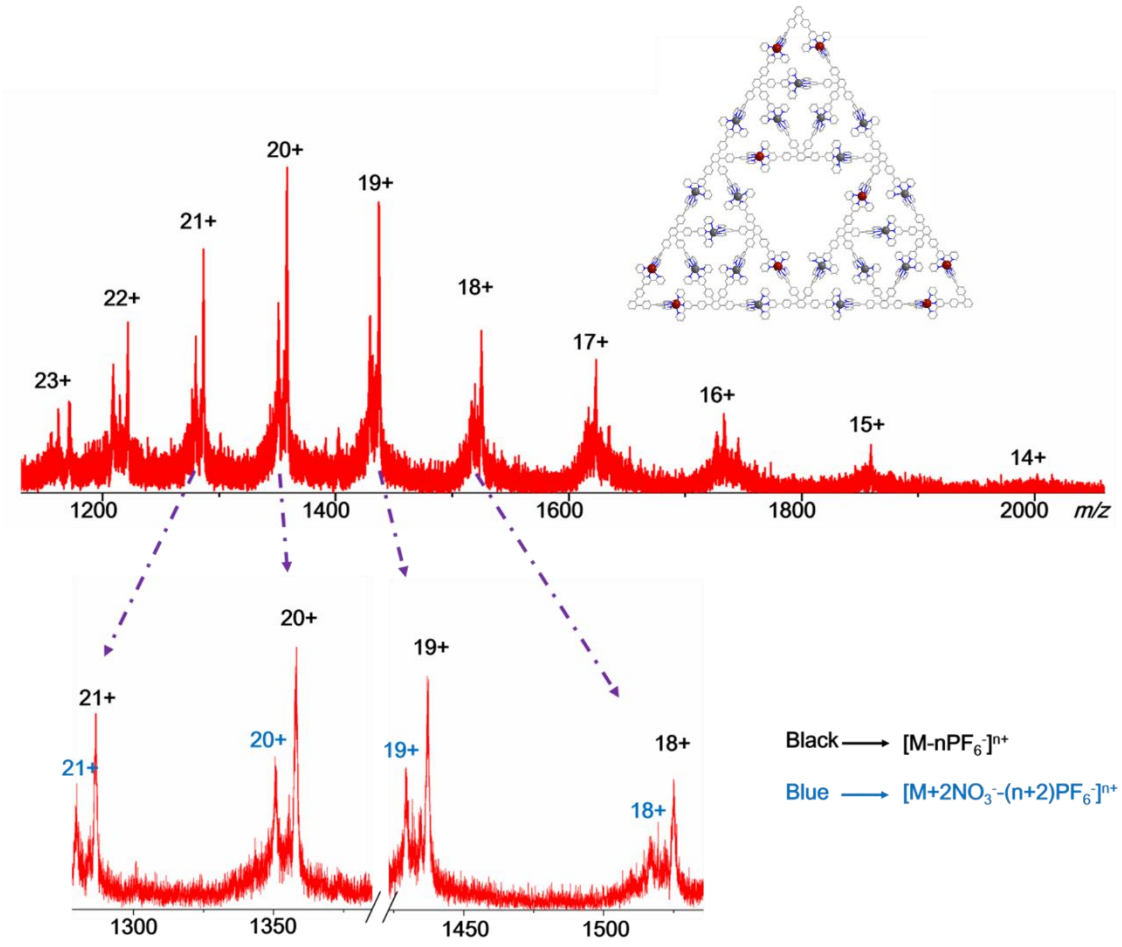

Figure S47. ESI-MS spectrum of G2 **ST** indicated the incomplete exchange of counterions (ion exchange was performed by adding excess amount of NH_4PF_6), the NO_3^- may held at the center of the little triangle structure (Ayme et al., 2012). Related to Figure 4.

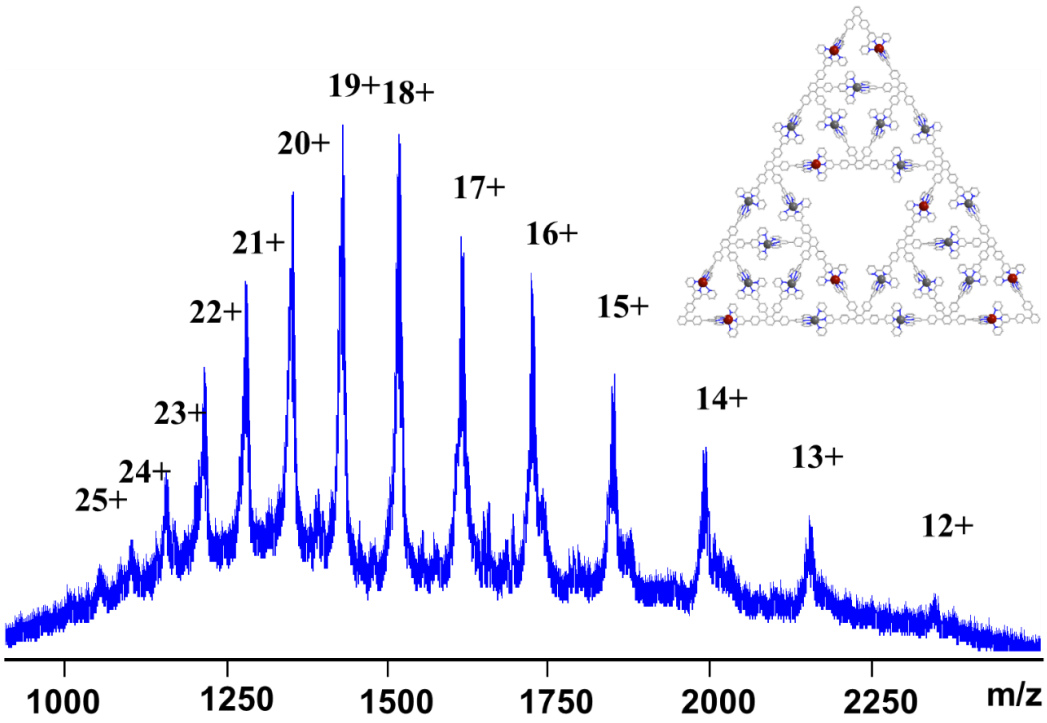

Figure S48. The ESI-MS spectrum of ligand G2 **ST** was obtained at low source and desolvation temperature. Therefore, supramolecules can form solvent adducts and/or salts adducts in ESI-MS (Sun et al., 2015). Related to Figure 4.

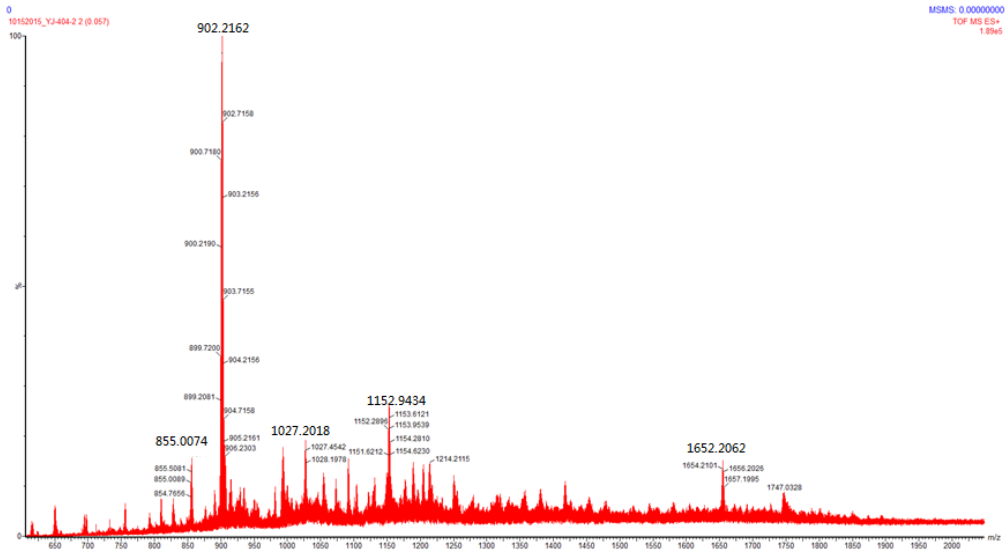

Figure S49. The ESI-MS Spectrum of assembled products by metal-organic ligand **L2** and K-shaped tetra*kis*-terpyridine **4** with Cd^{2+}, the resultant G2 **ST** was unidentified by ESI-MS. Related to Figure 4.

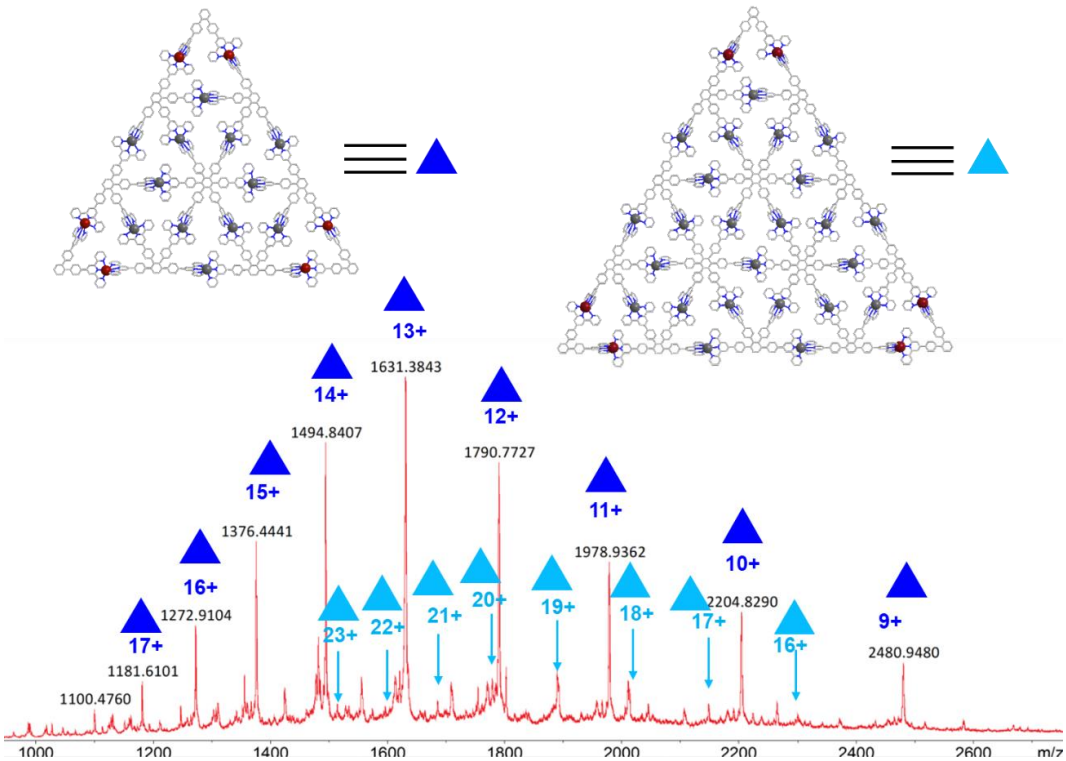

Figure S50. The ESI-MS Spectrum of assembled products by metal-organic ligand **L2**, K-shaped tetra*kis*-terpyridine **4** and star shaped **5** with Cd^{2+}. Only the G2 **PT** metallo-triangle architecture and a trace amount of G3 **PT** could be obtained. Related to Figure 4.

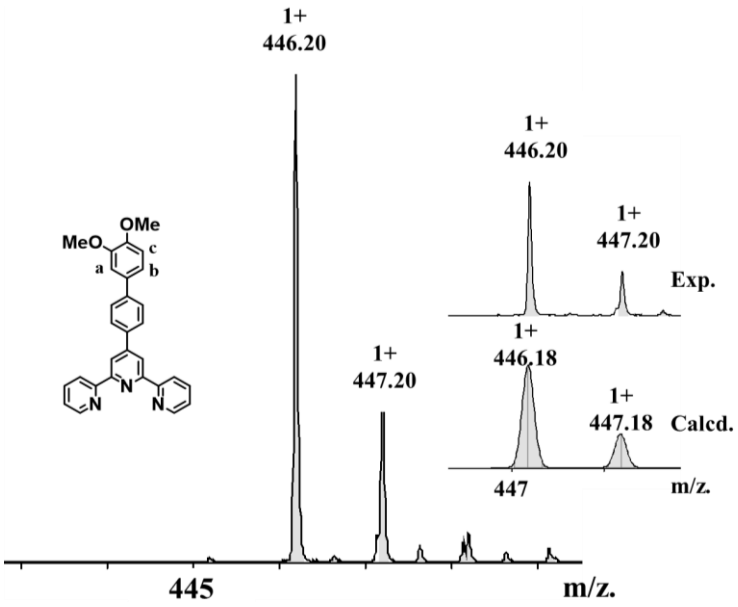

Figure S51. The ESI-MS spectrum of ligand **S6**. Related to Figure 2.

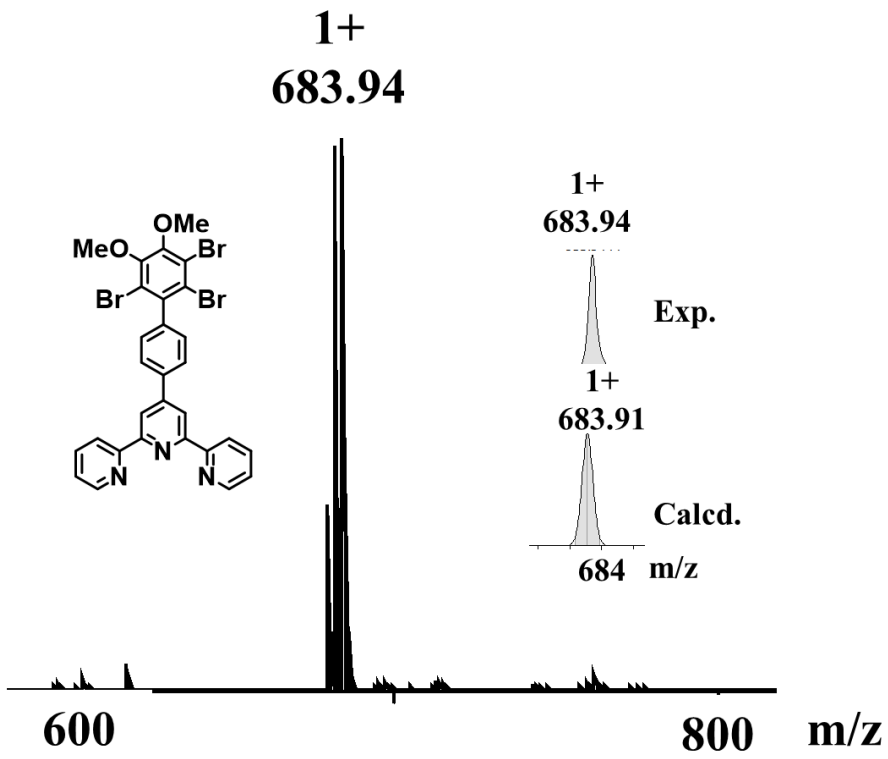

Figure S52. The ESI-MS spectrum of ligand **S7**. Related to Figure 2.

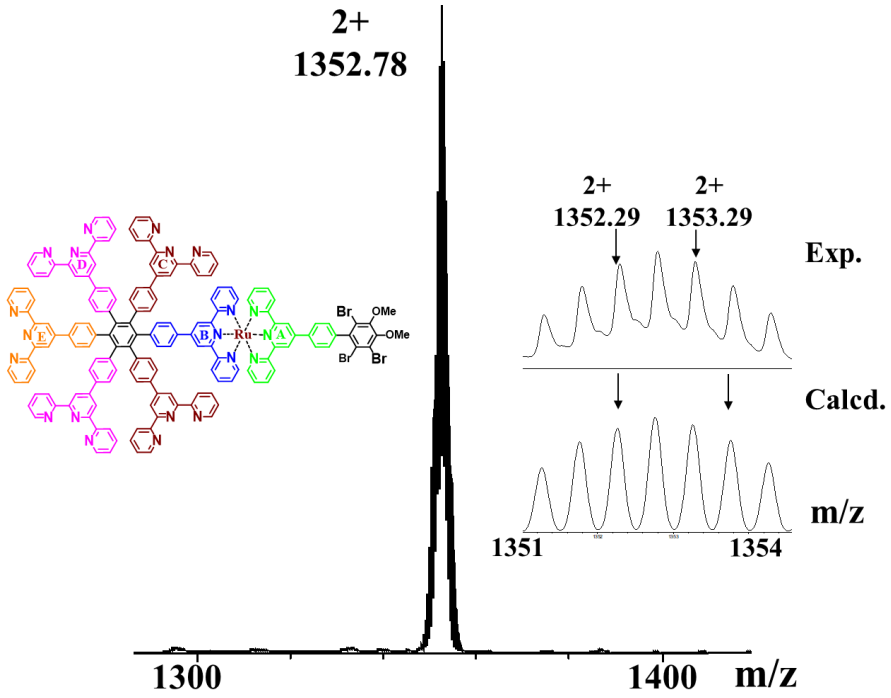

Figure S53. ESI-MS spectrum of ligand **6**. Related to Figure 2.

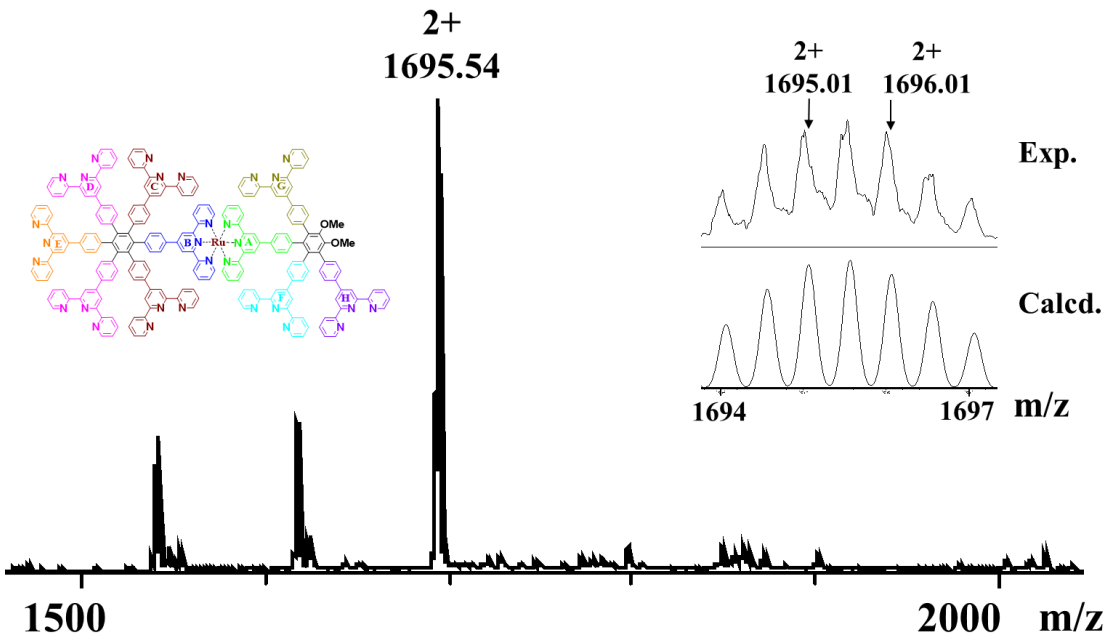

Figure S54. ESI-MS spectrum of ligand **L1**. Related to Figure 2.

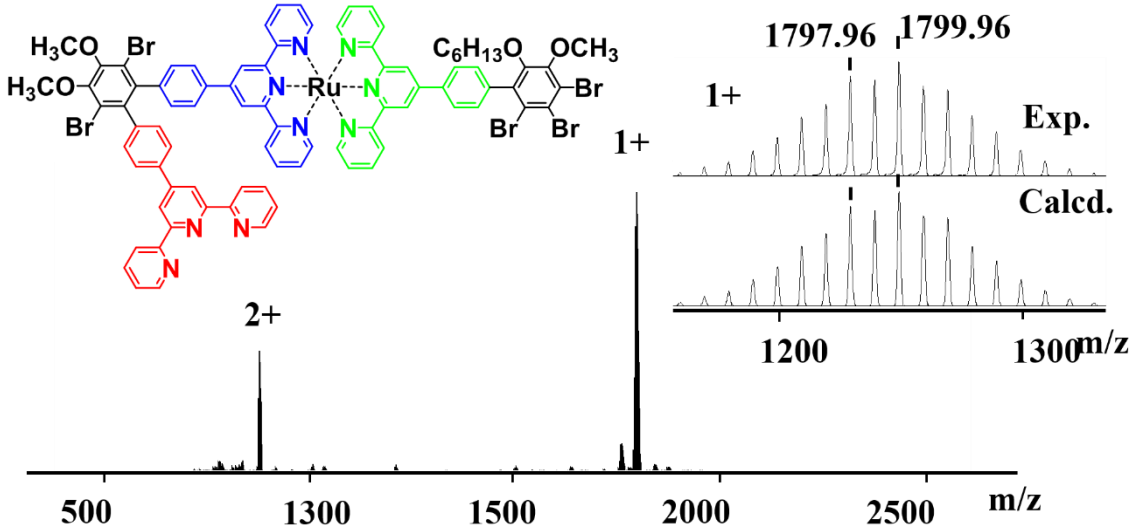

Figure S55. The HR-MS spectrum of complex **10**. Related to Figure 2.

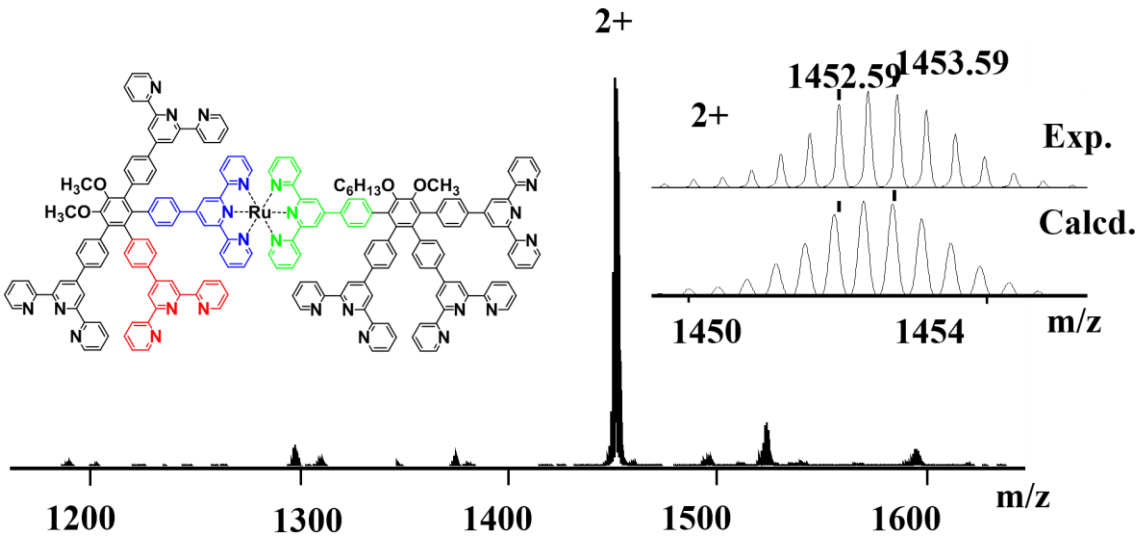

Figure S56. The MS spectrum of ligand **L3**. Related to Figure 2.

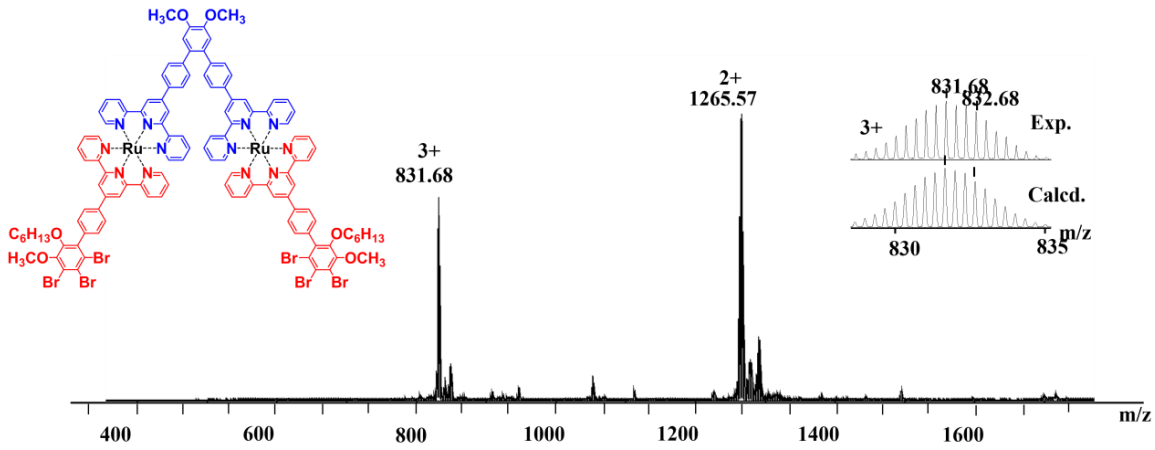

Figure S57. The ESI-MS spectrum of complex **8**. Related to Figure 2.

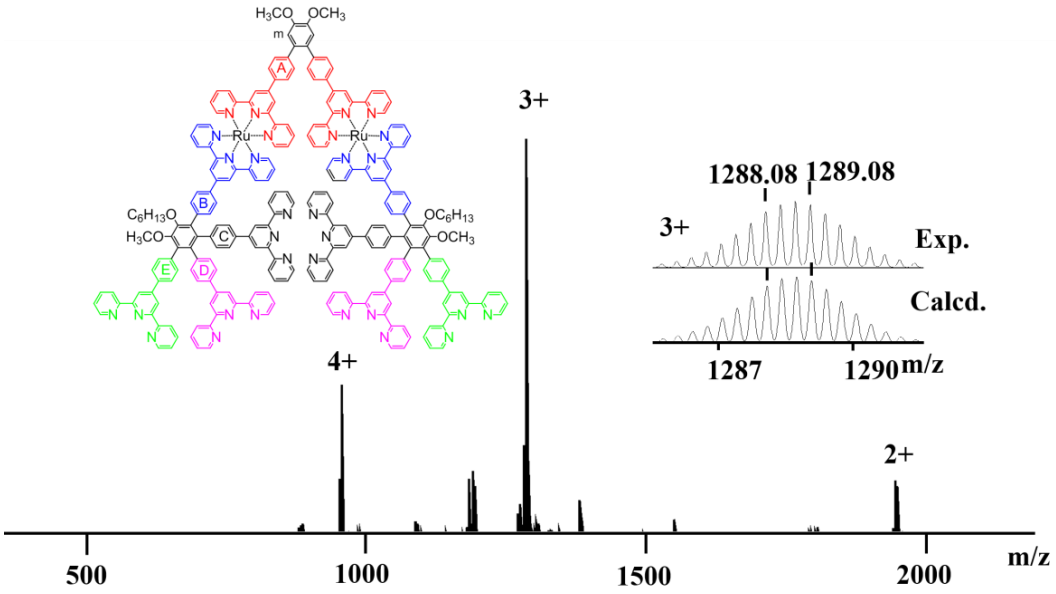

Figure S58. The ESI-MS spectrum of ligand **L2**. Related to Figure 2.

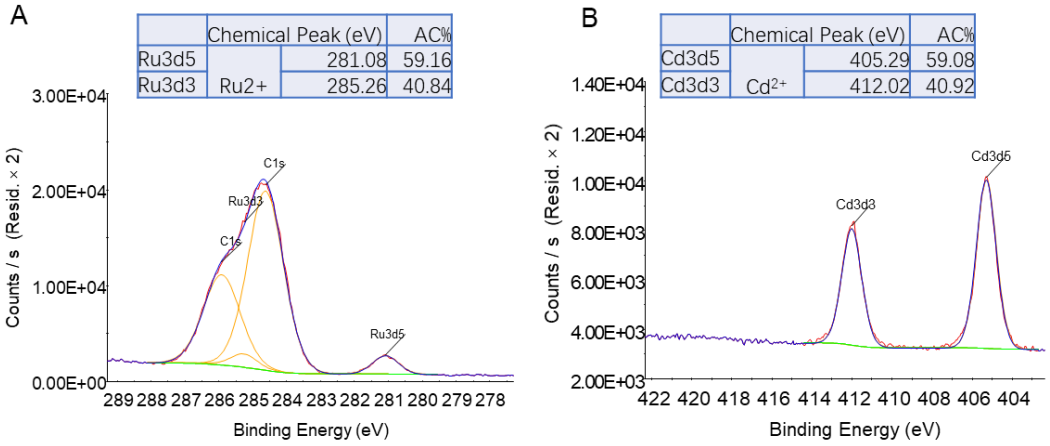

Figure S59. X-ray photoelectron spectrum of (A) Ru and (B) Cd of Pascal's Triangle G3 **PT**. Related to Figure 4.

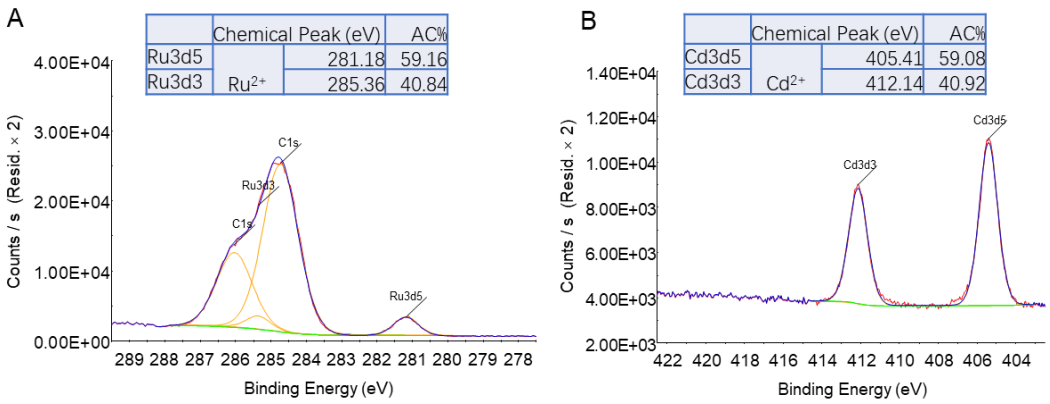

Figure S60. X-ray photoelectron spectrum of (A) Ru and (B) Cd of Sierpiński Triangle G2 **ST**. Related to Figure 4.

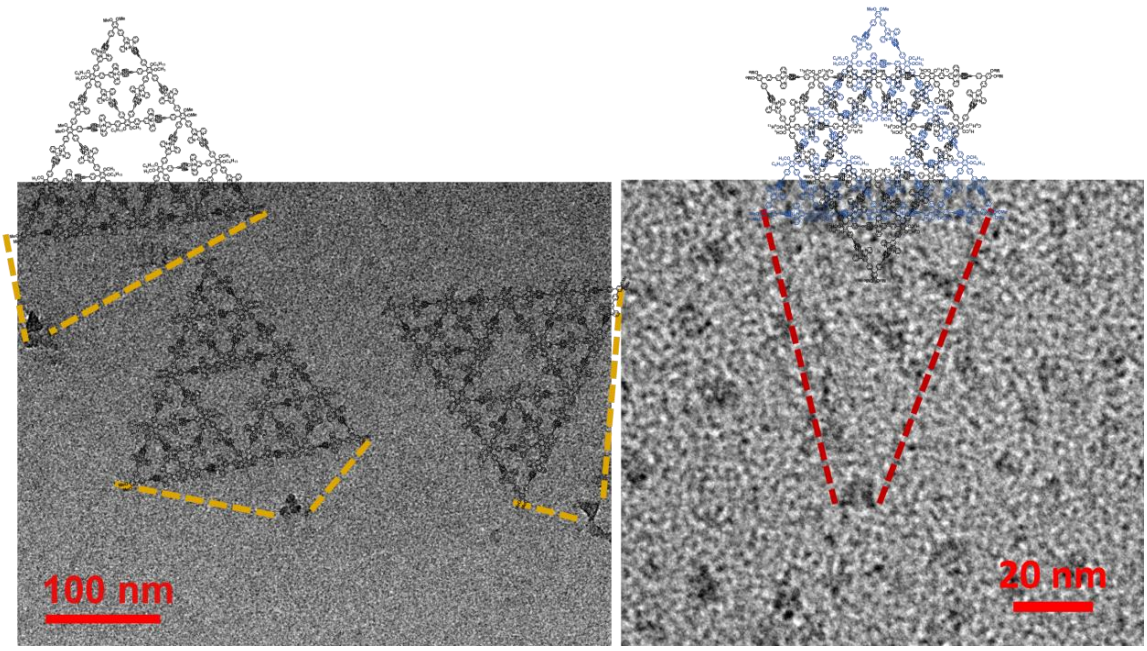

Figure S61. The TEM image of Sierpiński Triangle G2 **ST**. The architecture was observed as a triangle-shadow pattern and the length of sides that was comparable with the size of 11.6±0.5 nm calculated from molecular modeling. The overlapping of two triangles generated several Star-of-David patterns as well. Related to Figure 5.

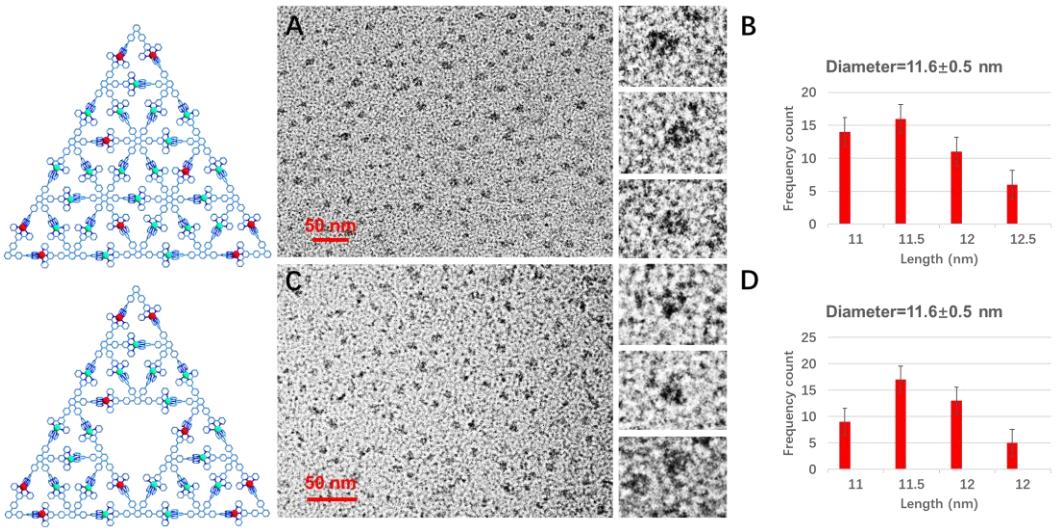

Figure S62. (A) TEM images of Pascal's Triangle G3 **PT** and (C) Sierpiński Triangle G2 **ST**; (B) TEM statistical size distributions of G3 **PT** and (C) G2 **ST**. Related to Figure 5.

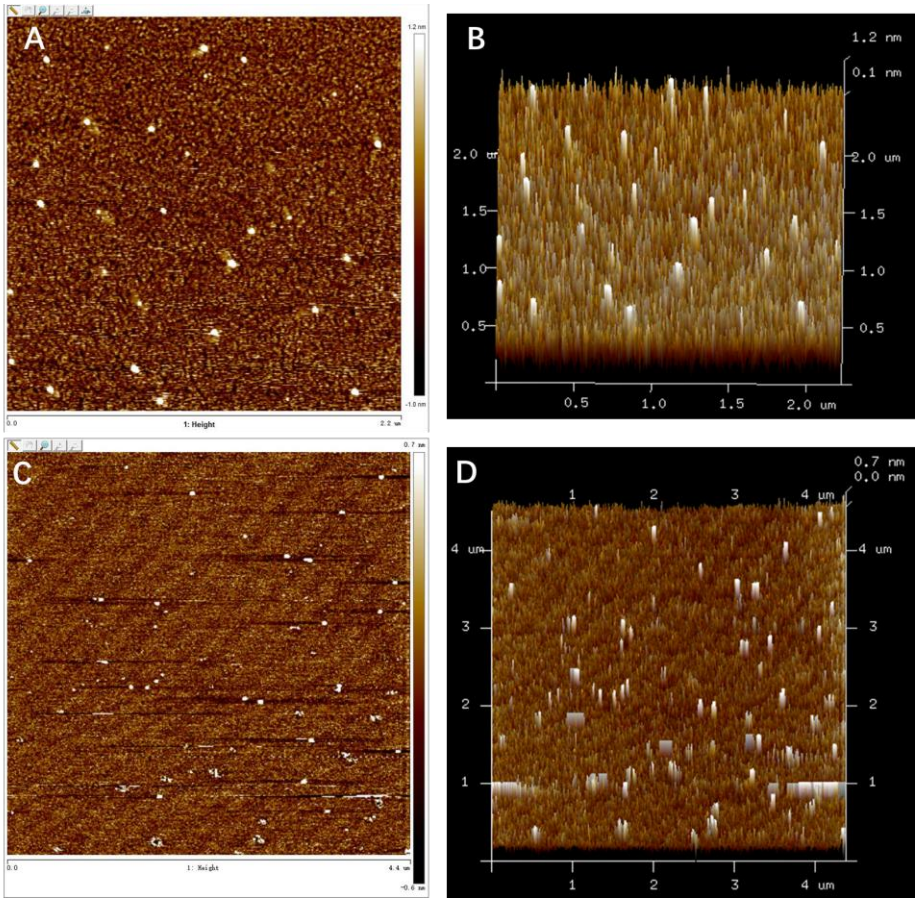

Figure S63. (A,B) AFM images of Pascal's Triangle G3 **PT** and (C,D) Sierpiński Triangle G2 **ST**. Related to Figure 5.

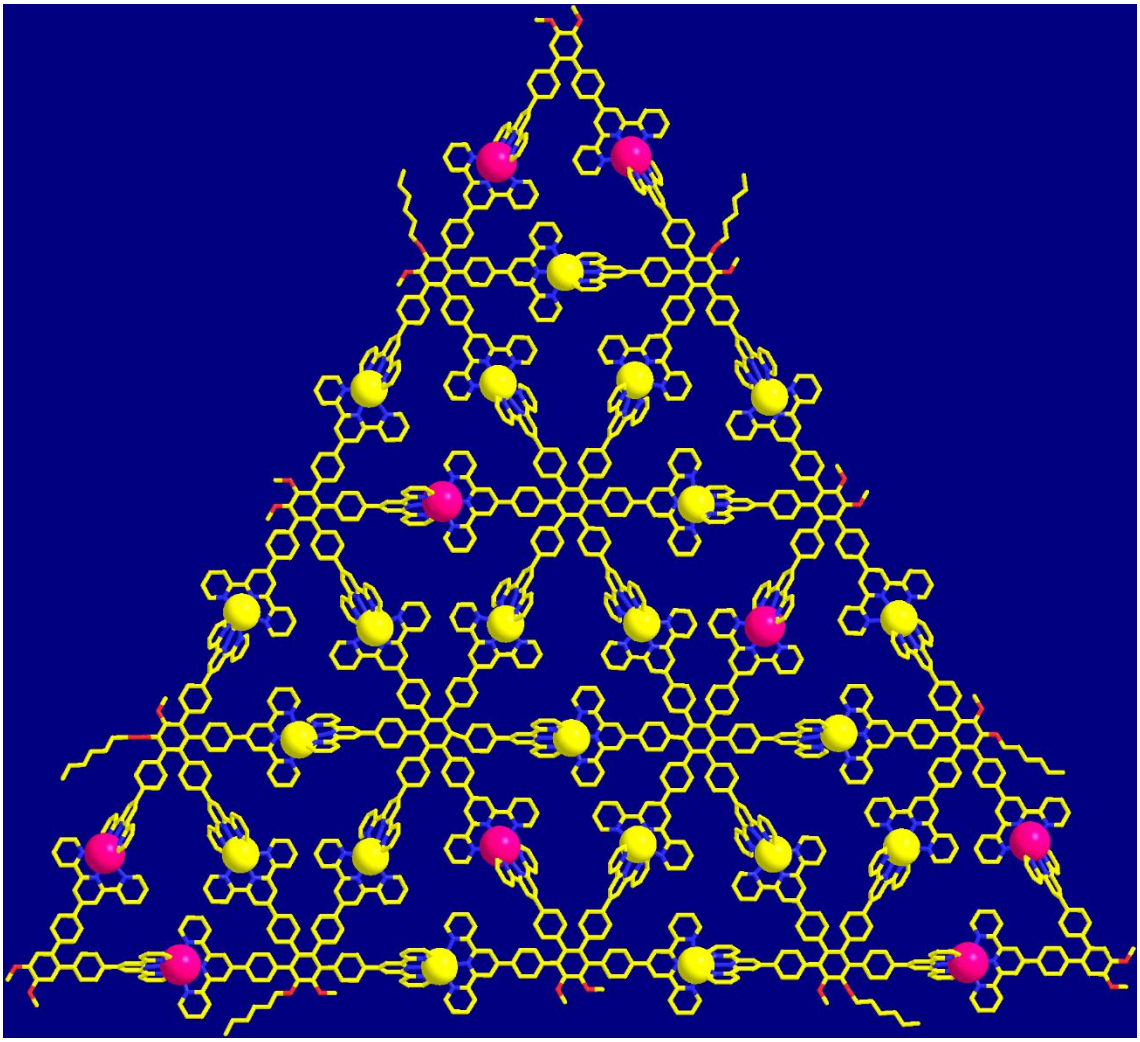

Figure S64. Representative energy-minimized structure from molecular modeling of G3 **PT**. Related to Figure 5.

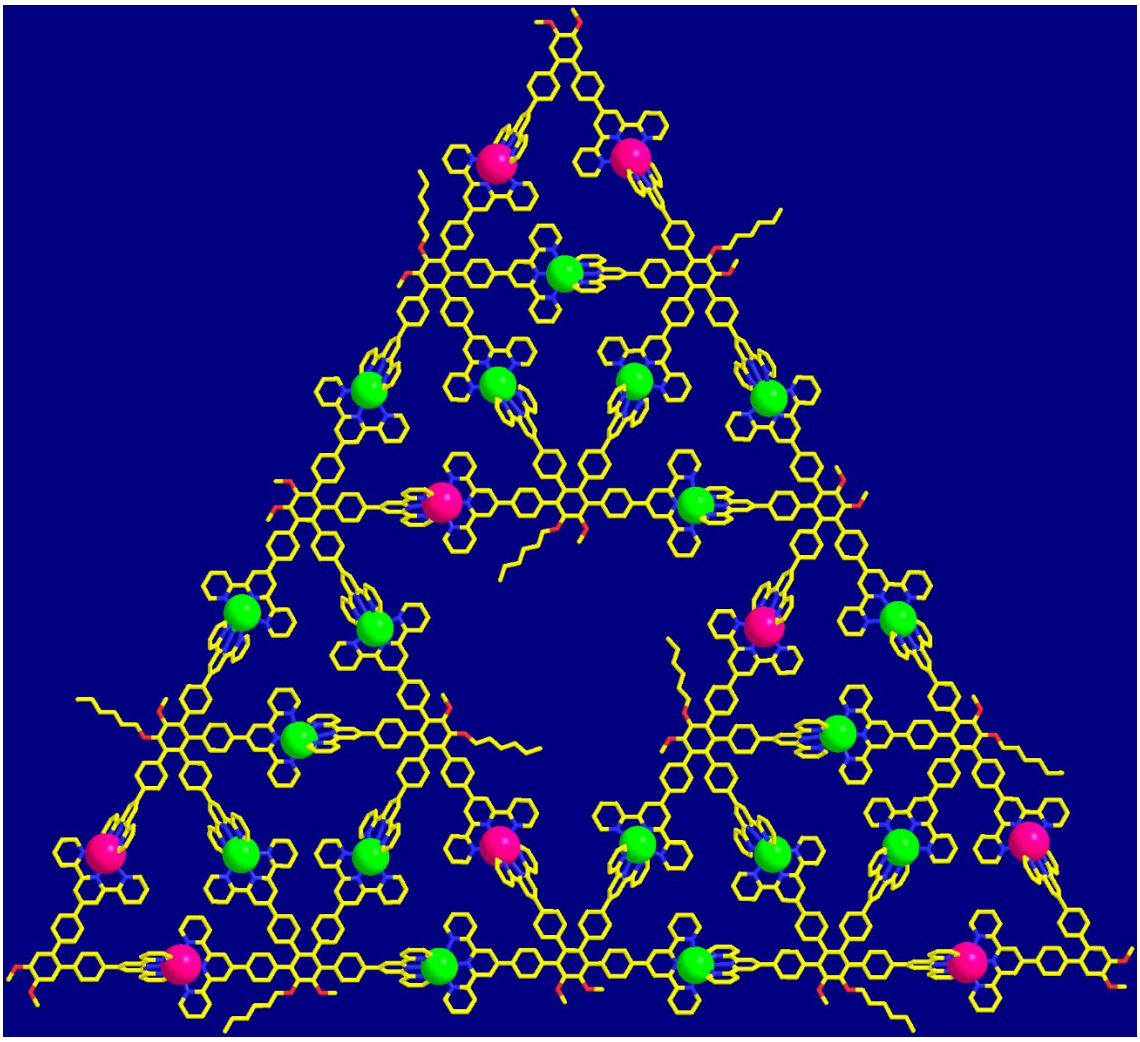

Figure S65. Representative energy-minimized structure from molecular modeling of G2 **ST**. Related to Figure 5.

Synthesis of the Ligands and Complexes

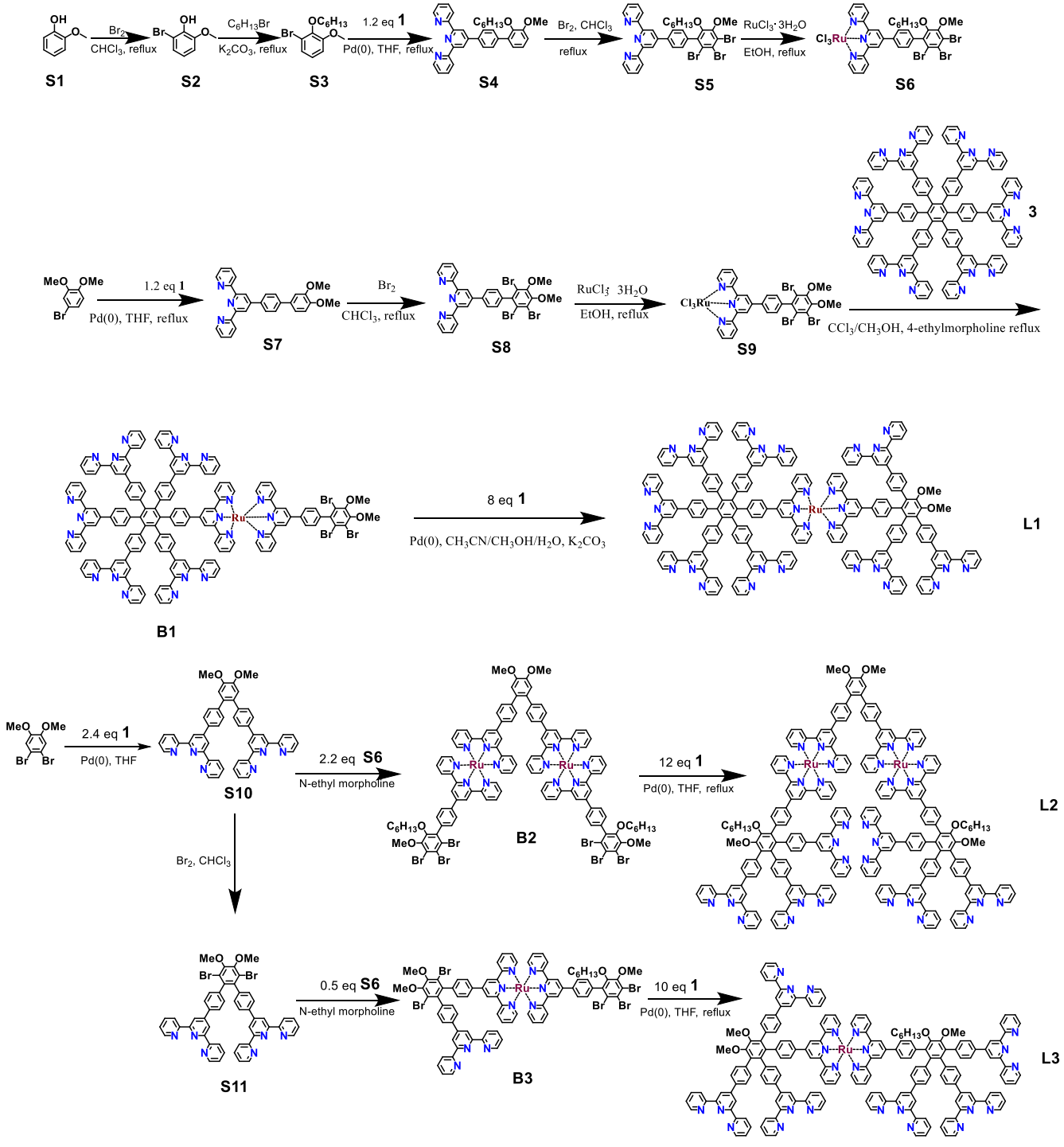

Scheme S1. The synthetic route of metallo-organic ligands module **L1-3**. Related to Figure 2.

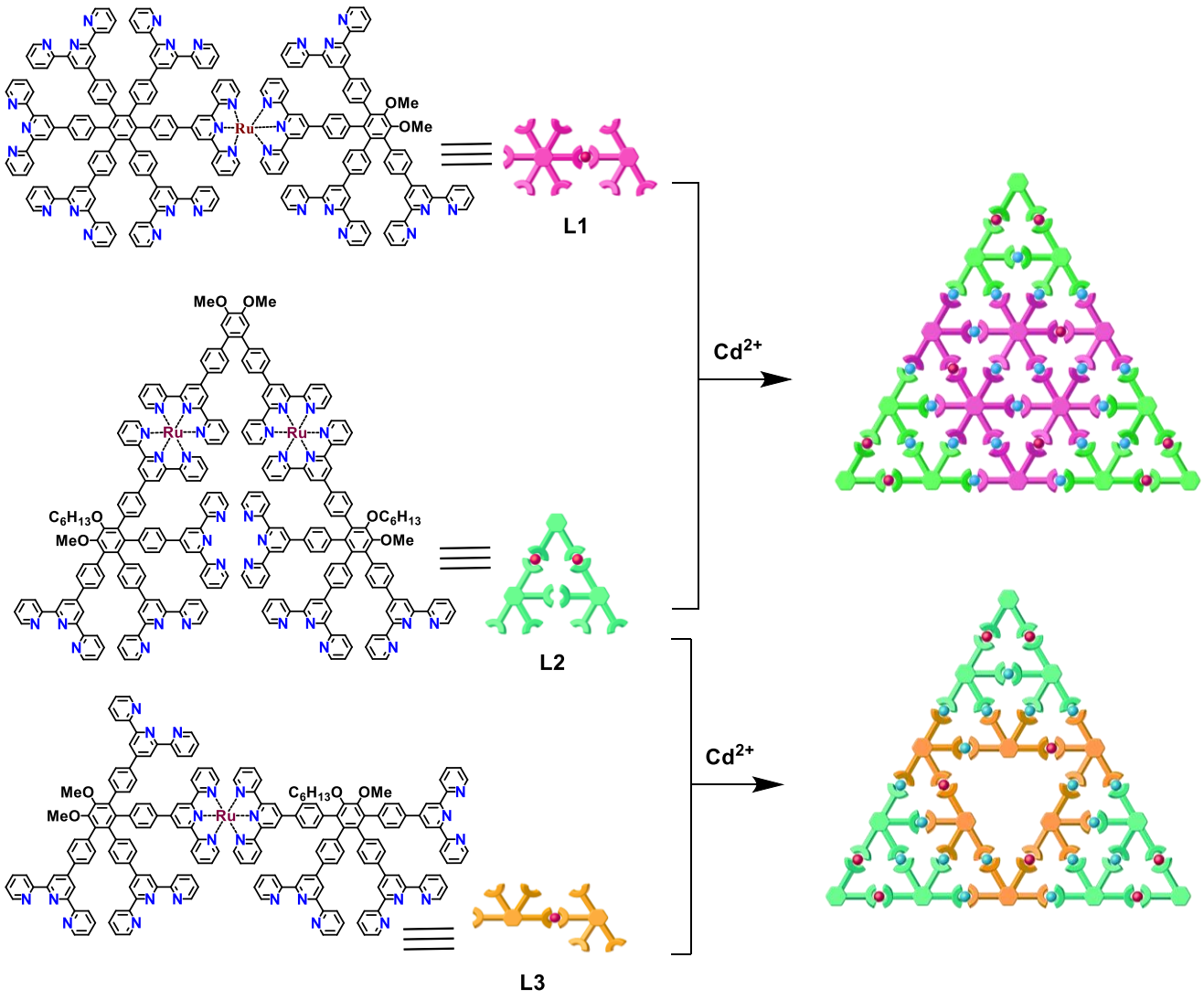

Scheme S2. The synthetic route of the third generation metallo-Pascal's Triangle G3 **PT** and the second generation metallo-Sierpiński Triangle G2 **ST**. Related to Figure 2.

Transparent Methods

2-Methoxyphenol and 1,2-dibromo-4,5-dimethoxybenzene were purchased from Aldrich and used without further purification. 4'-Boronatophenyl[2,2':6',2'']terpyridine **1,** tetra*kis*terpyridine **2** and star shaped ligand **3** were synthesized according to a reported method (Jarozs et al., 2009; Schultz et al., 2012; Wang et al., 2011). Column chromatography was conducted using basic Al_2O_3 (Sinopharm Chemical Reagents Co. Ltd, 200-300 mesh) or SiO_2 (Qingdao Haiyang Chemical Co., Ltd, 200-300 mesh) and the separated products were confirmed by ^1H NMR and ^{13}C NMR spectra using a Bruker Avance 400-MHz and 500-MHz NMR spectrometers in $CDCl_3$, DMSO-D_6, and CD_3CN with a TMS standard.

Electrospray ionization mass (ESI-MS). ESI-MS spectra were recorded with a Waters Synapt G2 tandem mass spectrometer, using solutions of 10 μg samples in 1 mL of $CHCl_3$/MeOH (1:3, v/v) for the ligands or 0.5 mg in 1 mL of MeCN/MeOH (3:1, v/v) for complexes. The ESI-MS experiments were performed under the following conditions: ESI capillary voltage, 3 kV; sample cone voltage, 30 V; extraction cone voltage, 3.5 V; source temperature 100 ºC; desolvation temperature, 100 ºC; cone gas flow, 10 L/h; desolvation gas flow, 700 L/h (N_2); source gas control, 0 mL/min; trap gas control, 2 mL/min; Helium cell gas control, 100 mL/min; ion mobility (IM) cell gas control, 30 mL/min; sample flow rate, 5 μL/min; IM traveling wave height, 25 V; and IM traveling wave velocity, 1000 m/s. Q was set in rf-only mode to transmit all ions produced by ESI into the triwave region for the acquisition of TWIM MS data.

The transmission electron microscope (TEM). TEM images were recorded with a JEOL 2010. The sample was prepared by drop-casting a sample MeCN solution (1×10^{-6} M) onto a carbon-coated Cu grid and extra solution was absorbed by filter paper to avoid aggregation, then dried *in vacuo* for 2 h, about 10 pictures were recorded for each architecture.

Atomic force microscopy (AFM). AFM was conducted on a Bruker Dimension Icon AFM system with ScanAsyst using non-contact/dynamic mode/tapping mode AFM probes, scan mode: contact mode; Scan rate, 2.00 Hz. The data were processed by NanoScope Analysis version 1.5 (Bruker Software, Inc.). The sample was prepared by drop-casting a sample MeCN solution (1×10^{-7} M) onto mica surface and the excess solvent was absorbed by filter paper to avoid aggregation, then dried *in vacuo* for 2 h, about 10 pictures were recorded for each architecture.

X-ray photoelectron spectroscopy (XPS). XPS data was obtained using an EscaLab Xi+ Versa Probe apparatus equipped with an Al Kα Xray source (1486.6 eV). Energy Step Size, 0.050 eV; Pass Energy 100.0 eV. All measurements were done at room temperature.

Molecular Modeling. All the structural optimization and energy calculation were carried out in Materials Studio version 6.1, using the Geometry Optimization and Energy tasks in the Forcite module (Accelrys Software, Inc.). The initial structural model was built up with all counterions omitted for clarity. The Geometry Optimization was performed by using Universal Force Field $(UFF)_2$ with atom-based summation and cubic spline truncation for both the electrostatic and Van der Waals parameters.

Synthesis of the Ligands and Complexes

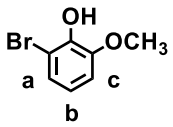

2-Bromo-6-methoxyphenol (**S2**). 2-Methoxyphenol **S1** (6.2 g, 50 mmol) was dissolved in dry THF (250 mL), then it was cooled to -50 °C with dry ice in an EtOH bath, then Br_2 (7.9 g, 50 mmol) was slowly dripped into the mixture maintaining this temperature for 2 h. The mixture was warmed to 25 °C with stirring for 4 hours; then the mixture was poured into an aqueous $NaHSO_3$ solution and extracted with CH_2Cl_2 (100 mL, ×3). The combined organic phase was washed sequentially with an aqueous $NaHCO_3$ solution, then brine. After drying over anh. Na_2SO_4, the solvent was removed *in vacuo* giving a residue, which was purified on a SiO_2 column (200-300 mesh), eluent with CH_2Cl_2: petroleum ether (1:3) to give **S2**, as a white solid: 5 g (65 %); ^{1}H NMR (400 MHz, $CDCl_3$): δ 7.12 (dd, *J* = 8.1, 1.4 Hz, Ph*H*^{a}, 1H), 6.84 (dd, *J* = 8.1, 1.4 Hz, Ph*H*^{b}, 1H), 6.77 (t, *J* = 8.1 Hz, Ph*H*^{c}, 1H), 3.92 (s, OC*H*$_3$, 3H); ^{13}C NMR (101 MHz, $CDCl_3$): δ 147.36, 143.16, 124.83, 120.66, 109.92, 108.38, 56.33; ESI/MS (m/z): Calcd. $[M+H]^+$: 204.0, Found: 204.1.

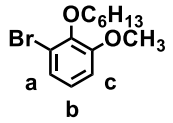

3-Bromo-2-hexyloxy-methoxybenzene (**S3**). A mixture of **S2** (2.03 g, 10 mmol), 1-bromohexane (1.64 g, 10 mmol), K_2CO_3 (1.48 g, 11 mmol), and DMF (100 mL) in a 250 mL 3-neck round bottom flask was stirred at 100 °C for 24 h under N_2, then cooled to 25 °C; the solvent was removed *in vacuo*. The residue was purified on a SiO_2 column eluting with petroleum ether (bp: 60-90 °C) to give the desired monomer, which was triturated with MeOH to generate (73 %) **S3**, as a white powder: 2.1 g; ^{1}H NMR (500 MHz, $CDCl_3$): δ 7.15 (dd, *J* = 8.0, 1.4 Hz, Ph*H*^{a}, 1H), 6.93 (t, *J* = 8.1 Hz, Ph*H*^{b}, 1H), 6.86 (dd, *J* = 8.2, 1.4 Hz, Ph*H*^{c}, 1H), 4.00 (t, *J* = 6.7 Hz, OC*H*$_2$R, 2H), 3.87 (s, OC*H*$_3$, 3H), 1.83 (m, *H*^{Alkyl}, 2H), 1.51 (m, *H*^{Alkyl}, 6H), 1.37 (dd, *J* = 7.4, 3.6 Hz, *H*^{Alkyl}, 3H); ^{13}C NMR (126 MHz, $CDCl_3$): δ 154.04, 146.05, 124.86, 124.62, 118.06, 111.78, 73.39, 56.06, 31.68, 30.17, 25.65, 22.66, 14.08; ESI/MS (m/z): Calcd. $[M+H]^+$: 287.2, Found: 287.2.

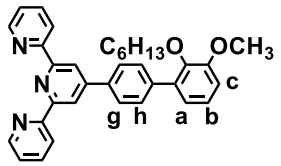

Monomer S4. To a solution of **S3** (287 mg, 1 mmol) and 4'-(4-boronatophenyl)[2, 2':6',2"]terpyridine (**1**; 391, 1.1 mmol) in THF (100 mL), aqueous Na_2CO_3 (2 mL, 1 M) was added. The mixture was freeze-pump-thawed (×3) and backfilled with Argon; then $Pd(PPh_3)_4$ (50 mg, 5% m/m) was added. After refluxing for 12 h under Argon, the mixture was cooled to 25 °C and poured into an aq. NH_4Cl solution. This aqueous layer was extracted with $CHCl_3$, then the combined organic phase was washed with brine and dried ($MgSO_4$). After concentration *in vacuo*, the residue was purified by flash column chromatography (Al_2O_3 200-300 mesh), eluting with $CHCl_3$:petroleum ether (2:1) to give **S4**, as a white solid: 320 mg (62%); ^{1}H NMR (500 MHz, $CDCl_3$): δ 8.84 (s, tpy$H^{3',5'}$, 2H), 8.80-8.73 (m, tpy$H^{6,6''}$, 2H), 8.71 (d, J = 7.9 Hz, tpy$H^{3,3''}$, 2H), 8.00 (d, J = 8.3 Hz, PhH^{g}, 2H), 7.91 (td, J = 7.8, 1.7 Hz, tpy$H^{4,4''}$, 2H), 7.75 (d, J = 8.3 Hz, PhH^{h}, 2H), 7.40–7.34 (m, tpy$H^{5,5''}$, 2H), 7.16 (t, J = 7.9 Hz, PhH^{a}, 1H), 7.05 (dd, J = 7.7, 1.3 Hz, PhH^{b}, 1H), 6.97 (dd, J = 8.1, 1.2 Hz, PhH^{c} ,1H), 3.94 (s, OCH_3, 3H), 3.73 (t, J = 6.6 Hz, OCH_2R, 2H), 1.61–1.51 (m, H^{Alkyl}, 2H), 1.32–1.11 (m, H^{Alkyl}, 6H), 0.82 (t, H^{Alkyl}, J = 7.2 Hz, 3H); ^{13}C NMR (126 MHz, $CDCl_3$): δ 156.35, 155.96, 153.39, 150.03, 149.14, 146.02, 139.35, 136.98, 136.81, 135.67, 130.06, 126.86, 123.95, 123.77, 122.49, 121.33, 118.78, 111.81, 73.50, 55.98, 31.54, 30.05, 25.58, 22.61, 14.01; ESI/MS (m/z): Calcd $[M+H]^+$: 516.4, Found: 516.2.

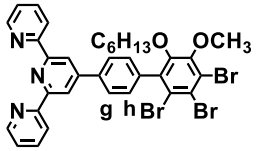

Monomer S5. Monomer **S4** (102 mg, 200 μmol) was dissolved in $CHCl_3$ (100 mL), Br_2 (1.58 g, 10 mmol) was slowly added under stirring, then the mixture was refluxed for 24 h with a tube to capture the HBr effluent. After the solution became colorless, the mixture was cooled to 25 °C and poured into cold aqueous $NaHSO_3$ solution, then extracted with CH_2Cl_2 (100 mL each, ×3). The organic phase was combined and washed with brine and purified on a SiO_2 column eluting with a 1:3 mixture of CH_2Cl_2 : petroleum ether, the desired **S5** was obtained, as a white solid: 100 mg (67%):.^{1}H NMR (400 MHz, $CDCl_3$): δ 8.83 (s, tpy$H^{3,3''}$,2H), 8.76 (ddd, J = 4.8, 1.7, 0.9 Hz, tpy$H^{6,6''}$ 2H), 8.72 (dt, J = 8.0, 1.0 Hz, tpy $H^{3,3''}$, 2H), 8.00 (d, PhH^{g}, 2H), 7.92 (m, tpy$H^{4,4''}$, 2H), 7.40 (ddd, J = 6.7, 3.8, 1.4 Hz, PhH^{h}, tpy$H^{5,5''}$, 4H), 3.96 (s, OCH_3, 3H), 3.76 (t, J = 6.5 Hz, OCH_2R, 2H), 1.12 (ddd, J = 11.0, 10.2, 4.5 Hz, H^{Alkyl}, 6H), 0.78 (t, J

= 7.0 Hz, H^{Alkyl}, 3H); ^{13}C NMR (126 MHz, $CDCl_3$): δ 156.24, 156.02, 151.52, 150.49, 149.90, 149.16, 138.78, 138.70, 138.21, 136.87, 130.28, 127.03, 123.86, 123.12, 121.99, 121.68, 121.35, 118.98, 74.29, 60.86, 31.41, 29.91, 25.34, 22.55, 13.93, 1.01; ESI/MS (m/z): Calcd $[M]^+$: 752.2, Found: 751.9.

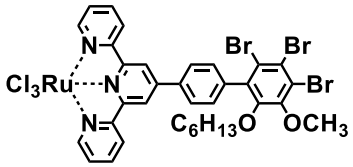

Monomer S6. A EtOH solution of **S5** (75 mg, 100 μmol) and $RuCl_3$•$3H_2O$ (30 mg, 120 μmol) was refluxed for 12 h, then cooled to 25 °C and filtered to generate a brown powder (75 mg), which was washed (3X) with MeOH until the filtrate is clean and colorless; the solid was collected and dried *in vacuo* for 12 h and used directly for the next step without further purification: m. p. >320°C, *Anal*. Calcd. for: $C_{34}H_{30}Br_3Cl_3N_3O_2Ru$: C, 32.71; H, 2.42; N, 3.37. Found: C, 32.88; H, 2.36; N, 3.31.

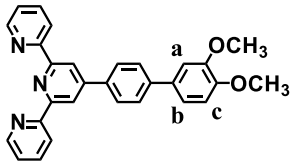

Monomer S7: To a solution of 4-Bromo-1,2-dimethoxybenzene (1 g, 2.25 mmol) and 4'-(4-boronatophenyl)[2, 2':6',2'']terpyridine (**1**; 1 g, 2.83 mmol) in THF (200 mL), aqueous Na_2CO_3 (7 mL, 1 M) was added. The mixture was freeze-pump-thawed and backfilled with Argon; then $Pd(PPh_3)_4$ (130 mg, 5% m/m) was added. After refluxing for 24 h under Argon, the mixture was cooled to 25 °C and poured into an aq. NH_4Cl solution. This aqueous layer was extracted with $CHCl_3$, then the combined organic phase was washed with brine and dried ($MgSO_4$). After concentration in vacuo, the residue was purified by flash column chromatography (Al_2O_3 200-300 mesh), eluting with $CHCl_3$:petroleum ether (2:1) to give **S7**, as a white solid: 1.1 g (70%). ^{1}H NMR (500 MHz, $CDCl_3$) δ 8.81(s, 2H, tpy-$H^{3',5'}$), 8.77-8.76(d, 2H, J=5 Hz tpy-$H^{6,6''}$), 8.72-8.70(d, 2H, J=10 Hz tpy-$H^{3,3''}$), 8.02-8.01(d, 2H, J=5 Hz, Ph-H^g), 7.93-7.90(t, 2H, J=5 Hz, tpy-$H^{4,4''}$), 7.74-7.72(d, 2H, J=5 Hz, Ph-H^h), 7.40-7.38(t, 2H, J=5 Hz, tpy-$H^{5,5''}$), 7.27-7.25(d, 1H, J=10 Hz, H^b), 7.21(s, 1H, H^a), 7.02-7.00(d, 1H, H^c), 4.02, 3.97. ^{13}C NMR (126 MHz, $CDCl_3$) δ 156.31, 155.98, 149.83, 149.29, 149.15, 148.97, 141.69, 136.89, 136.83, 133.41, 127.70, 127.27, 123.84, 121.41, 119.53, 118.65, 111.58, 110.39, 56.04. ESI/MS: Calculated $[M]^+$: 446.2, Found: 446.2.

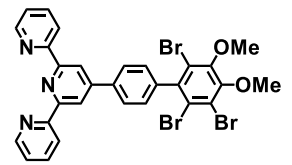

Monomer S8: The above **S7** (445 mg, 1 mmol) was dissolved in $CHCl_3$ (100 mL), then Br_2 (1.58 g, 10 mmol) was slowly added with stirring. After refluxing for 24 h, the mixture was cooled to 25 °C and poured into cold aq. $NaHSO_3$, then extracted with DCM (100 mL each, ×3). The organic extracts were combined and washed with a satd. NaCl solution. After in vacuo concentration, the residue was purified by flash column chromatography column (Al_2O_3, 200-300 mesh), with CH_2Cl_2: petroleum ether (1:3), as eluent, the desired monomer **S8** was obtained, as a white solid: 445 mg (65%). ^{1}H NMR (500 MHz, $CDCl_3$) δ 8.83(s, 2H, tpy-$H^{3',5'}$), 8.76-8.75(d, 2H, J=5 Hz tpy-$H^{6,6''}$), 8.73-8.71(d, 2H, J=10 Hz tpy-$H^{3,3''}$), 8.03-8.01((d, 2H, J=5 Hz, Ph-H^g), 7.93-7.90(t, 2H, J=5 Hz, tpy-$H^{4,4''}$), 7.40-7.38(t, 2H, J=5 Hz, tpy-$H^{5,5''}$), 7.34-7.32(d, 2H, J=5 Hz, Ph-H^h), 4.00, 3.98. ^{13}C NMR (126 MHz, $CDCl_3$) δ 156.19, 155.98, 151.57, 150.73, 149.90, 149.16, 142.72, 140.44, 138.44, 136.90, 129.72, 127.41, 123.88, 121.77, 121.39, 121.35, 119.48, 119.09, 60.98, 60.92. ESI/MS: Calculated $[M]^+$: 683.91, Found: 683.94.

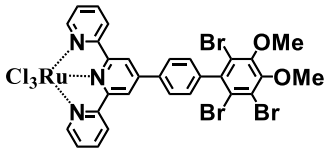

Monomer S9: A EtOH solution of **S8** (223 mg, 0.5 mmol) and $RuCl_3$•$3H_2O$ (195 mg, 0.75 mmol) was refluxed for 12 h, then cooled to 25 °C and filtered to generate a brown powder (300 mg), which was washed (×3) with MeOH until the filtrate is clean and colorless; the solid was collected and dried in vacuo for 12 h and used directly for the next step without further purification.

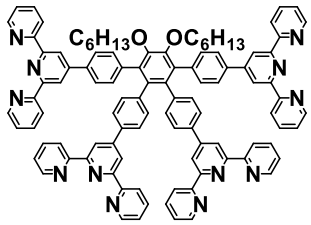

Monomer 3: 3 was synthesized according to the literature.[S2] ^{1}H NMR (500 MHz, $CDCl_3$) δ 8.74(s, 4H, tpyA $H^{3',5'}$), 8.70-8.69(d, J =5 Hz, 4H, tpyA $H^{6,6''}$), 8.65-8.63(d, J =10 Hz, 4H, tpyA $H^{3,3''}$), 8.59(s, 4H, tpyB $H^{3',5'}$, d, J =5 Hz, 4H, tpyB $H^{6,6''}$), 8.55-8.53(d, J =10 Hz, 4H, tpyB $H^{3,3''}$), 7.87-7.84(m, 4H, tpyA $H^{4,4''}$), 7.81-7.80(d, J =10 Hz, 4H, PhA H^g), 7.79-7.76 (m, 4H, tpyB $H^{4,4''}$), 7.57-7.55(d, J =10 Hz, 4H, PhB H^g), 7.39-7.37 (d, J =10 Hz, 4H, PhA H^h), 7.33-7.31(m, 4H, tpyA $H^{5,5''}$), 7.25-7.22 (m, 4H, tpyB $H^{5,5''}$), 7.06-7.05(d, J =10 Hz, 4H, PhB H^h), 3.88 (m, OCH_2, 4H), 1.79, 1.48, 1.15, 0.78(m, Halkyl, 22H). 13C NMR (101 MHz, $CDCl_3$) δ 156.39, 156.36, 155.78, 155.59, 150.08, 150.04, 149.61, 149.06, 148.94, 140.72, 138.28, 136.72, 136.57, 136.47, 136.14, 136.05, 135.21, 132.10, 131.72, 126.23, 126.00, 123.62,

123.45, 121.27, 121.17, 118.86, 118.69, 73.83, 31.62, 30.24, 25.63, 22.63, 14.01. ESI/MS (m/z): Calculated $[M+2H]^{2+}$: 753.9, Found: 753.9.

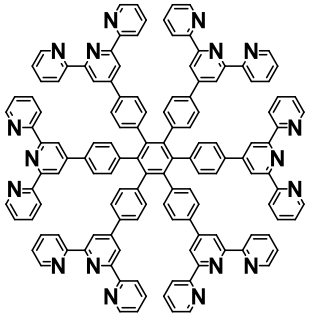

Monomer 3: 3 was synthesized according to the literature.[S3] ^{1}H NMR (400 MHz, $CDCl_3$) δ 8.59 (s, tpy- $H^{3',5'}$,12H), 8.57 (d, tpy-$H^{6,6"}$, 12H), 8.52 (d, J = 7.9 Hz, tpy-$H^{3,3"}$, 12H), 7.76 (td, J = 7.8, 1.6 Hz, Ph-H^{g}, 12H), 7.59 (d, J = 8.2 Hz, ph-H^{h} ,12H), 7.22 (dd, J = 6.8, 5.4 Hz, tpy-$H^{4,4"}$,12H), 7.16 (t, J = 8.2 Hz, tpy-$H^{5,5"}$, 12H).^{13}C NMR (101 MHz, $CDCl_3$) δ 167.11, 156.37, 155.60, 149.60, 148.94, 141.27, 140.29, 136.57, 131.90, 126.02, 123.44, 121.17, 118.75. ESI/MS (m/z): Calculated $[M+H]^{+}$: 1923.2, Found: 1923.2.

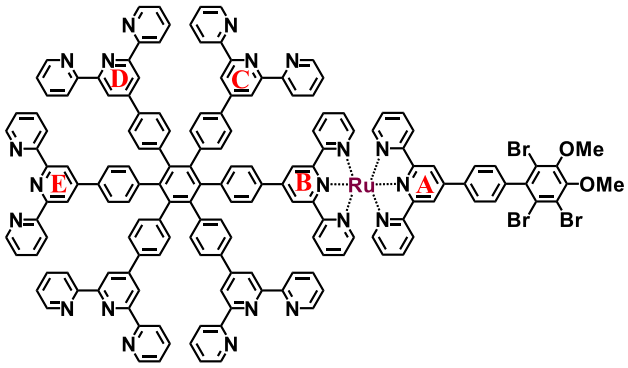

Complex B1: To a suspension of **3** (200 mg, 104 μmol) and **S9** (89 mg, 100 μmol) in $CHCl_3$/MeOH [200 mL, 1/1(v/v)], *N*-ethylmorpholine (5 drops), as a reductant, was added. The mixture was refluxed for 24 h giving a dark red solution, which was cooled to 25 °C and then the solvent was removed *in vacuo* giving a residue, which was extracted with $CHCl_3$ (3X). The combined organic phase was washed with brine and dried over anh. $MgSO_4$. After concentrating *in vacuo*, the residue was purified by flash column chromatography (Al_2O_3, 200-300 mesh) eluting with $CHCl_3$/MeOH (20/1) to give (70%) **6**, as a red powder. ^{1}H NMR (500 MHz, CDCl3) δ 9.09(s, 2H, A-tpy-$H^{3',5'}$), 8.84(s, 2H, B-tpy-$H^{3',5'}$), 8.74-8.73(d, 2H, A-tpy-$H^{3',3"}$), 8.60-8.57(m, 20H, C-tpy-$H^{3',5'}$, D-tpy-$H^{3',5'}$, E-tpy-$H^{3',5'}$, C-tpy-$H^{6,6"}$, D-tpy-$H^{6,6"}$, E-tpy-$H^{6,6"}$, B-tpy-$H^{3,3"}$), 8.51-8.48(m, 10H, C-tpy-$H^{3,3"}$, D-tpy-$H^{3,3"}$, E-tpy-$H^{3,3"}$), 8.31-8.29(d, 2H, J=10Hz, A-PH-

H^{g}), 7.95, 7.92(m, 4H, C-tpy-$H^{4,4"}$), 7.89-7.87(m, 2H, A-tpy-$H^{4,4"}$), 7.86-7.77(m, 10H, B-tpy-$H^{4,4"}$, D-tpy-$H^{4,4"}$, E-tpy-$H^{4,4"}$, B-PH-H^{g}), 7.67-7.66(d, 4H, J=5 Hz, C-PH-H^{g}), 7.59-7.57(d, 6H, J=5 Hz, D-PH-H^{g}, E-PH-H^{g}), 7.46-7.45(d, 2H, J= 5 Hz, A-PH-H^{h}), 7.39-7.37(m, 8H, B-PH-H^{h}, C-PH-H^{h}, E-PH-H^{h}), 7.33-7.26(m, 10H, A-tpy-$H^{6,6"}$, B-tpy-$H^{6,6"}$, E-tpy-$H^{5,5"}$ D-PH-H^{h}), 7.21-7.20(m, 8H, C-tpy-$H^{5,5"}$, D-tpy-$H^{5,5"}$), 7.14(m, 2H, B-tpy-$H^{5,5"}$), 7.01(m, 2H, A-tpy-$H^{5,5"}$), 3.97, 3.94. ^{13}C NMR (126 MHz, $CDCl_3$) δ 157.87, 157.55, 155.06, 154.98, 154.80, 154.74, 152.71, 152.03, 151.74, 151.35, 150.78, 149.85, 148.67, 148.20, 147.76, 145.87, 144.25, 141.71, 141.26, 140.37, 140.07, 138.88, 138.57, 138.21, 138.02, 135.99, 135.02, 132.75, 132.11, 131.95, 130.55, 128.01, 127.77, 126.06, 126.01, 124.52, 124.18, 122.36, 121.88, 119.17, 119.02. ESI/MS (m/z): Calculated $[M]^{2+}$: 1352.76, Found: 1352.78.

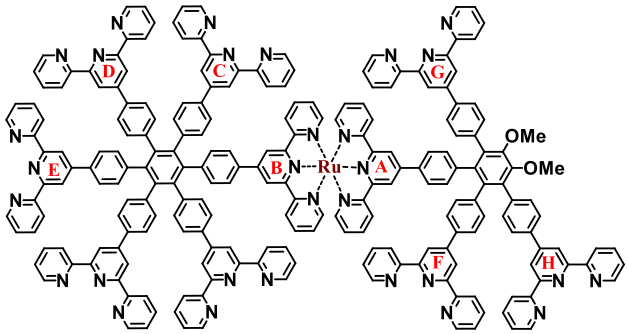

Ligand L1: To a solution of **B1** (60 mg, 16 μmol) and 4'-(4-boronatophenyl)[2,2':6',2"]terpyridine (**1**; 135 mg, 384 μmol) in DMSO (20 mL), aq. Na_2CO_3 (1 mL, 1 M) was added. The mixture was freeze-pump-thawed three (3X) and backfilled with Argon; then $Pd(PPh_3)_4$ (35 mg) was added. After refluxing for 72 h under Argon, the mixture was cooled to 25 °C and then poured into aq. NH_4Cl. The aqueous layer was extracted with $CHCl_3$, and then the combined organic phase was washed with brine and dried over anh. $MgSO_4$. After concentration *in vacuo*, the residue was purified by flash column chromatography (Al_2O_3, 200-300 mesh), eluting with $CHCl_3$:MeOH (40:1) to give (50 %) **L1**. ^{1}H NMR (400 MHz, $CDCl_3$) δ 8.75-8.74(m, 4H, A-tpy-$H^{3',5'}$, B-tpy-$H^{3',5'}$), 8.63(s, 2H, H-tpy-$H^{3',5'}$), 8.60-8.54(m, 12H, C-tpy-$H^{3',5'}$, D-tpy-$H^{3',5'}$, E-tpy-$H^{3',5'}$, F-tpy-$H^{3',5'}$, G-tpy-$H^{3',5'}$), 8.48-8.41(m, 38H, F-tpy-$H^{3',5'}$, C-tpy-$H^{6,6"}$, D-tpy-$H^{6,6"}$, E-tpy-$H^{6,6"}$, F-tpy-$H^{6,6"}$, G-tpy-$H^{6,6"}$, H-tpy-$H^{6,6"}$, A-tpy-$H^{3,3"}$, B-tpy-$H^{3,3"}$, C-tpy-$H^{3,3"}$, D-tpy-$H^{3,3"}$, E-tpy-$H^{3,3"}$, F-tpy-$H^{3,3"}$, G-tpy-$H^{3,3"}$, H-tpy-$H^{3,3"}$), 7.85-7.80(m, 6H, A-PH-H^{g}, B-PH-H^{g}, H-PH-H^{g}), 7.79-7.65(m, 32H, A-tpy-$H^{4,4"}$, B-tpy-$H^{4,4"}$, D-tpy-$H^{4,4"}$, C-tpy-$H^{4,4"}$, E-tpy-$H^{4,4"}$, F-tpy-$H^{4,4"}$, G-tpy-$H^{4,4"}$, G-PH-H^{g}, E-PH-H^{g}, F-PH-H^{g}), 7.59-7.54(m, 14H, C-PH-H^{g}, D-PH-H^{g}, H-tpy-$H^{4,4"}$, A-PH-H^{h}, B-PH-H^{h}), 7.42-7.40(m, 2H, H-PH-H^{h},), 7.36-7.26(m, 14H, C-PH-H^{h}, D-PH-H^{h}, E-PH-H^{h}, F-PH-H^{h}, G-PH-H^{h}), 7.25-7.19(m, 10H, C-tpy-$H^{5,5"}$, D-tpy-$H^{5,5"}$, F-tpy-$H^{5,5"}$), 7.16-7.15(m, 6H, F-tpy-$H^{5,5"}$, G-tpy-$H^{5,5"}$, H-tpy-$H^{5,5"}$), 7.10-7.07(m,

4H, A-tpy-H$^{6,6''}$, B-tpy-H$^{6,6''}$), 6.93-6.92(m, 4H, A-tpy-H$^{5,5''}$, B-tpy-H$^{5,5''}$), 3.75, 3.74. ESI/MS: Calculated $[M]^{2+}$: 1695.56, Found: 1695.54.

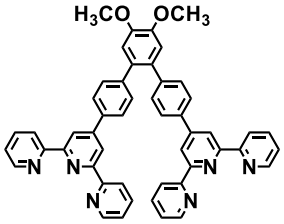

"V" Monomer S10. To a solution of 1,2-dibromo-4,5-dimethoxybenzene (1.48 g, 5 mmol) and 4'-(4-boronatophenyl)[2,2':6',2"]terpyridine (**1**; 3.54 g, 10.00 mmol) in THF (200 mL), aq. Na_2CO_3 (20 mL, 2 M) was added. The mixture was freeze-pump-thawed (3X) and backfilled with Argon; then $Pd(PPh_3)_4$ (100 mg) was added. After refluxing for 12 h under Argon, the mixture was cooled to 25 °C and poured into an aq. NH_4Cl solution. The aqueous layer was extracted with $CHCl_3$, and then the combined organic phase was washed with brine and dried with anh. $MgSO_4$. After concentration *in vacuo*, the residue was purified by flash column chromatography (Al_2O_3 200-300 mesh), eluting with $CHCl_3$: petroleum ether (2:1) to give the desired "**V**" ligand, as a white solid: 2.4 g (64%); ^{1}H NMR (400 MHz, $CDCl_3$): δ 8.76 (s, 4H), 8.70 (ddd, *J* = 4.8, 1.7, 0.8 Hz, 4H), 8.66 (d, *J* = 7.9 Hz, 4H), 7.86 (ddd, *J* = 8.3, 6.6, 2.8 Hz, 8H), 7.34 (m, 8H), 7.28 (s, 2H), 4.03 (s, 6H); ^{13}C NMR (101 MHz, $CDCl_3$) δ 156.31, 155.88, 149.77, 149.09, 148.54, 142.22, 136.82, 136.37, 132.42, 130.51, 127.05, 123.74, 121.34, 118.79, 113.70, 113.70, 56.19.

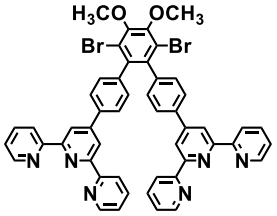

"V" Monomer S11. The above **S10** (102 mg, 200 μmol) was dissolved in $CHCl_3$ (100 mL), then Br_2 (1.58 g, 10 mmol) was slowly added with stirring. After refluxing for 24 h, the mixture was cooled to 25 °C and poured into cold aq. $NaHSO_3$, then extracted with DCM (100 mL each, X3). The organic extracts were combined and washed with a satd. NaCl solution. After *in vacuo* concentration, the residue was purified by flash column chromatography column (Al_2O_3, 200-300 mesh), with CH_2Cl_2 : petroleum ether (1:3), as a eluent, the desired monomer **S11** was obtained, as a white solid: 100 mg (67%), m. p. = 301 °C; ^{1}H NMR (500 MHz, $CDCl_3$): δ 8.73–8.64 (m, 8H), 8.63 (d, *J* = 7.9 Hz, 4H), 7.84 (t, *J* = 7.7 Hz, 4H), 7.79 (d, *J* = 8.1 Hz, 4H), 7.34–7.29 (m, 4H), 7.21 (d, *J* = 8.0 Hz, 4H), 4.06 (s, 6H); ^{13}C NMR (126

MHz, $CDCl_3$): δ 156.29, 155.83, 150.70, 149.69, 149.06, 140.57, 139.09, 137.20, 136.73, 130.67, 126.75, 123.67, 121.27, 119.50, 118.93, 60.91; 2D-COSY spectrum: ESI-MS: $[M + H]^+$ = 909.11 (found = 909.1).

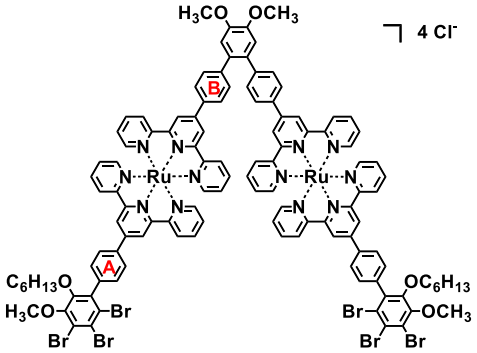

Complex B2. To a mixture of **S10** (37.2 mg, 50 μmol) and **S6** (105.6 mg, 110 μmol) in $CHCl_3$/MeOH (200 mL), a few drops of *N*-ethylmorpholine was added, as a catalyst. The mixture was refluxed for 24 h, then cooled to 25 °C and the solvent was removed *in vacuo* leaving a residue that was purified on an Al_2O_3 column with CH_2Cl_2/MeOH (40:1), as a eluent, then drying *in vacuo* to give (50%) pure complex **B2**, as a red powder: 62 mg: ^{1}H NMR (400 MHz, MeOD): δ 9.38 (s, tpy^B*H*$^{3',5'}$, 4H), 9.35 (s, tpy^A*H*$^{3',5',}$ 4H), 8.94 (dd, *J* = 8.0, 4.5 Hz, tpy^A*H*$^{3,3"}$, tpy^B*H*$^{3,3"}$, 8H), 8.44 (d, *J* = 8.4 Hz, Ph^B*H*^{g}, 4H), 8.32 (d, *J* = 8.4 Hz, Ph^A*H*^{g}, 4H), 8.03 (ddd, *J* = 5.7, 4.8, 2.4 Hz, tpy^A*H*$^{4,4"}$, tpy^B*H*$^{4,4"}$, 8H), 7.71 (d, *J* = 8.3 Hz, Ph^B*H*^{h}, 4H), 7.66 (d, *J* = 8.3 Hz, Ph^A*H*^{h}, 4H), 7.58 (t, *J* = 6.2 Hz, tpy^A*H*$^{6,6"}$, tpy^B*H*$^{6,6"}$, 8H), 7.30 (m, tpy^A*H*$^{5,5"}$, tpy^B*H*$^{5,5"}$, 8H), 7.25 (s, Ph*H*^{J}, 2H), 4.06 (s, OC*H*$_3$, 6H), 3.98 (s, OC*H*$_3$,6H), 3.90 (t, *J* = 6.3 Hz, OC*H*$_2$R, 4H), 1.47 (d, *J* = 6.7 Hz, *H*^{alkyl}, 4H), 1.21 (m, *H*^{alkyl}, 12H), 0.82 (t, *J* = 7.0 Hz, *H*^{alkyl}, 6H); ^{13}C NMR (101 MHz, $CDCl_3$): δ 162.34, 162.27, 159.60, 159.49, 155.91, 155.79, 154.42, 153.24, 152.26, 152.07, 147.93, 144.16, 142.41, 142.05, 142.02, 142.00, 140.12, 138.63, 136.21, 135.06, 134.90, 131.60, 131.48, 131.35, 131.17, 128.67, 128.53, 126.72, 125.58, 125.22, 125.14, 125.05, 124.90, 77.54, 63.70, 35.03, 33.85, 33.39, 33.19, 30.55, 28.66, 26.27, 17.00; ESI/MS (m/z): Calcd $[M]^{4+}$: 613.52, Found: 613.64; $[M+Cl^-]^{3+}$: 829.68; Found: 829.78.

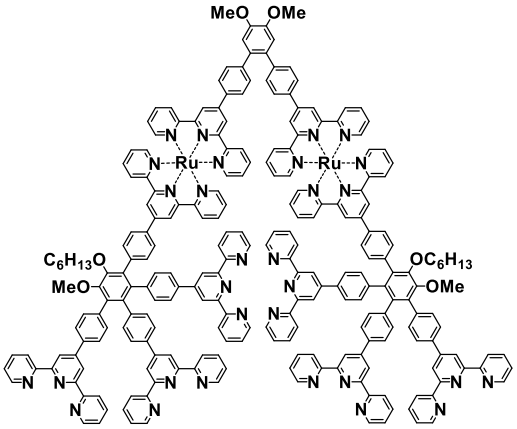

Ligand L2. To a solution of **B2** (25.85 mg, 10 μmol) and 4'-(4-boronato-phenyl)[2,2':6',2"]terpyridine (**1**; 70.8 mg, 200 μmol) in DMSO (20 mL), aqueous Na_2CO_3 (0.5 mL, 1 M) was added. The mixture was freeze-pump-thawed (3X) and backfilled with Argon; then $Pd(PPh_3)_4$ (10 mg) was added. After refluxing for 96 h under Argon, the mixture was cooled to 25 °C and then poured into aq. NH_4Cl. The aqueous layer was extracted with $CHCl_3$, and the combined organic phase was washed with brine and dried over anh $MgSO_4$. After concentration *in vacuo*, the residue was flash column chromatographed (Al_2O_3, 200-300 mesh) eluting with $CHCl_3$:MeOH (30:1) to give (62%) **L2**, as a red solid: 25 mg; ^{1}H NMR (500 MHz, $CDCl_3$,): δ 9.41 (s, tpy^B*H*$^{3',5'}$, 4H), 9.23 (d, *J* = 7.7 Hz, tpy^B*H*$^{3,3"}$, 4H), 9.02 (s, tpy^B*H*$^{3',5'}$, 4H), 8.77 (d, *J* = 8.7 Hz, tpy^A*H*$^{3,3"}$, 4H), 8.73 -8.69 (m, tpy^C*H*$^{3',5'}$, tpy^D*H*$^{3',5'}$, tpy^E*H*$^{3',5'}$, 12H), 8.64 (d, *J* = 7.7 Hz, tpy^C*H*$^{6,6"}$, tpy^D*H*$^{6,6"}$, tpy^E*H*$^{6,6"}$, 12H), 8.54 (ddd, *J* = 24.2, 15.2, 8.1 Hz, tpy^C*H*$^{3,3"}$, tpy^D*H*$^{3,3"}$, tpy^E*H*$^{3,3"}$, 12H), 8.32 (d, *J* = 7.6 Hz, Ph^B*H*^{g}, 4H), 8.18 (d, *J* = 7.6 Hz, Ph^A*H*^{g}, 4H), 7.86 (m, Ph^C*H*^{g}, Ph^D*H*^{g}, Ph^E*H*^{g}, 12H), 7.79 (m, tpy^B*H*$^{4,4"}$, tpy^A*H*$^{4,4"}$, 8H), 7.58 (dd, *J* = 20.8, 8.6 Hz, Ph^B*H*^{h}, Ph^A*H*^{h}, 8H), 7.38 (m, tpy^B*H*$^{6,6"}$, tpy^A*H*$^{6,6"}$, 8H), 7.24 (m, Ph^C*H*^{h}, Ph^D*H*^{h}, Ph^E*H*^{h}, 12H), 7.10 (m, tpy^B*H*$^{5,5"}$, tpy^A*H*$^{5,5"}$, tpy^C*H*$^{5,5"}$, tpy^D*H*$^{5,5"}$, tpy^E*H*$^{5,5"}$, 20H), 6.94 (d, *J* = 8.5 Hz, ph*H*^{J}, 2H), 4.05 (s, OC*H*$_3$, 6H), 3.99 (s, OC*H*$_3$, 6H), 3.75 (d, OC*H*$_2$R, 4H), 1.43 (m, *H*^{alkyl}, 6H), 1.26 (d, *J* = 12.6 Hz, *H*^{alkyl}, 8H), 0.90 (d, *J* = 7.0 Hz, *H*^{alkyl}, 4H), 0.83 (t, *J* = 6.8 Hz, *H*^{alkyl}, 6H); ^{13}C NMR (126 MHz, $CDCl_3$): δ 158.18, 157.59, 156.34, 156.27, 155.81, 155.66, 155.61, 155.02, 149.05, 148.91, 138.24, 136.66, 132.01, 131.35, 127.96, 126.49, 126.04, 123.93, 123.67, 123.54, 121.31, 121.21, 118.93, 118.64, 118.37, 117.78, 116.39, 116.00, 60.84, 56.34, 31.91, 31.62, 31.59, 30.28, 29.68, 29.34, 25.64, 22.72, 14.14, 14.08; ESI/MS (m/z): Calcd $[M]^{4+}$: 957.5, Found: 957.5; $[M+Cl]^{3+}$:1288.6, Found:1288.6.

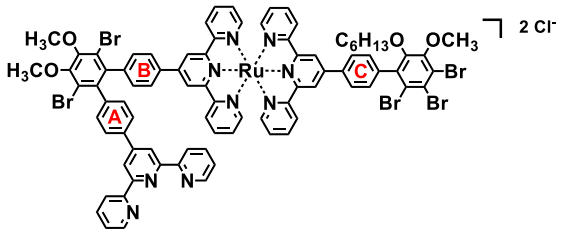

Complex B3. To a suspension of **S11** (48 mg, 50 μmol) and **S6** (91.1 mg, 100 μmol) in $CHCl_3$/MeOH (100 mL, 1:1(v/v)), 5 drops of *N*-ethylmorpholine, as a reductant, were added. The mixture was refluxed for 12 h becoming dark red over time. The mixture was cooled to 25 °C and then concentrated *in vacuo* to give a residue that was extracted (3X) with $CHCl_3$, and then the combined organic phase was washed with brine and dried with anh $MgSO_4$. After concentrated *in vacuo*, the residue was flash column chromatographed (Al_2O_3, 200-300 mesh) eluting with $CHCl_3$:MeOH (20:1) to give (30 %) **B3**, as a red powder: 35 mg, m.p. > 320 °C; ^{1}H NMR (500 MHz, $CDCl_3$): δ 9.39 (s, 2H), 9.17 (s, 2H), 9.13 (d, *J* = 8.1 Hz, 2H), 8.94 (d, *J* = 8.1 Hz, 2H), 8.69 (s, 2H), 8.64 (dd, *J* = 9.6, 6.7 Hz, 3H), 8.58 (d, *J* = 7.8 Hz, 2H), 8.27 (d, *J* = 7.7 Hz, 2H), 8.01 – 7.83 (m, 6H), 7.80 (d, *J* = 7.8 Hz, 2H), 7.58 (d, *J* = 7.8 Hz, 2H), 7.46 – 7.37 (m, 4H), 7.34 (t, *J* = 6.2 Hz, 4H), 7.29 – 7.20 (m, 6H), 7.22 – 7.10 (m, 2H), 4.08 (d, *J* = 4.9 Hz, 6H), 3.96 (s, 3H), 3.80 (t, *J* = 6.4 Hz, 2H), 0.90 (t, *J* = 6.4 Hz, 2H), 0.80 (t, *J* = 6.8 Hz, 3H); ^{13}C NMR (126 MHz, $CDCl_3$): δ 157.99, 155.90, 155.07, 152.62–151.50, 150.91, 150.51, 149.81, 149.33–149.00, 148.80, 148.50, 142.42, 140.77, 140.39, 139.28, 138.58, 137.24, 136.90, 135.54, 134.73, 131.68, 131.44–131.27, 131.03, 128.00, 127.70, 126.76, 125.83, 125.52, 124.05, 123.19, 122.16, 121.75, 121.55, 119.55, 119.26, 118.82, 114.06, 60.96, 33.81, 31.92, 31.43, 30.20, 29.92, 29.52, 29.34–29.27, 29.15, 28.95, 27.21, 25.37, 22.66, 14.09; ESI/MS m/z: Calcd $[M]^{2+}$: 882.5004, Found: 882.4975, Calcd $[M+Cl^-]^-$: 1797.9605, Found: 1797.9694.

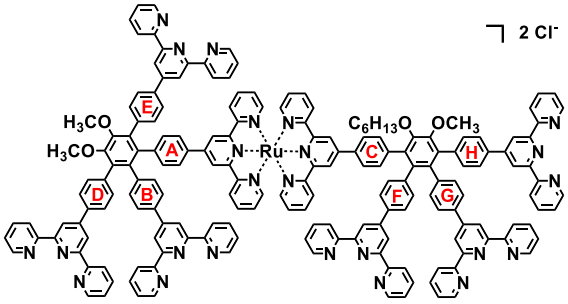

Ligand L3. To a solution of **B3** (32 mg, 20 μmol) and 4'-(4-boronatophenyl)[2,2':6',2"]terpyridine (**1**; 70.8 mg, 200 μmol) in DMSO (20 mL), aqueous Na_2CO_3 (0.5 mL, 1 M) was added. The mixture was freeze-pump-thawed (3X) and backfilled with Argon; then $Pd(PPh_3)_4$ (5 mg) was added. After refluxing

for 96 h under Argon, the mixture was cooled to 25 °C and poured into an aq. NH_4Cl solution. The aqueous layer was extracted with $CHCl_3$, and then the combined organic extract was washed with brine and dried over anh $MgSO_4$. After concentration *in vacuo*, the residue was flash column chromatographed (Al_2O_3, 200-300 mesh) eluting with $CHCl_3$: MeOH (40:1) to give (42%) **L3**, as a red solid: 20 mg, m. p. >320°C; ^{1}H NMR (400 MHz, $CDCl_3$): δ 9.06 (s, 2H), 8.87 (s, 2H), 8.78 (d, *J* = 8.0 Hz, 3H), 8.73 (d, *J* = 2.3 Hz, 4H), 8.71 – 8.61 (m, 17H), 8.60 – 8.43 (m, 20H), 8.21 (d, *J* = 8.4 Hz, 2H), 7.92 (d, *J* = 8.4 Hz, 3H), 7.89 – 7.69 (m, 24H), 7.61 – 7.56 (m, 5H), 7.53 (t, *J* = 6.1 Hz, 4H), 7.47 (d, *J* = 8.2 Hz, 3H), 7.45 – 7.39 (m, 6H), 7.39 – 7.29 (m, 11H), 7.26 – 7.19 (m, 8H), 7.12 (dt, *J* = 16.8, 5.4 Hz, 11H), 7.01 (dd, *J* = 10.8, 3.8 Hz, 3H), 6.89 (d, *J* = 8.7 Hz, 2H), 3.97 (t, *J* = 6.5 Hz, 2H), 3.81 (d, *J* = 3.2 Hz, 6H), 3.75 (s, 3H), 0.89 (q, *J* = 6.8 Hz, 6H), 0.82 (t, *J* = 6.8 Hz, 4H); ^{13}C NMR (126 MHz, $CDCl_3$): δ 156.30, 155.80, 148.99, 136.88–136.55, 131.36–128.79, 126.65–126.49, 123.71, 121.35, 118.73, 118.42, 77.26, 77.01, 76.76, 60.85, 50.84, 31.76, 30.82, 29.69, 29.35, 25.71–25.48, 22.68, 14.10, 1.01; ESI/MS (m/z): Calculated $[M]^{2+}$: 1453.16, Found: 1452.95

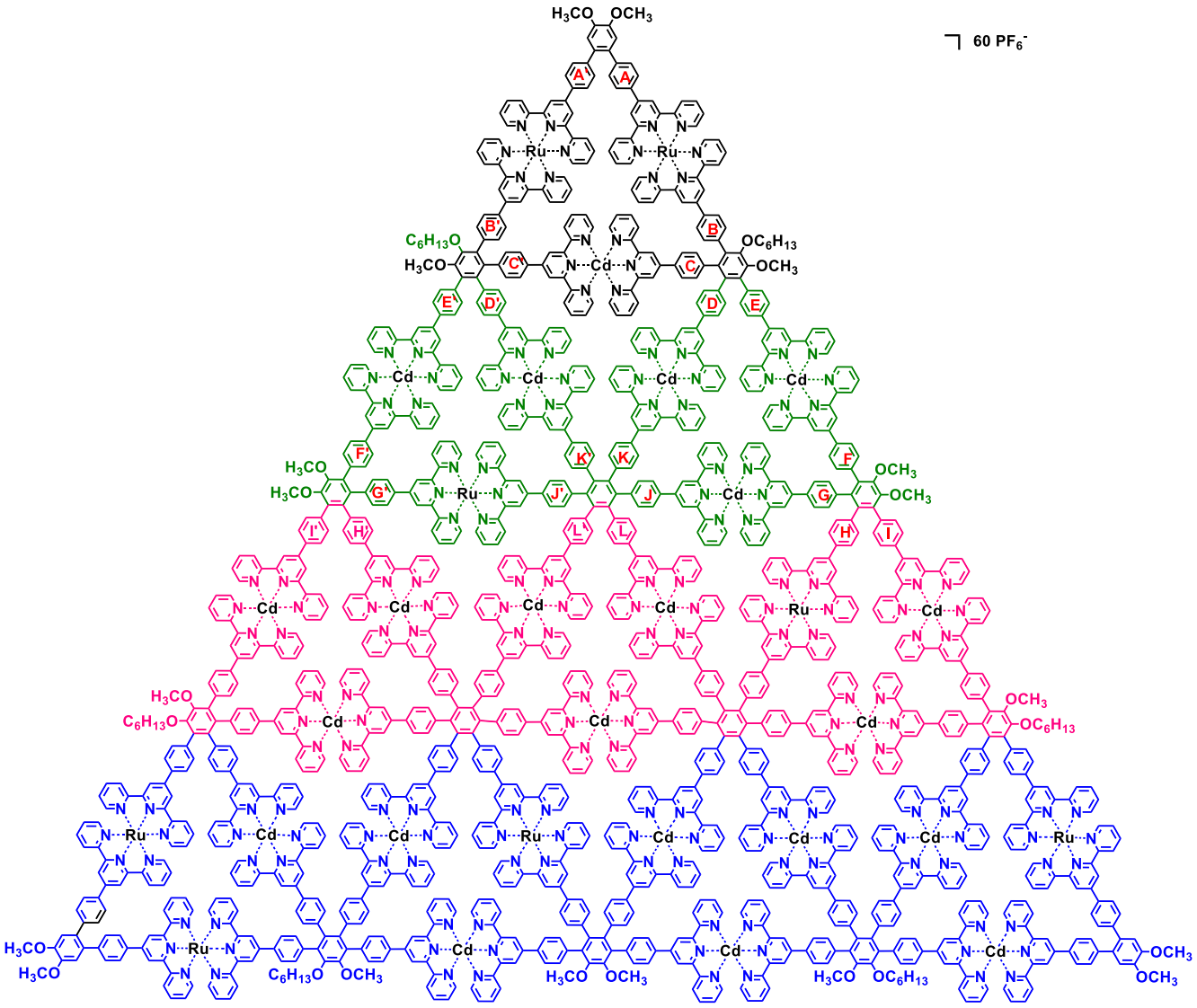

G3 Pascal Triangle (G3 **PT)**. To a solution of **L2**(5.00 mg, 1 μmol) and L1 (3.95 mg, 1 μmol) in $CHCl_3$/MeOH (10 mL, 1:1 v/v), a solution of $Cd(NO_3)_2$•$6H_2O$ (2.31 mg, 7.50 μmol) in MeOH (5 mL) was added dropwise, then the mixture was stirred at 25 °C for 8h. NH_4PF_6 (200 mg) was added resulting in the formation of an orange precipitate, which was filtered, then washed with water and MeOH to give (95%) the Pascal triangle (G3 **PT**): 8.5 mg; ^{1}H NMR (500 MHz, CD_3CN) δ 9.05 (m, 42H), 8.94 (m, 34H), 8.71-8.49 (m, 164H), 8.11 (m, 120H), 7.93-7.67 (m, 199H), 7.62–7.58 (m, 119H), 7.45 (m, 94H), 7.36 – 7.33-7.29 (m, 72H), 7.18-7.12(m, 73H), 7.07 – 6.95 (m, 48H), 4.15 – 4.12 (m, 12H), 4.07 (m, 18H), 4.00 (m, 10H), 3.93 (m, 24H), 1.30 (m, 76H), 0.91 (m, 24H); ESI-MS (m/z): 1898.20 [M-16 PF_6^-]$^{16+}$ (calcd *m/z*: 1900.18), 1780.04 [M-17 PF_6^-]$^{17+}$ (calcd m/z: 1779.88), 1673.49 [M-18PF_6^-]$^{18+}$ (calcd m/z: 1672.94), 1577.27 [M-19 PF_6^-]$^{19+}$ (calcd m/z: 1577.26), 1491.28 [M-20 PF_6^-]$^{20+}$ (calcd m/z: 1491.15), 1413.47 [M-

21 PF_6^-]$^{21+}$ (calcd m/z: 1413.24), 1342.58 [M-22 PF_6^-]$^{22+}$ (calcd m/z: 1342.41), 1277.56 [M-23 PF_6^-]$^{23+}$ (calcd m/z: 1277.74), 1218.59 [M-24 PF_6^-]$^{24+}$ (calcd. m/z: 1218.46), 1164.32 [M-25 PF_6^-]$^{25+}$(calcd *m/z*: 1163.93), 1113.54 [M-26 PF_6^-]$^{26+}$(calcd *m/z*: 1113.59).

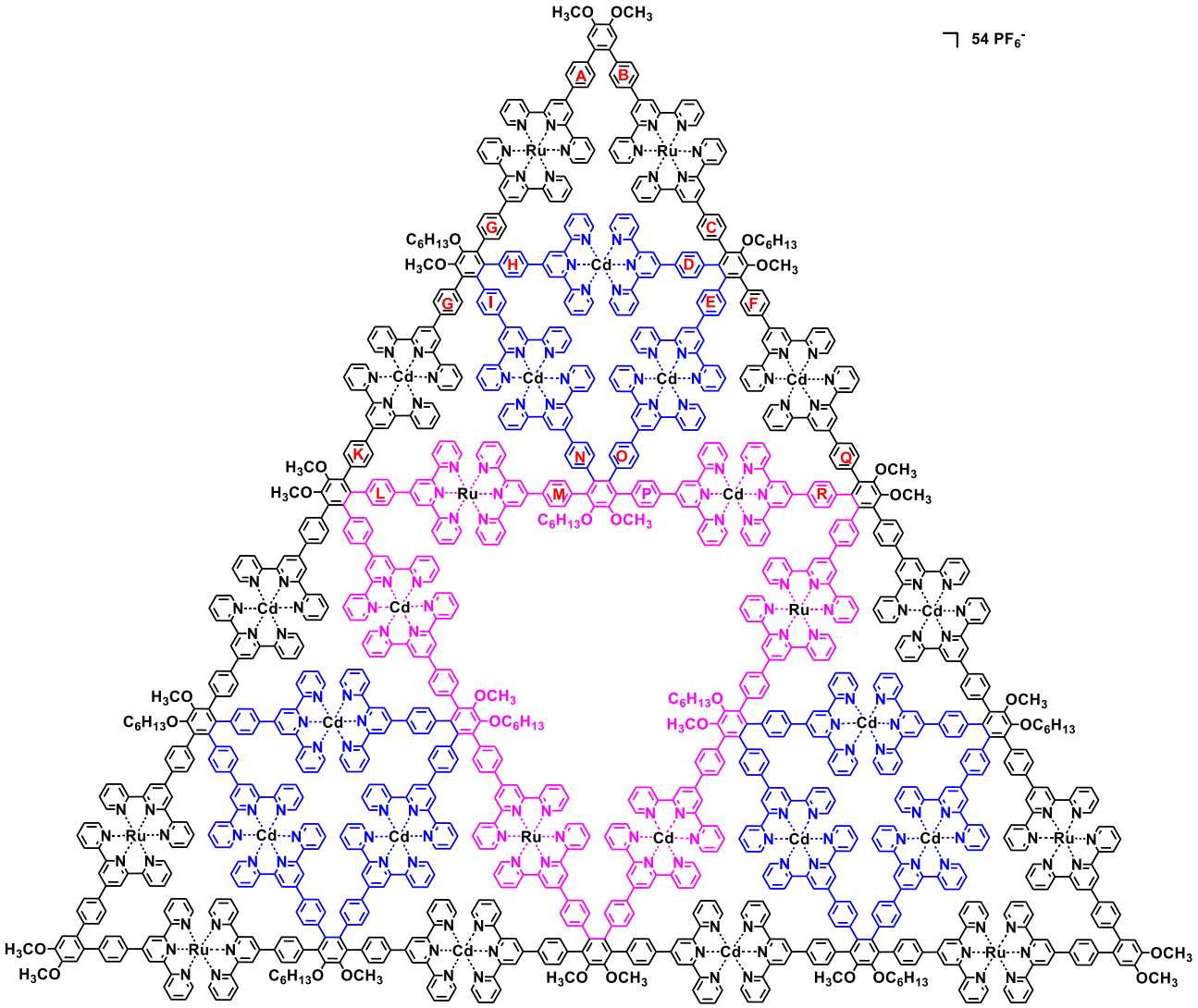

G2 Sierpinski Triangle (G2 **ST**). To a solution of ligand **L2** (3.956 mg, 1 μmol) and **L3** (3.01 mg, 1 μmol) in $CHCl_3$/MeOH (10 mL, 1:1 v/v), a solution of $Cd(NO_3)_2$•$6H_2O$ (1.848 mg, 6 μmol) in MeOH (5 mL) was added dropwise; then the mixture was stirred at 60 °C for 8h. NH_4PF_6 (200 mg) was added to give an orange precipitate, which was filtrated, washed with water and MeOH to afford the desired triangle G2 **ST**, as an orange solid: 8.2 mg (92%); ^{1}H NMR (500 MHz, CD_3CN): δ 9.05 (m, 24H), 9.01 (m, 24H), 8.98 – 8.94 (m, 16H), 8.97 – 8.92 (m, 18H), 8.89 (m, 16H), 8.82 – 8.58 (m, 140H), 8.14 (m, 106H), 7.88 (m, 170H), 7.70 (m, 84H), 7.42 (m, 100H), 7.29 (m, 46H), 7.17 (m, 28H), 7.12 – 7.05 (m, 26H), 4.14 – 4.11 (m, 12H), 4.06 (m, 18H), 3.92 (m, 21H), 3.89 (m, 9H), 1.30 (m, 71H), 0.90 (m, 48H); ESI-MS (m/z):

2002.20 [M-14 PF_6^-]$^{14+}$ (calcd. m/z: 2002.33), 1859.26 [M-15 PF_6^-]$^{15+}$(calcd *m/z*:1859.18), 1734.22 [M-16 PF_6^-]$^{16+}$ (calcd *m/z*: 1733.93), 1623.59 [M-17 PF_6^-]$^{17+}$ (calcd m/z: 1623.40), 1525.42 [M-18PF_6^-]$^{18+}$ (calcd m/z: 1525.16), 1437.47 [M-19 PF_6^-]$^{19+}$ (calcd m/z: 1437.29), 1358.27 [M-20 PF_6^-]$^{20+}$ (calcd m/z: 1358.15), 1286.74 [M-21 PF_6^-]$^{21+}$ (calcd m/z: 1286.57), 1220.99 [M-22 PF_6^-]$^{22+}$ (calcd m/z: 1221.50), 1161.72 [M-23 PF_6^-]$^{23+}$ (calcd m/z: 1162.09

References

Jarozs, P.; Lotito, K.; Schneider, J.; Kumaresan, D.; Schmehl, R.; Eisenberg, R. *Inorg. Chem*. **2009**, *48*. 2420.

Schultz, A.; Li, X.; Barkakaty, B.; Moorefield, C. N.; Wesdemiotis, C.; Newkome, G. R. *J. Am. Chem. Soc*. **2012**, *134*, 7672.

Wang, J.-L., Li, X., Lu, X. C., Hsieh, I-F., Cao, Y., Moorefield, C. N., Wesdemiotis, C., Cheng, S. Z. D., Newkome, G. R., *J. Am. Chem. Soc*. **2011**, *133*, 11450-11453.

Ayme, J.-F.; Beves, J. E.; Leigh, D. A.; McBurney, R. T.; Rissanen, K.; Schultz, D. *Nat. Chem.* **2012**, *4*, 15.

Sun, B.; Wang, M.; Lou, Z.; Huang, M.; Xu, C.; Li, X.; Chen, L.-J.; Yu, Y.; Davis, G. L.; Xu, B.; Yang, H.-B.; Li, X. *J. Am. Chem. Soc.* **2015**, *137*, 1556.